FACILE HIGHLY SCALABLE METHOD FOR TEMPLATING HOLLOW SILICA SPHERES USING A TWO STEP SYNTHESIS

by

Spyridon Monastiriotis

A Dissertation Submitted to the Graduate Faculty in Engineering
in Partial Fulfillment of the Requirements for
the Degree of Doctor of Philosophy

The City University of New York

2010

This manuscript has been read and accepted for the
Graduate Faculty in Engineering in satisfaction of the
dissertation requirement for the Degree of Doctor of Philosophy.

Prof. Alexander Couzis

_____

_____ _____

Date Chair of Examining Committee

Prof. Mumtaz Kassir

_____

_____ _____

Date Executive Officer

Prof. Charles Maldarelli

_____

Prof. Ilona Kretzschmar

_____

Prof. Raymond Tu

_____

Prof. Steven O'Brien

_____

Supervisory Committee

THE CITY UNIVERSITY OF NEW YORK

ABSTRACT

FACILE HIGHLY SCALABLE METHOD FOR TEMPLATING HOLLOW SILICA SPHERES USING A TWO STEP SYNTHESIS

by

Spyridon Monastiriotis

Advisor: Professor Alexander Couzis

In this work we have developed a facile highly scalable two step method for templating hollow silica nanospheres using catanionic vesicles as templates. The template consisted of equilibrium unilamelar catanionic vesicles formed from mixtures of cationic and anionic surfactants. A thorough investigation of the template's behavior was necessary in order to proceed in templating synthesis. The template's (catanionic vesicles) structure, phase and stability were characterized by independent techniques such as cryo-Transmission Electron Microscopy, Small Angle Neutron Scattering and Dynamic Light Scattering. Hollow silica spheres were synthesized using catanionic vesicles as a template and tetramethoxysilane (TMOS) as the silica precursor under acidic conditions. Transmission Electron Microscopy, Scanning Electron Microscopy, Atomic Force Microscopy and Dynamic Light

Scattering were the techniques that helped us to characterize the hollow silica nanospheres, further understand and face the challenges of the particular templating sol-gel process. The competition between the adsorption of the hydrolyzed silica precursor onto the vesicular surface and the homogeneous nucleation in the bulk (resulting in gel formation and particle trapping-caging into the gel) was never faced as an optimization challenge. We find that by introducing a second step, under conditions close to the Stöber synthesis, non adsorbed silicate species condense resulting in solid particle formation and produce two distinctly different particle size populations of hollow and solid silica beads, which can easily be separated due to their significant density difference. Thus, the second step maximizes the yield of the templated synthesis and optimizes the sol-gel batch process.

ACKNOWLEDGMENTS

First and foremost, I offer my sincerest gratitude to my advisor, Professor Alexander Couzis for his guidance, advice and motivation. His scientific intuition and unique way of discovering answers to obstacles that arise in research, not only broadened my knowledge, but also, and most importantly, provided me with the tools needed to enrich and cultivate an independent way of approaching and investigating a challenge. I would like to thank the other members of my committee, Professors Charles Maldarelli, Ilona Kretzschmar, Raymond Tu and Stephen O'Brien, for providing their valuable feedback and advice.

I would also like to thank Dr. Paul Butler and Dr. Lionel Porcar at National Institute of Standards and Technology (Center for Neutron Research) for their assistance and support during Small Angle Neutron Scattering experiments.

I had the privilege to share ideas, learn with and from great colleagues and friends, during the five years of pursuing my doctorate. Many thanks to Kevin, Makonnen, Nikhil, Shyam, Lorraine, Tieuvi and Vikas.

Over the last few years, I was fortunate enough to have the continuous support and encouragement of a wonderful person, Carrie, who I now share my life with. Without her faith and patience, this work would have never been accomplished.

Finally, I dedicate this thesis to my parents Mihalis and Ellie, and my brother Alexander. Their fundamental influence, love and devotion have always been instrumental in achieving the various goals in my life.

TABLE OF CONTENTS

LIST OF TABLES

LIST OF FIGURES

CHAPTER 1

INTRODUCTION

1.1 Background

Thomas Graham,[1] in his fundamental paper "Liquid Diffusion Applied to Analysis," first coined the term *colloids*, derived from the Greek *kolla*, meaning glue, also terms such as dialysis, sol, gel, and so forth. He pointed out the differences between what he called "the two worlds of matter." He showed that substances such as certain inorganic salts, sugar and glycerol will diffuse through water and membranes much more rapidly than substances such as gelatin and the hydrous oxides which are gelatinous. Substances which diffuse rapidly were categorized as *crystalloids*, and those which exhibit little or no tendency to diffuse were termed *colloids*. Von Weymarn[2] generalized further, that any crystalline material can be made to assume the colloidal state under suitable conditions. The term colloid should be used only as an adjective to define a physical system of matter usually made up of more than one substance. The leader in what now we call modern colloid chemistry was Wolfgang Ostwald (1883-1943). He first classified dispersed systems depending on the size of the dispersed phase and set the limits of the colloidal zone.[3] Ostwald referred to this zone as "The world of neglected dimensions."[4,5] Colloidal particles are usually spherical and dense. However, the definition does not preclude other shapes or even hollow particles, which are the topic of this research.

The design and fabrication of hollow inorganic spheres with nanometer to micrometer dimensions have attracted a lot of attention because of their many potential applications. Their hollow structure provides them with relative low

density and large specific area, compared to their solid counterparts, and makes them attractive for numerous uses in applications such as catalysts (larger number of active sites), pigments, coatings, thermal and electronic insulators, controlled drug delivery agents, protection of biologically active agents, and gas sensors. Various methods of fabrication of inorganic materials with hollow spherical structures have been reported including nozzle reactor processes, aerosols, microemulsions, solvothermal and sacrificial template techniques.

During the last three decades, template synthesis of hollow nanomaterials (nanocoatings), using a sol-gel coating procedure, has attracted a lot of attention.[6,7] Templated synthesis involves coating a sacrificial template and subsequently removing it by calcination or selectively dissolving it with a solvent.[8,9] Templates can serve as casts for a reverse casting in order to fabricate nanomaterials and nanocomposites. In templated synthesis of hollow spheres, the inner diameter of hollow spheres is confined by the dimensions of the template. The interface between the template and the solution of inorganic precursors (sol-gel synthesis), acts as a site for selective adsorption[10] and growth of inorganic material from the solution.

Sacrificial templates that have been frequently used are aerosol droplets,[11] liquid droplets,[12,13] silica spheres,[14-16] colloidal carbon spheres,[17] resin spheres,[18] polystyrene spheres,[19-22] gas bubbles,[23] vesicles,[24-28] cellulose,[29] bacterial superstructures,[30] water in oil as well as oil in water emulsions[31,32] and triblock copolymers.[33,34] Self-assembled nanostructures that serve as templates is an area of great, not only

scientific and technological, but also biological and medical interest. For example, biomineralization in living organisms[35] can resemble by the selective growth of inorganic materials onto or into self-assembled molecular nanostructures.[36]

Hubert et al.,[25] first described the use of unilamellar vesicles as templates for the deposition of silica from aqueous solution to produce silica coated vesicles. Fluorocarbon surfactants have been used for templated synthesis of silica hollow spheres. Qiao et al.[37] used a fluorocarbon surfactant FC4 to synthesize the vesicular template in order to form the hollow silica structure and a cationic surfactant cetyltrimethylammonium bromide (CTAB) as the liquid-crystal template to produce the mesoporous silica shell. Tan et al.[38] describes the synergistic interaction of a fluorocarbon surfactant and silica in the presence of ammonium hydroxide as they co-assembled and formed vesicle-like hollow silica spheres. Finally, mixtures of fluorocarbon/hydrocarbon[39,40] and fluorocarbon/fluorocarbon[40] surfactants have been used to form vesicular templates for synthesis of hollow silica spheres.

1.2 Scope of Research

Solid templates such as polystyrene latex beads, carbon spheres, silver, gold and iron particles[15,41] have been used for numerous syntheses of inorganic hollow or composite materials, but hollow soft templates such as droplets, gas bubbles, liposomes and vesicles represent a very fascinating class of casting materials, due to the fact that simply they are hollow themselves, therefore exhibit encapsulation capabilities and contribute to a much cleaner synthesis-process, as there is less material (template) to be removed in order to obtain the inorganic hollow structure. However, the complexity of these systems is elevated, since the stability and the structural behavior of these templates, compared to their solid counterparts, are not only a function of the interfacial phenomena between the template's surface and the solution, but also a function of the template itself. Once the silica precursor is introduced to the solution and polymerization reactions occur, the vesicles cannot be considered as stable colloidal structures such as solid templates. Dynamic interactions between the vesicles, precursor and already shaped silica hollow spheres, during the sol-gel coating, play a significant role during the template synthesis. Conditions such as type of solvents, pH, temperature, time, and concentrations are the tools (and needed to be investigated) to maintain the integrity of the template during the nanocoating, and have direct influence in the sol-gel process.

The purpose of this work is to determine the parameters that influence the templated synthesis of hollow silica nanospheres using catanionic vesicles as templates. Our goal is first to investigate the stability of the template during the template synthesis. The binary system of the two surfactants used to form the vesicular templates has the ability to form lamellar, coexistence of lamellar and vesicular structures, rodlike micelles and vesicular phases. Concentration, ratio (of the two surfactants), and pH are the tools needed to form solely the vesicular phase. Characterization of the surfactant mixtures was essential in order to confirm the vesicular unilamellar phase.

Surface chemistry plays a significant role, since the templating mechanism (transcriptive synthesis) is directly dependent on the stability of the template and the receptiveness for silica of the vesicular surface. Surface charge role would be investigated by using amidine functionalized polystyrene spheres with diameter similar to the vesicular templates.

The competition between the adsorption of the hydrolyzed silica precursor onto the vesicular surface and the homogeneous nucleation in the bulk (resulting in gel formation and particle trapping-caging into the gel) has been identified as one of the serious challenges in templated synthesis of hollow inorganic materials. Usually, the sol-gel (batch) process has been terminated by subsequent repeated washing and centrifugation-separation steps in order to obtain the hollow nanomaterial-powders and discard the unreacted silica precursor's oligomers-gels. Additional steps in the

process, such as pH modification, have been reported in order to ensure colloidal stability.[40]

To our knowledge, there have been no reported studies of any additional processing steps toward optimization (gel minimization) and product yield. Control of the concentration of the inorganic precursor[39,40] can be used to minimize the gel formation but it is not adequate, especially when considering the scale-up of the process. Steps-mechanisms that favored adsorption-condensation onto the vesicular template and simultaneously reduce the condensation of the hydrolyzed non-adsorbed silica species in the bulk (that would eventually form the by-product: gel) were investigated and proposed as an approach to optimize the process.

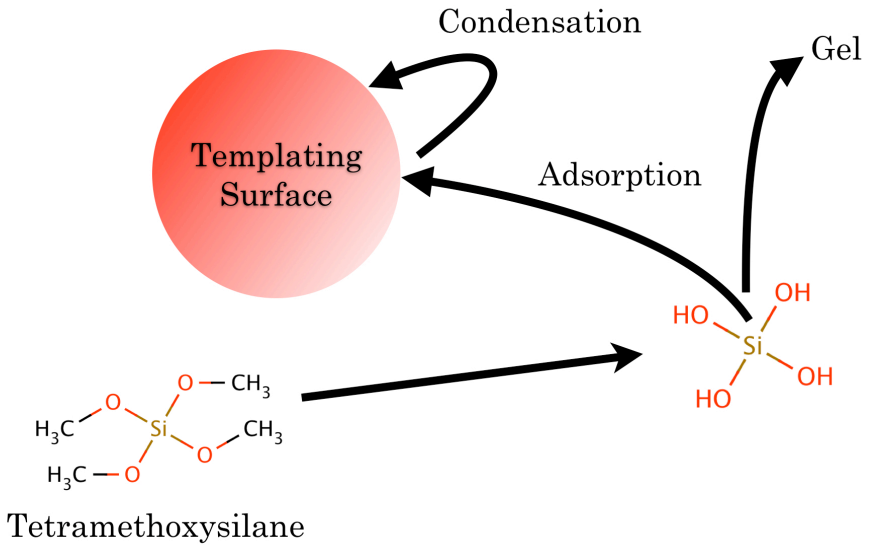

Figure 1.1 Schematic representation of the competition between the adsorption of the hydrolyzed silica precursor species (tetramethoxysilane, TMOS) onto the vesicular surface and their homogeneous nucleation in the bulk (resulting in gel formation and particle trapping-caging into the gel).

CHAPTER 2

INVESTIGATION OF THE BEHAVIOR AND STABILITY OF VESICULAR TEMPLATES FORMED FROM AN AQUEOUS BINARY MIXTURE OF CATIONIC AND ANIONIC SURFACTANTS

2.1 Introduction

Surfactants are bi-functional molecules that are amphiphilic (i.e., contain a hydrophilic head and a hydrophobic tail).[42] As a result of their amphiphilic nature, surfactants can associate into supramolecular arrays. Bangham et al.,[43] in 1965, first reported that phospholipids in water form liposomes, closed multibilayer aggregates that separate an internal volume from the bulk solution. Self-organizing of amphiphiles in solution is spontaneous, thermodynamically driven and depends on their molecular structure. Israelachvili et al.,[44,45] introduced the concept of molecular packing parameter which makes it possible to predict the shape and size of equilibrium structures based on geometrical considerations.[46] Packing parameter, P, is defined by the ratio of the volume of the hydrocarbon tail of the surfactant in the core (v) and the product of the optimal head group area (α) and the critical chain length of the tail (l) :

$$P = \frac{v}{al}$$

The importance of the hydrocarbon chain length and head surface area was first reported by Tartar et al.[47] in 1956 and theoretically interpreted by Tanford[48,49] and Israelachvili.[44,50] Additional important factors in the prediction of the structures are temperature, ionic strength, and pH.

Mixtures of cationic and anionic surfactants ("catanionic surfactants" or "ion pair amphiphiles") were first described by Jokela et al.[51] as solutions of water and the oppositely charged surfactant ions formed from an organic hydroxide and an organic acid, so the common ancillary product is water rather than a salt. Specifically in our research, we were interested in mixtures of anionic and cationic surfactants from which the co-ion simple salt has not been removed.

Catanionic surfactant systems in water mix in a highly non-ideal way, and can form various different self-organization nanostructures in solution (such as spherical and cylindrical micelles, discs, unilamellar vesicles and multilayered lamellar phases) depending on the surfactant architecture, the strength of the intra- and intermolecular interactions, cationic and anionic surfactant ratio, total surfactant concentration and solution properties. Mixtures of cationic and anionic surfactants form vesicles with considerably lower critical aggregation concentrations (cac's) than the critical micelle concentration (cmc) of individual surfactant. Vesicle formation as aqueous mixtures of anionic and cationic surfactant is well documented.[52-57] Several applications rely on their colloidal, chemical, microencapsulating and surface properties such as drug encapsulation and delivery devices, cancer therapy, cosmetic formulations, diagnostics and food industry, etc.[58,59] Unlike unilamellar vesicles prepared by mechanical and chemical treatment of multilayered liposome[60], those formed from anionic and cationic surfactants remain stable and do not aggregate over periods of years.[53,61,62] The unique aspect of these vesicular systems is that the formation proceeds spontaneously upon mixing.[62] The stability of the vesicle phase

has been of special interest,[63-65] with a variety of work showing that composition range over which vesicles form can be expanded by increasing the asymmetry between the two surfactant chains or by branching one of the surfactant chains.[54,57] Stability and formation of any surfactant aggregate are directly dependent on their thermodynamics; whether that system represents the minimum free energy for any given composition. Helfrich,[66] in 1973, was the first to describe the properties of a bilayer in terms of its local state of curvature. The harmonic approximation of the bending free energy of a bilayer is given by:

$$\frac{E}{A} = \frac{1}{2}\kappa\left(c_1 + c_2 + 2c_0\right)^2 + \bar{\kappa} c_1 c_2 \qquad (1)$$

A is the area of the bilayer membrane, $c_1 = 1/R_1$ and $c_2 = 1/R_2$ are the principle curvatures of the structures, $c_o = 1/R_o$ is the spontaneous curvature of the bilayer, κ is the bending modulus, and $\bar{\kappa}$ is the saddle splay or Gaussian modulus. The origin of spontaneous formation of vesicles was described by Safran et al.,[67] in surfactant mixtures. The harmonic approximation states that deviations of the mean curvature c_o are associated with an energy penalty known as the bending or curvature modulus, κ which is always positive ($\kappa > 0$) for a stable film.[66] The saddle splay modulus $\bar{\kappa}$, measures the energy cost of saddle deformations where $\bar{\kappa} > 0$ for surfaces that prefer hyperbolic shapes (where the centers of curvature are on opposite sides of the surface, $c_1 c_2 < 0$), and $\bar{\kappa} < 0$ for surfaces that prefer elliptical shapes (spheres, cylinders, etc., where the centers of curvature are on the same side

of the surface, $c_1c_2 > 0$).[67-69] The spontaneous curvature c_o describes the tendency of a surfactant bilayer to bend toward either the water ($c_o < 0$) or the oil ($c_o > 0$). For a symmetric bilayer, such as a single component bilayer, the spontaneous curvature $c_o = 0$. Physical and or chemical asymmetry are essential for a spontaneous curvature to exist.[67] Helfrich[70] showed that thermally driven elastic fluctuations of the fluid membranes give an important contribution to the total free energy of interaction. The physical mechanism responsible for this interaction is the coupling between confinement forces and undulation disorder of the membrane surfaces. Thermal fluctuations of the bilayers lead to a repulsive interaction, as the bilayers come into contact.[70] For bilayers separated by a distance d, the undulation interaction energy is:

$$E_{fl} = \frac{3\pi^2}{128}\frac{\left(k_B T\right)^2}{\kappa d^2} \qquad (2)$$

Van der Waals attraction between the bilayers (which is also $\propto d^{-2}$) can be overwhelmed by the repulsive undulation interaction E_{fl} when κ is small, resulting in a net repulsive interaction between the bilayers and therefore, stable unilamellar vesicles.[71] This repulsive interaction between bilayers is enhanced in charged systems.[72]

Stabilization of vesicles can be achieved by either an entropic or an enthalpic mechanism. The bending modulus κ plays a significant role in these two mechanisms. The magnitute of κ represents the amount of energy needed to bend the

bilayer away from its spontaneous curvature, c_o. Entropically stabilized vesicles have a low bending modulus ($\kappa \sim k_BT$) which leads to a low bending free energy and high undulation interaction, therefore a net repulsive interaction between vesicles in short distances. The vesicles are stabilized over multilamellar liposomes by this steric repulsion and the gain in entropy resulting from the large number of finite sized vesicles.[73,74] Enthalpically stabilized vesicles, on the other hand, require larger values of bending modulus ($\kappa >> k_BT$) and a non-zero spontaneous curvature, $c_o \neq 0$. Non-ideal surfactant mixing sastisfies the non-zero spontaneous curvature and can cause the interior and exterior monolayers of the vesicle bilayer to have different compositions. The vesicles population is monodisperse, distributed around a particular vesicle radius dictated by the spontaneous curvature. The curvature energy of adding a second bilayer to the vesicle can overcome the attractive interaction between bilayers, leading to unilamellar vesicles. In this case any curvature variations, such as multilamellar phases, are energetically unfavored.[73,75,76]

In our study, we formed equilibrium catanionic vesicles by using a aqueous mixture of Cetytrimethylammonium Bromide (CTAB) and Sodium Perfluorooctanoate (SPFO). By equilibrium we are not describing their equilibrium size or the time to reach their equilibrium size (equilibration time), but we refer to the following three criteria as described by Kaler et al.:[77]

i. Unilamellar vesicles are formed spontaneously upon dispersing dry surfactant into water without mechanical or chemical perturbation;

ii. Vesicles do not aggregate with time; and

iii. Any physical or chemical process to which the vesicles are exposed will result in spontaneous reformation of unilamellar vesicles on reversing the process.

The anionic surfactant Sodium Perfluorooctanoate (SPFO) has a completely fluorinated hydrophobic part. Fluorination of the hydrophobe increases the surface activity of the surfactant over that of the analogous hydrocarbon surfactant. Similar to hydrocarbon surfactants the fluorocarbon surfactants self-assemble into various aggregates such as micelles, threadlike micelles, vesicles, and other lamellar aggregates. A distinctive property of fluorocarbon surfactants is their tendency to form structures with little curvature, such as cylindrical micelles and bilayer structures.[78] For a given chain length, fluorocarbon surfactants have a lower critical micellar concentration (actually fluorocarbon vs. hydrocarbon surfactants with CF_2/CH_2 ratio of 1.5 between alkyl chains have nearly the same cmc)[79] and are more effective at lowering the surface tension of water than hydrocarbon surfactants.[80] The fluorocarbon chain is both hydrophobic and oleophobic, so fluorocarbon surfactants can be used in applications where both water and oil repellence are required. Furthermore, the ability of fluorinated surfactants to solubilize a variety of compounds has led to their proposed use in emulsion polymerizations[81] and in vivo oxygen transport.[82] Hydrocarbon/fluorocarbon surfactant mixtures are of interest because of physical and chemical differences between the two hydrophobic moieties.

Physically, the fluorocarbon chain is bulkier (the volume of the CF_2 group is 50% larger than that of the corresponding CH_2 group) and considerably more rigid than the hydrocarbon chain.[82,83] An interested review about the properties and significant advances of fluorinated surfactants has been reported by Kissa[80] and Hoffmann and Wurtz.[84]

The combination of hydrocarbon and fluorocarbon chains in the vesicle bilayer of the CTAB/SPFO system leads to a a high effective bending modulus K ($K = 6 \pm 2\ k_BT$, where $K = 2\kappa + \bar{\kappa}$) for the bilayer. The fact that CTAB/SPFO vesicles are stabilized by a spontaneous curvature of the bilayer,[75] which arises due to nonideal surfactant mixing,[67,68] and a high bending modulus κ, reveals an enthalpic stabilization mechanism, and explains their size monodispersity. Ristori et al.[85] reported the spontaneous formation of enthalpically stabilized monodisperse vesicles of a different mixture of hydrocarbon and fluorocarbon surfactants in aqueous solution.

Phase behavior of aqueous mixtures of cationic (R^+X^-) and anionic surfactants (R^-Y^+) is rather complex because it constitutes a five-component system: two ionic surfactants (R^+X^-, R^-Y^+), an ionic pair of amphiphiles (R^+R^-), inorganic salt (Y^+X^-) and H_2O. The phase behavior of the CTAB/SPFO system has been reported.[77,86] The ternary phase diagram of CTAB, SPFO and H_2O in rectangular coordinates (Figure 2.1) is only a portion of the complete phase diagram. But since precipitation was not observed, in any case of formation of CTAB/SPFO vesicular solutions, the ternary phase diagram was sufficient enough. The phase diagram consists predominantly of

a two phase region composed of vesicles in equilibrium with a lamellar phase (V+Lα) (see Figure 2.1). Rodlike micelles (R) exist on the CTAB-H_2O and SPFO-H_2O binary axes. There is a single vesicle phase (V) on the SPFO rich side of the phase map and that was the region that we were focused on experimentally in order to form the vesicular template.

2.2 Experimental Section

2.2.1 Materials

Cetyltrimethylammonium Bromide (CTAB) 97% wt., and Sodium Perfluoro-octanoate (SPFO) 98% wt., were obtained from Alfa Aesar and were used as received.

2.2.2 Vesicles Solution Preparation

Stock solutions of CTAB/SPFO vesicles were made under 2 different methods:

i. The required amount of the two surfactants for a 250 mL solution was measured on a scale of 0.1 mg accuracy. CTAB was placed on a flask of 250 mL of deionized water (water resistivity greater than 18 MΩ·cm, Millipore system). Then the solution was heated under stirring to 31°C for 10 min in order to achieve complete dissolution of CTAB (exceed the Krafft point of CTAB where the surfactant remains in crystalline form). Then SPFO was added to the solution and the binary mixture was aged for one (1) day under vigorous stirring (700 rpm). The second (2) day the solution was filtered (Nylon filter, 450 nm pore size, Whatman) and stirred at room temperature for 21 days to reach equilibrium size. Hydrodynamic average diameter and polydispersity were monitored by dynamic light scattering (DLS).

ii. Stock solutions of CTAB (2% wt.) and SPFO (2.8% wt.) were prepared, in deionized water, in 2 different 250 mL flasks. CTAB solution was heated under stirring to 31°C for 10 min in order to achieve complete dissolution of CTAB (exceed the Krafft point of CTAB where the surfactant remains in crystalline form). Then the appropriate volume of the two stock solutions was added to a separate flask and the remained volume in order to achieve the designed concentration was filled with deionized water. The solution was aged for one (1) day under vigorous stirring (700 rpm). The second (2) day the solution was filtered (Nylon filter, 450 nm pore size, Whatman) and stirred at room temperature for 21 days to reach equilibrium size. Hydrodynamic average diameter and polydispersity were monitored by dynamic light scattering (DLS).

The two different preparation protocols resulted in vesicular solutions that showed no major differences in particle size, average diameter, and size polydispersity index. For the rest of this study the vesicular solutions were prepared under the second protocol.

Total concentrations (both surfactants) of CTAB/SPFO were chosen to 0.5, 1.0, 1.5, 2.0, 2.5% wt. and the ratios of the two surfactants were 15/85, 20/80, 25/75% wt.

2.2.3 Methods

Dynamic Light Scattering

Dynamic Light Scattering (DLS) experiments were performed using the Malvern Zetasizer nano ZS. DLS measures Brownian motion and relates this to the size of the particles. Brownian motion is the random movement of particles due to the bombardment by the solvent molecules that surround them. The larger the particle, the slower the Brownian motion will be. Smaller particles are "kicked" further by the solvent molecules and move more rapidly. Constant temperature is necessary for DLS because the viscosity of a liquid is related to its temperature. The velocity of the Brownian motion is defined by the translational diffusion from the translational diffusion coefficient by using the Stokes-Einstein equation:

$$d_H = \frac{k_B T}{3\pi\eta D}$$

where:

d_H: hydrodynamic diameter

D: translational diffusion coefficient

k_B: Boltzmann's constant

T: absolute temperature

η: viscosity

In dynamic light scattering, the speed at which the particles are diffusing due to Brownian motion is measured. This is done by measuring the rate at which the intensity of the scattered light fluctuates. A corellator (a signal comparator) measures the degree of similarity (correlation) between the signal with itself at varying time intervals. The correlation reduces with time. If the signals at $t+2\delta t$, $t+3\delta t$, $t+4\delta t$ etc. are compared with the signal at t, the correlation of a signal will decrease with time until at some time, effectively $t = \infty$, there will be no correlation. If the particles are large, the signal will be changing slowly and the correlation will persist for a long time. If the particles are small and moving rapidly then correlation will reduce more quickly. The correlator will construct the correlation function $G(\tau)$ of the scattered intensity:

$$G(\tau) = \langle I(t).I(t+\tau) \rangle$$

where:

τ : the time difference (the sample time) of the correlator.

For a large number of monodisperse particles in Brownian motion, the correlation function (G) is an exponential decaying function of the correlator time delay τ:

$$G(\tau) = A[1 + B\ exp(-2\Gamma\tau)]$$

where:

A: the baseline of the correlation function

B: intercept of the correlation function

$\Gamma = D\,q^2$

where:

D: translational diffusion coefficient

$q = (4\pi n/\lambda_o)\,\sin(\theta/2)$

where:

n: refractive index of dispersant

λ_o: wavelength of the laser

θ: scattering angle.

Size is obtained from the correlation function by using various algorithms. The diameter that is obtained by this technique is the diameter of a sphere that has the same translational diffusion coefficient as the particle. The size distribution obtained is a plot of the relative intensity of light scattered by particles in various sizes and is known as an intensity size distribution. 1 mL of the desired sample was poured into a polystyrene cuvette that had been previously blown out with compressed nitrogen. Temperature was set at 20°C.

Small Angle Neutron Scattering

Small Angle Neutron Scattering (SANS) probes structures in materials on the nanometer (10^{-9} m) to micrometer (10^{-6} m) scale. SANS experiments were carried out at the National Institute for Standards and Technology (NIST) Center for Neutron Research (NCNR, Gaithersburg, MD) on the 30 m NG7 beamline. The SANS

intensity, I, was recorded as a function of the magnitude of the scattering vector $q=(4\pi/\lambda)\sin(\theta/2)$, where θ is the scattering angle and λ is the neutron wavelength). The detector angle was set at 2°, and the sample-to-detector distance was set to 2 and 13 m to cover the widest possible range of q (0.001 to 0.45 $Å^{-1}$). Samples were contained in demountable titanium cells with quartz windows that provided a path length of 2 mm. The sample is held in the cell by two quartz windows, and each window was sealed by a viton o-ring. After assembling the cells, liquid samples can be inserted through the top using a syringe. The sample temperature was maintained at 25ºC. The vesicular solutions were prepared in D_2O instead of H_2O using the same protocol as previously described.

Cryogenic Transmission Electron Microscopy

Cryogenic Transmission Electron Microscopy (Cryo-TEM) was performed using a FEI Tecnai TF20 with a 200 kV tungsten filament field emission gun (FEG) fitted with standard side entry cryo-stage and a CCD camera with a 4k x 4k resolution. The microscope, located at the New York Structural Biology Center (NYSBC), was used to obtain images of the surfactant aggregate structures that were created by the binary surfactant systems of catanionic vesicles [2% wt. total surfactant (CTAB/SPFO) at 1:4 wt. ratio]. Cryo-TEM is a very useful technique to validate vesicle microstructure. Phase diagrams of catanionic mixtures has been created by using Electron Microscopy. The samples were prepared on a Quantifoil R2/4 Copper, 200-mesh, holey carbon grids, with 2 μm holes on a 4 μm lattice spacing, which were

purchased from Quantifoil Micro Tools GmbH and were used as received. In order to prepare the sample, a Plexiglas chamber with access openings, was humidified using a water pump until the chamber had a humidity of at least 80%. Placed inside the chamber was a vessel of liquid ethane, which was cooled using liquid nitrogen. A drop of the solution (4 μL) was placed on the grid held 5 tweezers, using a micropipette. The tweezers, with the grid, were then placed in the humidified chamber, in a holder designed specifically to hold the tweezers over the liquid ethane. A strip of filter paper was used to blot the excess fluid from grid. Once all of the excess solution was removed, the grid was immediately plunged into the liquid ethane by stepping on a pedal that activated the plunger holding the tweezers. The freshly frozen sample was placed into a cryogenic holder until it was time to image the sample.

2.3 Results and Discussion

Figure 2.2, shows a typical size distribution of number of particles, volume of particles and intensity of particles vs. diameter, obtained by dynamic light scattering experiments of catanionic vesicles solution [2% wt. total surfactant (CTAB/SPFO) at 1:4 wt. ratio]. The differences we observe in these three (3) size distributions are due to the fact that the measurement is based on intensity and the number and volume curves are obtained from the instrument. For example, if the number distribution was converted into volume, then the measurement would change to a 1:1000 ratio (because the volume of a sphere is equal to $4/3 \cdot \pi \cdot (d/2)^3$). If this was further converted into an intensity distribution, a 1:1000000 ratio would be obtained (because the intensity of scattering is proportional to d^6 from Rayleigh's approximation). The vesicle size distribution was independent of the method of preparation as it is mentioned in the experimental section. Vesicular solutions recovered their size distribution after filtering, sonication, and heat treatment confirming that their size is a thermodynamic equilibrium property of the particular surfactant mixture.[75] Using dynamic light scattering we were able to obtain a hydrodynamic average diameter (based on intensity) of the two surfactant solutions upon mixing and once per day. The hydrodynamic average size of the vesicles was increasing with time (Figure 2.3) and in 14 days reached 93 % of their equilibrium size, which takes approximately three weeks.

Cryogenic electron microscopy (cryo-TEM) is a very useful technique to validate vesicle microstructure. It is not reliable to characterize vesicles without imaging, therefore cryo-TEM paired with small angle neutron scattering (SANS) can actually distinguish between unilamellar vesicles, multilamellar vesicles and discs.[87] Samples of the catanionic vesicles were equilibrated for at least 2 weeks before cryo-TEM or SANS experiments. Equilibration time is necessary for the catanionic vesicles in order to confirm the existence of any vesicle/lamellar phase since lamellar structures develop slowly compared to other phases. In cryo-TEM images (Figure 2.4) catanionic vesicles are shown as dark circular rings (surfactant bilayer) on a uniform brighter background. The inside region of the rings appears a little darker than the background. A zoom of two of the catanionic vesicles in Figure 2.5 shows clearly the dark surfactant bilayer with a brighter outer layer which is an imaging artifact. We also observed the existence of cylindrical shaped vesicles (Figure 2.4, Figure 2.6) with hemispherical ends that had the same curvature as the spherical catanionic vesicles, which indicates that the cylindrical bilayers were composed from the same cationic/anionic surfactant ratio as the corresponded spherical vesicles for the same radius. No double bilayer vesicular phase was observed in any of our samples.

In mixtures of cationic and anionic surfactants, the spontaneous formation of vesicular structures evolves from micelles, which immediately break up to form bilayer discs that slowly grow (minutes to hours) and close to form closed structures such as cylindrical and spherical vesicles.[88,89] Jung et al.,[75] reported the coexistence of spherical unilamellar vesicles with open flat discs and cylindrical bilayer

structures for three different weight ratios (15/85% wt., 20/80% wt. and 25/75% wt.) of CTAB/SPFO solution. Using cryo-TEM images, he showed that as the weight ratio of CTAB increases from 15% to 25%, the population of open flat disks increases, and the population of cylindrical bilayers decreases to an insignificant population for the ratio of CTAB/SPFO 25/75% wt.. The size of the main spherical vesicular structure (mean diameter of 50 ± 5.8 nm, obtained by cryo-TEM images) was practically the same for all three different surfactant weight ratios. The population of the open flat discs was highly monodisperse for all the samples, and their mean length (70 ± 8 nm), was close to the unilamellar spherical vesicles. The cylindrical bilayers had a mean length of 136 ± 36 nm.

Figure 2.7 shows three different size distributions, that we obtained by dynamic light scattering, for the two surfactants (CTAB/SPFO) solution at three different ratios (15/85% wt., 20/80% wt. and 25/75% wt.), under the same total concentration 2% wt. We found that as the weight ratio of CTAB increases from 15% to 25% the size distribution of the (CTAB/SPFO) solution decreases. Since the population of open flat discs is highly monodisperse, and their size is almost in the same range of the unilamellar spherical vesicles, for all three different weight surfactant ratios, the assumption that the open flat discs population cannot affect the overall size distribution at different weight ratios, is fairly valid. On the other hand, the fact that the population of cylindrical bilayers decreases as the weight fraction of CTAB increases from 15% to 25%, explains the different size distributions (Figure 2.7) we obtained for the three different weight ratios. For the ratio of CTAB/SPFO 15/85%

wt., we obtained the largest size distribution because the population of cylindrical bilayers is high. A decreased amount of cylindrical bilayers for CTAB/SPFO 20/80% wt. explains the smaller size distribution, and the absence of cylindrical bilayers for the CTAB/SPFO 25/75% wt. gave us the smallest size distribution. Hence, the average hydrodynamic diameter (58.15 nm) obtained from the CTAB/SPFO 25/75% wt. (in absence of cylindrical bilayers) is the most appropriate, out of the three different CTAB/SPFO weight ratios, to represent the unilamellar spherical vesicular population, and it is in an agreement with the findings of Jung et al.[75] The small size variation of the unilamellar spherical vesicles at the three different surfactant weight ratios is contributed to the enthalpic stabilization mechanism (the unilamellar spherical vesicles are stabilized by a spontaneous curvature and a high effective bending modulus *K*). Any curvature variations, such as size polydispersity or multilamellar phases, are energetically unfavored.

Dynamic light scattering experiments data showed (Figure 2.8) no significant change in size distributions of catanionic vesicles by lowering the pH from neutral (pH=7.7) to acidic (pH=3.3). This is a strong indication that the system does not undergo any phase transition and the unilamellar vesicular population remains constant.

Small angle neutron scattering experiments (SANS) were used to examine the structure of the catanionic vesicles. The solvent (water) of the vesicular solutions was replaced by deuterium oxide due to the significant higher scattering length density of deuterium vs. hydrogen. Plotting the total scattering intensity I(q) corrected for

background intensity as a function of the magnitude of the scattering vector q (using standards provided by NCNR) and then fitting to a scattering polycore model (i.e., in our case there is only one core, which is D_2O), where the vesicles are assumed to have a polydisperse core with a constant shell thickness (vesicle's bilayer), we can back out the dimension of the CTAB/SPFO vesicles, as shown in Figure 2.9.[90] The model indicates the existence of spherical vesicular structures and most importantly the absence of any multilamellar phases. A minimum is observed over the range $0.01<q<0.02$ which is a characteristic for a monodisperse population of spherical vesicles of a mean diameter of 42-48 nm, and is in an agreement with Jung et al.[74] experimental data for the same particular system. The adjustable parameters for the model are the average vesicle radius, vesicle shell thickness, and polydispersity. The model resulted in a vesicle diameter of 40 nm, size polydispersity of 0.21 and the bilayer thickness was 3 nm, which are in remarkable agreement with the size distribution obtained by dynamic light scattering (Figure 2.10, average hydrodynamic diameter of 39.5 nm and size polydispersity of 0.2) for the same sample.

2.4 Conclusion

Catanionic monodisperse equilibrium unilamellar vesicles of CTAB/SPFO were formed in aqueous solutions. It was very important to investigate any co-existence of multilamellar phases and the stability of the vesicular solutions. We confirmed the stability of the vesicular structures in low pH values. Stability in low pH would enable us to use the catanionic vesicles as templates in acidic template synthesis of hollow silica spheres. Weight ratio of the two surfactants seems to have a small effect on their equilibrium size. Cryo-TEM experiments showed monodisperse unilamellar spherical vesicles in the range of 30 to 120 nm. There was no evidence of double or triple bilayer of the two surfactants. Small angle neutron scattering experiments paired with dynamic light scattering experiments confirmed the unilamellar vesicular phase, average size and polydispersity.

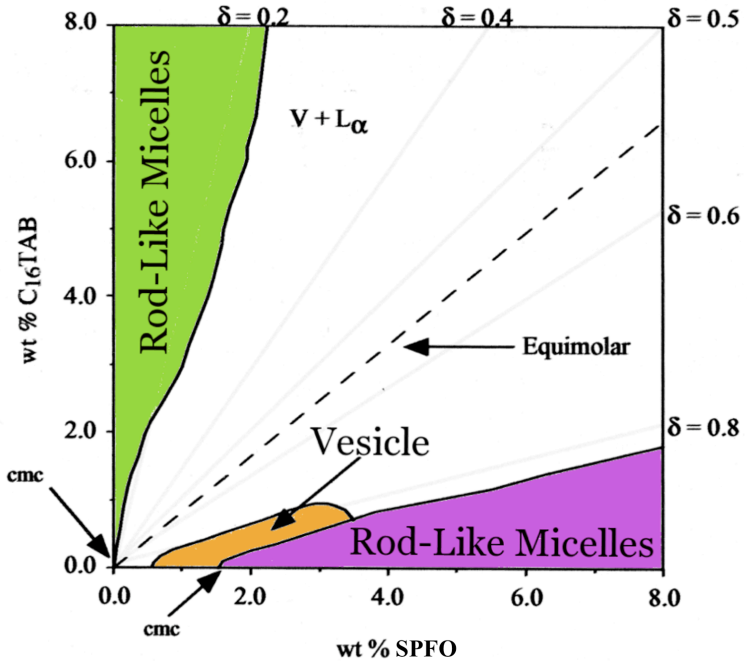

Figure 2.1 Phase diagram of CTAB/SPFO/H_2O at neutral pH and 25°C.[77]

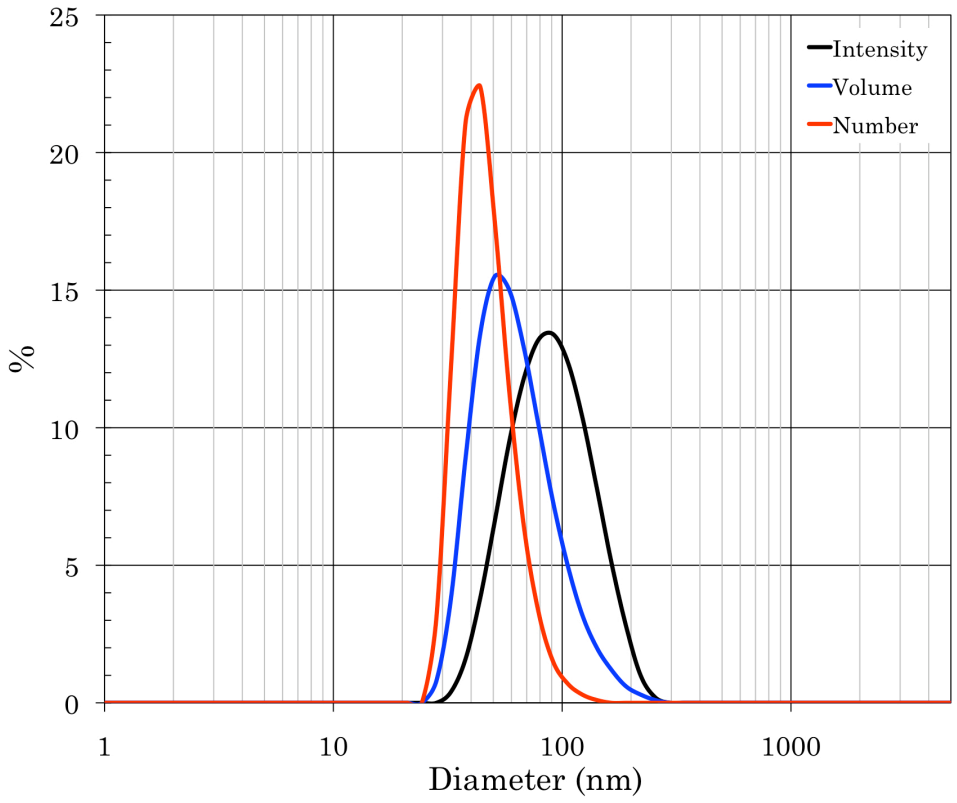

Figure 2.2 Hydrodynamic average diameter vs. % of Intensity, Volume and Number of catanionic vesicles [2% wt. total surfactant (CTAB/SPFO) at 1:4 wt. ratio].

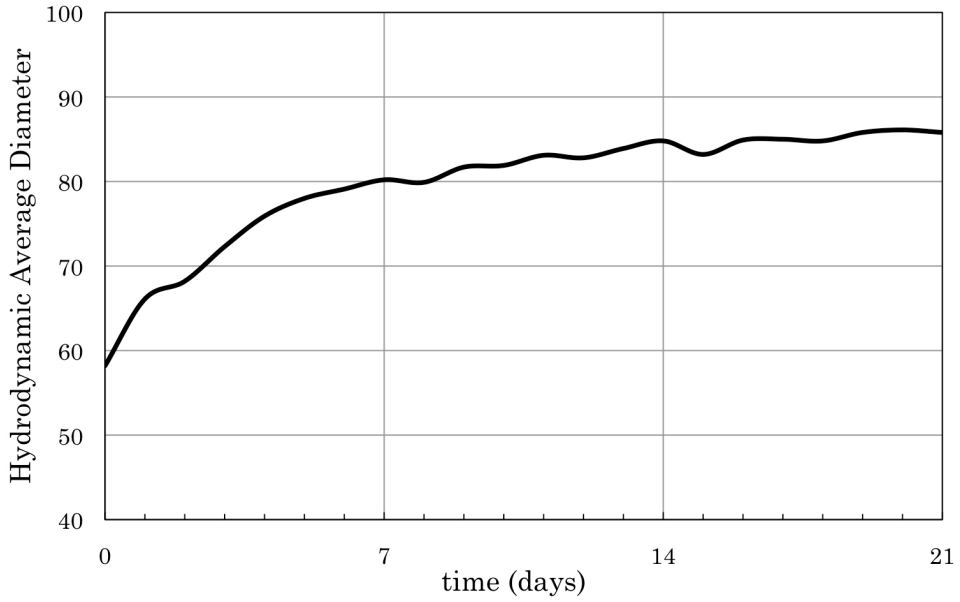

Figure 2.3 Hydrodynamic average diameter (obtained from intensity measurements) of catanionic vesicles [2% wt. total surfactant (CTAB/SPFO) at 1:4 wt. ratio] over the period of 21 days.

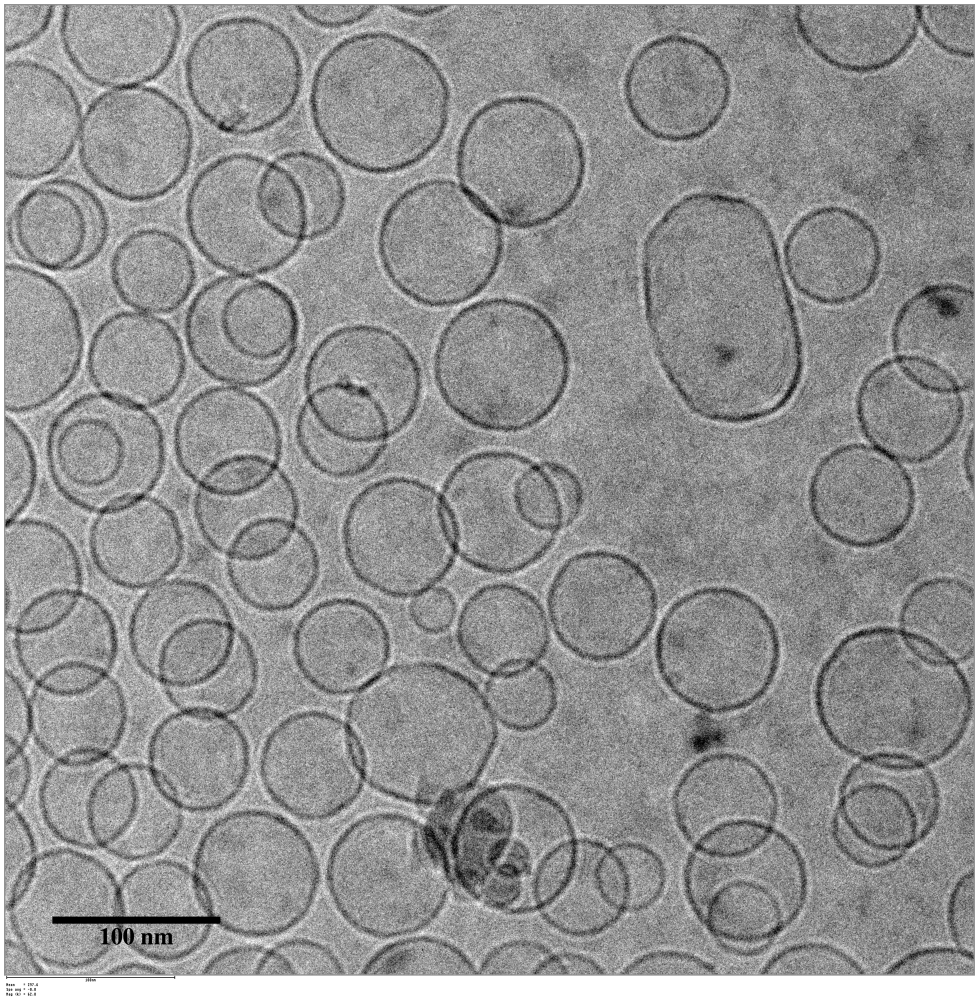

Figure 2.4 Cryo-TEM image of catanionic vesicles [2% wt. total surfactant (CTAB/SPFO) at 1:4 wt. ratio].

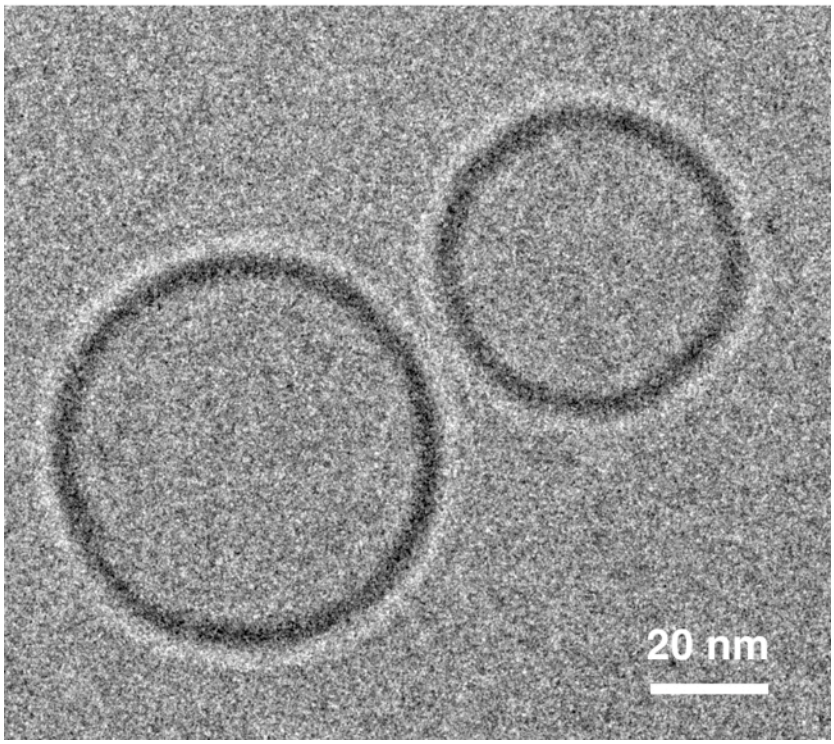

Figure 2.5 Cryo-TEM image of catanionic vesicles [2% wt. total surfactant (CTAB/SPFO) at 1:4 wt. ratio].

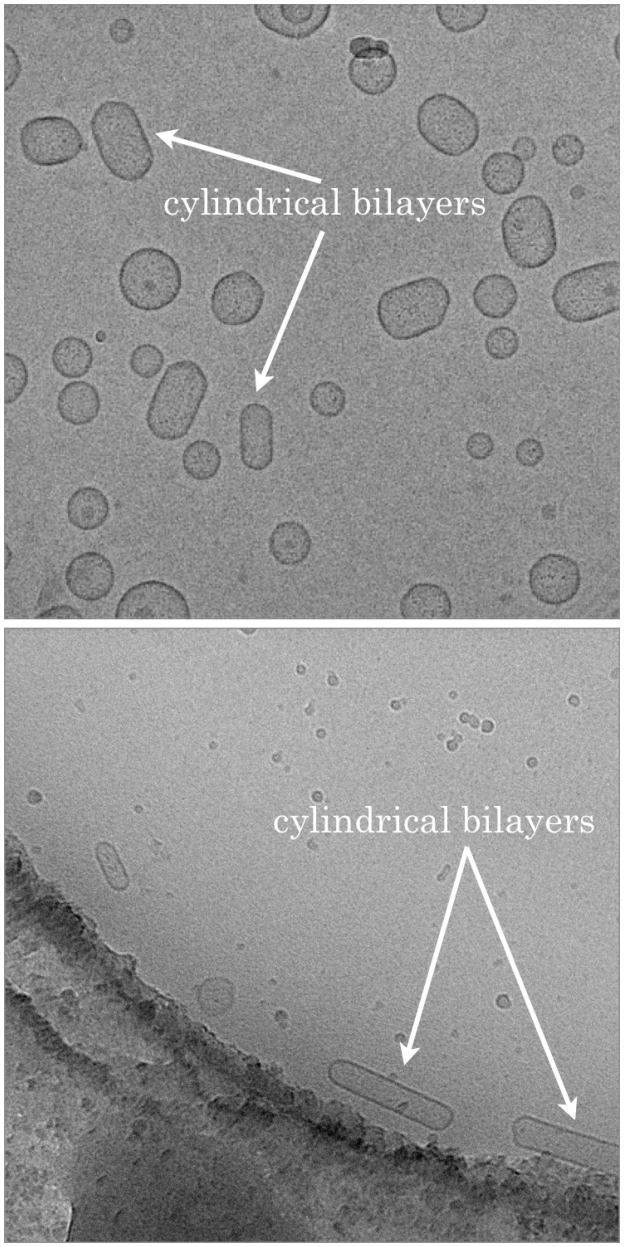

Figure 2.6 Cryo-TEM image of catanionic vesicles [2% wt. total surfactant (CTAB/SPFO) at 1:4 wt. ratio]. Arrows indicate cylindrical bilayers.

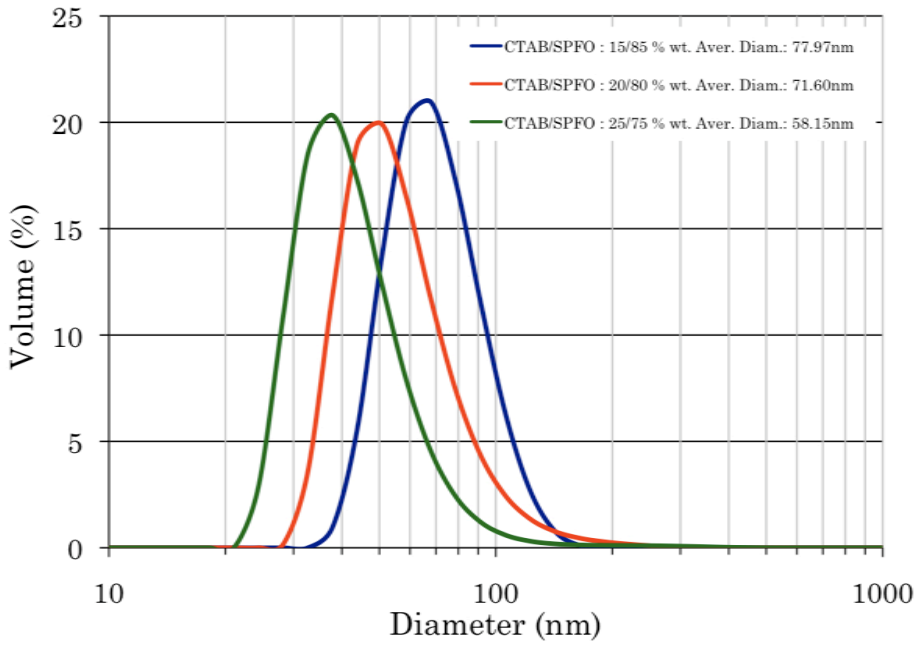

Figure 2.7 Particle size distributions (volume vs. diameter) of catanionic vesicles 2% wt. total surfactant (CTAB/SPFO) at three different weight ratios (15/85% wt. blue, 20/80% wt. red, 25/75% wt. green).

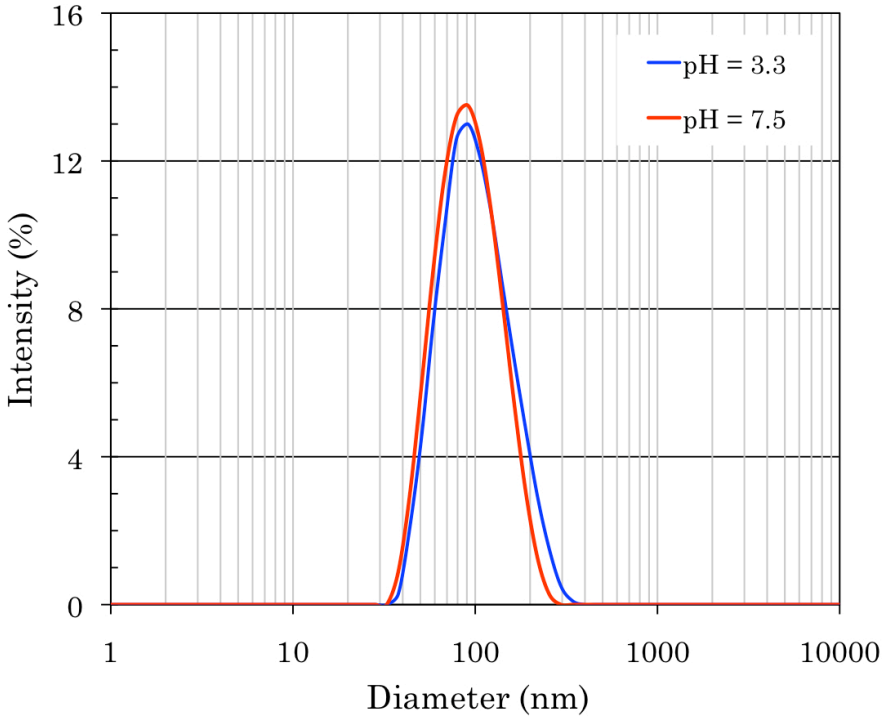

Figure 2.8 Particle size distributions (intensity vs. diameter) of catanionic vesicles [2% wt. total surfactant [(CTAB/SPFO) at 1:4 wt. ratio] at pH=7.5 and pH=3.3.

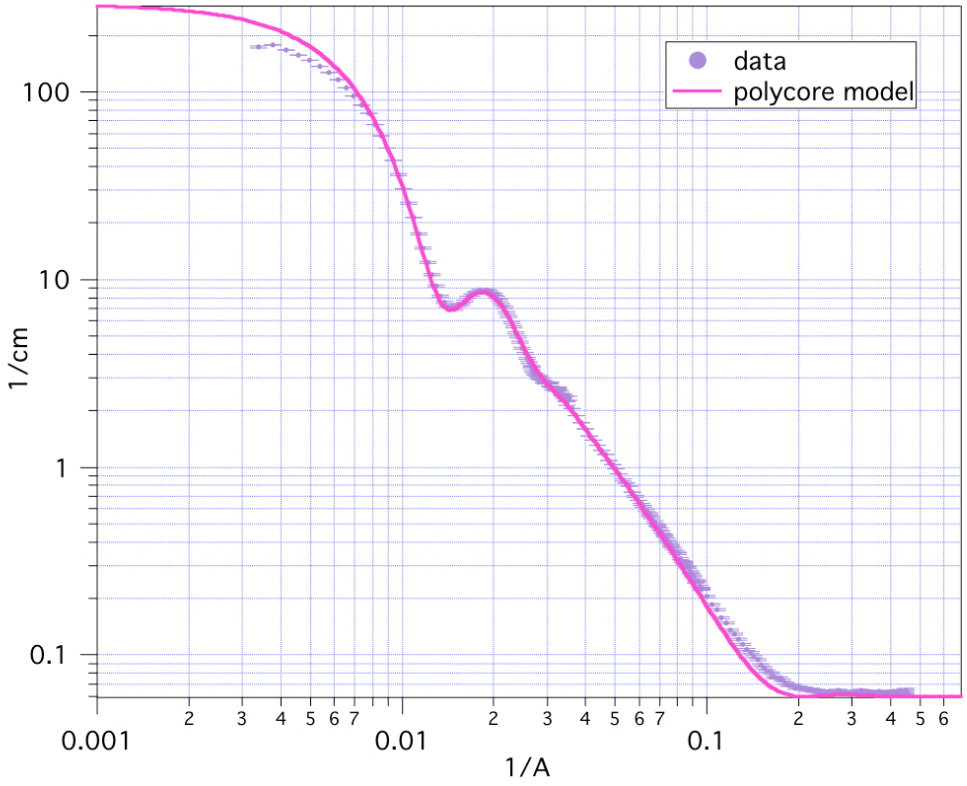

Figure 2.9 Small angle neutron scattering data of I(q)(cm^{-1}) versus q($Å^{-1}$) for catanionic vesicles [2% wt. total surfactant (CTAB/SPFO) at 1:4 wt. ratio]. The solid line corresponds to the polycore model.

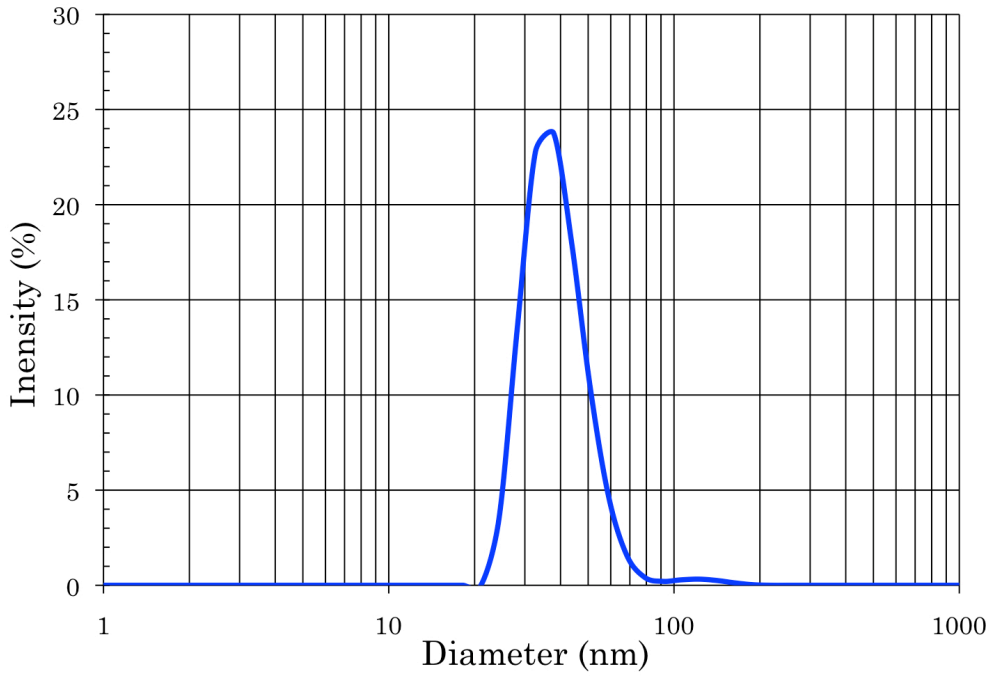

Figure 2.10 Particle size distribution (intensity vs diameter) of catanionic vesicles [2% wt. total surfactant (CTAB/SPFO) at 1:4 wt. ratio] in D_2O with a hydrodynamic average diameter of 39.5 nm.

CHAPTER 3

ORGANOSILANE CHEMISTRY FOR PARTICLE FORMATION

3.1 Introduction

The first preparation of silicon tetrachloride ($SiCl_4$) was reported in 1824.[91] Ebelmen[92] reacted $SiCl_4$ with ethanol to form tetraethoxysilane (TEOS) as early as 1845 (eq.1).

$$SiCl_4 + 4CH_3CH_2OH \rightarrow Si\left(OC_2H_5\right)_4 + 4HCl \qquad (1)$$

Mendeleyev[93,94] observed that hydrolysis of $SiCl_4$ produces a product $Si(OH)_4$ that undergoes condensation reactions to form high molecular weight polysiloxanes. Ebelemen,[95] in 1846, was the first to investigate the reaction of an alcoxysilane. He studied the hydrolysis and condensation of $Si(OC_2H_5)_4$, and observed the existence of oligomers such as hexaethoxydisiloxane and octaethoxytrisiloxane as a function of the added water.

$$Si(OR)_4 \xrightarrow[\text{catalyst}]{H_2O} SiO_2 + 4ROH \qquad (2)$$

He reported that hydrolysis and condensation led to silica gel, and after months of storage at room temperature to solid products (crystalline quartz) of a specific weight of 1.77 g/cm^3. Between 1865 and 1868, Friedel et al.[96-98] reported similar results. Ebelman and Friedel et al. had proved that eq. 2 is an oversimplification of the reactions that take place during the sol-gel process.

Konrad et al.,[99] in 1929, were the first to investigate the role of water in its reactions with alkoxysilanes. They studied the hydrolysis of $Si(OC_2H_5)_4$ with under-stoichiometric water and they noted the important reacting role of water. Water starvation of the system leads to linear types of oligomers and excess of water produces three-dimensional crosslinking. Linear polymerization was supported by Bechtold et al.,[100] and Sakka and Kamiya.[101] Yoldas[102] proposed a spherical network expanding system during the particle growth, with different structural models and different degrees of network complexity. Theoretical analysis about condensation mechanisms and particle growth are given by Weyl[103] in 1951 and Iler[104] in 1979.[105]

According to Iler,[104] condensation takes place in order to maximize the number of Si-O-Si bonds and minimize the number of terminal hydroxyl groups through internal condensation. When the concentration of hydrolyzed species reaches a critical supersaturation value, nucleation occurs. Rings are rapidly formed and monomers are added to form three-dimensional particles, leaving –OH groups on the outside. These particles serve as nuclei for further growth by an Ostwald ripening mechanism where particles grow in size and decrease in number as highly soluble small particles dissolve and re-precipitate on larger less soluble nuclei. Depending on the conditions, (Figure 3.1) particle growth continues to larger sizes especially above pH=7 or, particles aggregate into three-dimensional networks and form a gel at pH<7. Figure 3.2 shows that near the isoelectric point (IEP) (pH=2), where the electrical mobility of the silica particles is zero, gelation time is maximized.[93,104,106,107] At pH≈7 gelation time is minimized, since silica solubility and dissolution rates are

maximized. Above pH=7, the silica particles are adequately ionized so that particle growth occurs without aggregation and the gelation time is significantly large.

3.2 Hydrolysis and Condensation of Alkoxysilanes

Hydrolysis and condensation of alkoxides is one of the most common approaches in producing inorganic powders such as silica, titania and zirconia. Silicate gels can be produced by hydrolysis and condensation of alkoxide precursors with a mineral acid (e.g., HCl) or a base (e.g., NH_3) as a catalyst. The most common tetraalkoxysilanes are tetramethoxysilane $Si(OCH_3)_4$ (TMOS), tetraethoxysilane $Si(OC_2H_5)_4$ (TEOS) and tetra-n-propoxysilane $Si(OC_3H_7)_4$ (TPOS). The sol-gel process can be described by the following three reactions, where R is an alkyl group:

Hydrolysis:

$$Si(OR)_4 + nH_2O \xrightarrow{\text{hydrolysis}} Si(OR)_{4-n}(OH)_n + nROH$$

Alcohol condensation:

$$\equiv Si - OR + HO - Si \equiv \xrightarrow{\text{alcohol condensation}} \equiv Si - O - Si \equiv + ROH$$

Water condensation

$$\equiv Si - OH + HO - Si \equiv \xrightarrow{\text{water condensation}} \equiv Si - O - Si \equiv + H_2O$$

Hydrolysis replaces alkoxide groups and produces alcohol. Condensation reactions produce the silanol groups and alcohol and water as by-products. Due to the hydrophobicity of the tetra-alkoxysilanes, an alcohol is usually used as a co-solvent in order to increase solubility and homogeneity. In fact, gels can be produced without added solvent since alcohol, produced as a by-product of the hydrolysis reaction, can actually homogenize and dissolve the initially phase separated system.

Kolbe[108] first reported the formation of uniform spherical silica particles by reacting tetraethyl silicate in alcoholic solutions with water in basic conditions. Stöber et al.,[109] investigated the experimental conditions necessary to form spherical silica particles by hydrolysis and condensation of tetra-alkoxysilanes using various alcoholic solutions in presence of ammonia as a catalyst. The reaction parameters (ranges of tetra-alkoxysilanes, ammonia and water) were further investigated by Van Helden et al.,[110] Bogush et al.[111] and later by Green et al.[112]

The formation and growth of uniform silica spheres was initially explained using LaMer's[113] model on mechanisms of formation of monodispersed hydrosols. According to LaMer's model, nucleation occurs when the concentration of the dissolved precursor species exceeds a certain critical supersaturation value. When the formation of nuclei decreases the concentration of precursor species under the supersaturation value, nucleation stops and the particles grow by the addition of precursor species (diffusion controlled) onto the particles surface. Monodispersity is achieved because all the particles formed at the same time (rapid nucleation), and grew at the same rate.

Matsoukas and Gulari[114-116] proposed the monomer addition growth model. Particle growth is controlled by the hydrolysis of the monomers, which is the rate-limiting step. Nucleation is a result of condensation of two hydrolyzed monomers. Further growth occurs only by monomer addition since hydrolysis is the rate-limiting step. The monomer addition mechanism is described as either reaction-limited process

(i.e., growth is limited by the condensation of hydrolyzed monomers onto the particle surface) or a diffusion-limited process (i.e., growth is depended on the diffusion of monomers onto the particle surface). The two different growth mechanisms cannot change the particle growth rate because the overall rate is limited by the rate of hydrolysis. However, size polydispersity and particle size are influenced by the differences of the growth mechanisms.

Zukoski and co-workers[117-119] proposed a controlled aggregation mechanism of subparticles of a few nanometers in size that are slowly produced during the entire reaction time. Particle growth occurs from the aggregation of the subparticles. Hydrolysis is not the rate-limiting step in the particle growth, but a step in the condensation process. The proposed mechanism was defined as "controlled", because once the aggregates/particles reach a certain size and therefore a certain colloidal stability due to their surface charge, then growth continues only by aggregation of smaller subparticles with large particles. Polydispersity and particle size are controlled by the size of the subparticles and the particles' surface charge.

Bailey and Mecartney[120] used cryogenic transmission electron microscopy (cryo-TEM) in order to provide direct observation of the growth mechanism in colloidal particle formation from alkoxides. They described the formation of low density particles initially, which undergo a collapse to form colloidally stable small primary particles, and argued that the small particles reported by Zukoski et al., were

artifacts during the sample preparation (i.e., drying process of the solution on the TEM grid).

Van Blaaderen et al.[121] proposed a mechanism that the incorporation of hydrolyzed monomers proceeds through a reaction-limited process but the overall rate of the particle growth is limited by the first-order hydrolysis rate of the alkoxide. The particle formation proceeds through an aggregation process of siloxane substructures (polymeric clusters) that are influenced by the surface potential of the silica particles and the ionic strength of the reaction medium. These siloxane substructures undergo polymerization until they collapse and condense to form dense particles that aggregate in order to form stable silica particles. Colloidal stability is an important factor (in agreement with Zukoski and co-workers) that determines how many particles are formed early in the reaction and at which size aggregation stops. Also, concentrations of ammonia and water influence the particle size based on the stability behavior.

3.2.1 pH Dependence – Acidic Conditions

The mechanism of the hydrolysis reaction of tetraalkoxysilanes has been studied by Aelion et al.,[122] Assink and Kay,[123] Brinker[124] and others.[105] Under acidic conditions, there is a fast protonation of the alkoxy groups (Eq. 2), then a nucleophilic attack of water on the silicon atoms (Eq. 3) and a release of an alcohol.[123,125,126] This an S_N2 reaction involving a pentacoordinate intermediate.

Hydrolysis

$$\mathrm{Si-OR + H^+ \xrightarrow{fast} Si-O^+HR} \quad (3)$$

$$\mathrm{Si-O^+HR + H_2O \xrightarrow{slow} Si-OH + ROH + H^+} \quad (4)$$

Condensation

$$\mathrm{Si-O^+HR + HO-Si \xrightarrow{alcohol\ condensation} Si-O-Si + ROH + H^+} \quad (5)$$

$$\mathrm{Si-OH + HO-Si \xrightarrow{water\ condensation} Si-O-Si + H_2O} \quad (6)$$

The water molecule attacks and acquires a partial positive charge. The positive charge of the protonated alkoxide is reduced, making alcohol a better leaving group. Electron density is reduced from silicon, making it more electrophilic and thus more susceptible to be attacked by water. Overall, in acidic conditions, hydrolysis reactions are fast (Eq. 3, 4) and condensation reactions (Eq. 5, 6) are the rate-limiting steps.

3.2.2 pH Dependence – Basic Conditions

In basic conditions, hydrolysis has been shown to be the rate-limiting step.[93,126] Water dissociates to produce nucleophilic hydroxyl groups in a rapid first step.

Hydrolysis

$$\equiv Si\text{-}OR + OH^- \xrightarrow{slow} \equiv Si\text{-}OH + RO^- \quad (7)$$

$$RO^- + H_2O \xrightarrow{fast} ROH + OH^- \quad (8)$$

Transesterification

$$\equiv Si\text{-}OR + R'OH \xrightarrow{transesterification} \equiv Si\text{-}OR' + ROH \quad (9)$$

Condensation

$$\equiv Si\text{-}OH + OH^- \xrightarrow{deprotonated\ hydrolyzed\ monomer} \equiv Si\text{-}O^- + H_2O \quad (10a)$$

$$\equiv Si\text{-}O^- + \equiv Si\text{-}OR \xrightarrow{alcohol\ condensation} \equiv Si\text{-}O\text{-}Si \equiv + RO^- \quad (10b)$$

$$\equiv Si\text{-}OH + HO\text{-}Si \equiv \xrightarrow{water\ condensation} \equiv Si\text{-}O\text{-}Si \equiv + H_2O \quad (11)$$

Nucleophilic attack of OH^- on alkoxide groups forms an intermediate complex OR^- which, by reacting with water, regenerates OH^- groups and speeds hydrolysis (Eq. 7,8). Transesterification (Eq. 9) occurs when an –OR is exchanged with the solvent alcohol to produce a substitute ligand and alcohol. Condensation consists of the polymerization of hydrolyzed and esterified silica species which involves deprotonated hydrolyzed monomers[127 128] (Eq. 10a, 10b) and the polymerization of hydrolyzed species (Eq. 11).

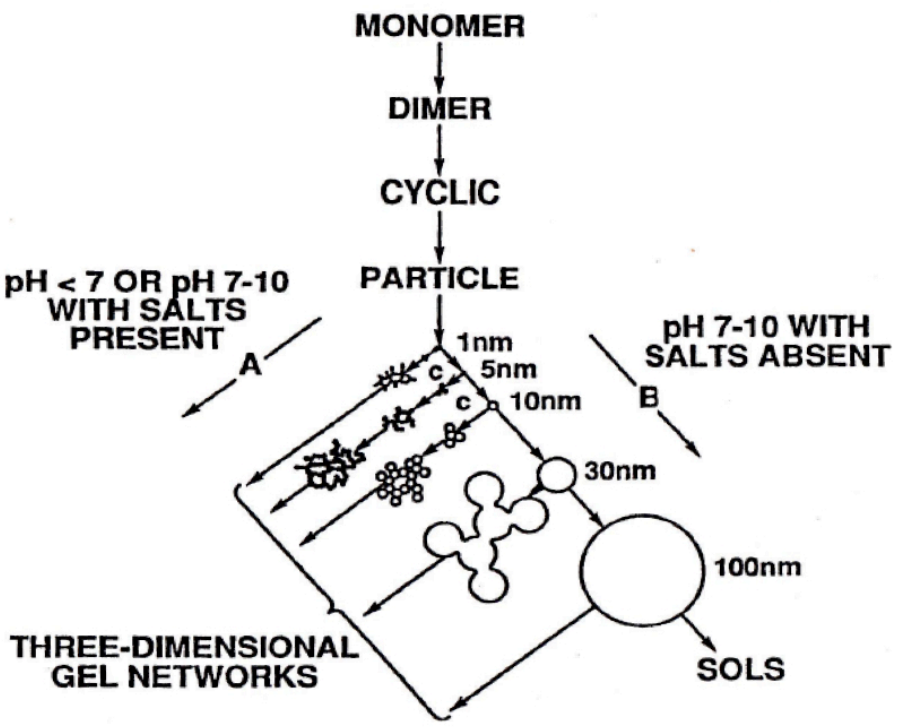

Figure 3.1 Polymerization behavior of aqueous silica. In acidic conditions, or in the present of flocculating salts, particles aggregate into three-dimensional networks and form gels. In basic conditions particles grow in size with decrease in number. From Iler.[104]

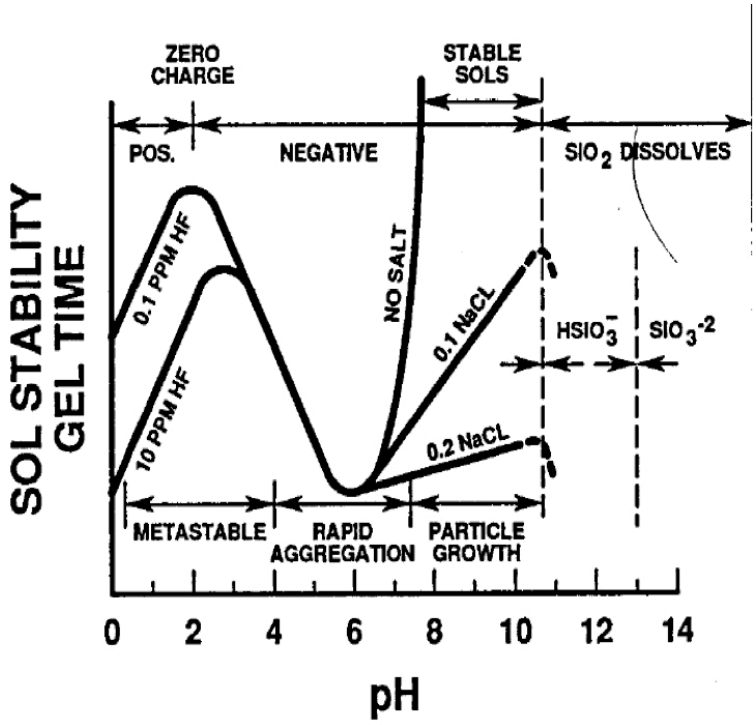

Figure 3.2 Effect of pH in the colloidal silica-water system.[104]

CHAPTER 4

SHELL FORMATION

4.1 Introduction

Templated synthesis of organic-inorganic materials involves a sacrificial template and a synthesis solution. Two main templating strategies have been extensively explored. In the first approach (*morphosynthesis*), inorganic materials synthesis is carried out within the organized organic media (template) and produces complex materials. This is a spatially restricted growth of the inorganic materials, which actually adopt the shape and morphology of the template due to the confinement of the reaction solutions within the template, and the interface between the template and the solution is maintained.[129] In the second approach (*transcriptive synthesis*), templates serve as directing agents in the synthesis solution. The organic template can be self-assembled before or during synthesis. The template's surface is used as a specific site for adsorption and growth of inorganic materials from the synthesis solution leading to coating the template.[129]

In transcriptive synthesis of organic-inorganic materials, the organic template should have an affinity with the inorganic reaction solution (inorganic precursor) in order to direct the adsorption and condensation of the inorganic materials onto its surface, and be stable throughout the material synthesis. Hubert et al.[25] was the first to introduce templated synthesis of hollow silica particles using unilamellar vesicles of dioctadecyldimethylammonium bromide (DODAB) cationic surfactant as a template, and tetramethoxysilane (TMOS) and tetraethoxysilane (TEOS) as the inorganic silica precursors. His motivation was to successfully coat the unilamellar

DODAB vesicles with silica in an aqueous solution, since these template structures are sensitive to alcoholic solvents, pH, and ionic strength. It was reported that the morphology of the silica-coated vesicles was dependent on the precursor used to form the silica coating. The authors suggested that the deformations in the case of TEOS were caused by either the different alcohols that were produced from the hydrolysis and condensation of the two different silica precursors, or by the mechanical stresses exerted by the condensation of the silica network onto the surface of the template.

The hydrolysis reaction of alkoxysilanes has a direct influence on the templating synthesis. Silica precursors, such as tetramethoxysilane (TMOS), tetraethoxysilane (TEOS), tetra-n-propoxysilane (TPOS), and tetra-n-butoxysilane (TBOS), have significantly different rates of hydrolysis, which decrease dramatically with the chain length of the alkoxide group. For example, TMOS hydrolysis is complete within minutes, whereas TEOS hydrolysis exceeds several hours. During hydrolysis, the release of alcohols for different type of alkoxides occurs at a different time scale and the alcohols can behave as co-solvents or co-surfactants (for long-chain alcohols).

In addition, long time scales of hydrolysis result in an increased time of available non-hydrolyzed species of alkoxides, that could be directed into the bilayer due to their hydrophobicity, thus reducing the integrity of the template. Also, fast hydrolysis (e.g., TMOS) has the advantage of the rapid availability of a relatively large amount of hydrolyzed species within a short period of time. The concentration of hydrolyzed alkoxide species in the bulk reaches a maximum rapidly and

simultaneously adsorbs and condenses onto the template's surface. On the other hand, slow hydrolysis translates to the presence of less hydrolyzed silica species in the solution over time, and a slow templating synthesis with non-uniform growth. In the case of a vesicular template, a low rate of hydrolysis in the beginning of the process would result in successfully coating a fraction of the vesicles. Consequently, this would eventually drop the effective concentration of the surfactant in the solution to a lower value of the critical aggregate concentration of the vesicular system, and a phase transition of the vesicles will occur.

Catanionic vesicles of mixtures of fluorocarbon and hydrocarbon chains are excellent candidates for templating synthesis due to the high rigidity of the bilayer (as described in Chapter 2), their highly monodisperse vesicular populations, and the distinct properties of the fluorocarbon surfactant. The hydrophobic and oleophobic properties of a fluorinated chain reduce the permeability of non-hydrolyzed hydrophobic silica precursors into the bilayer ensuring the transcriptive synthesis mechanism of material adsorption and structuring.

4.2 Experimental Section

4.2.1 Materials

Sodium Perfluorooctanoate (SPFO, Alfa Aesar 97%), Cetyltrimethylammonium Bromide (CTAB, Alfa Aesar 98%), Tetramethoxysilane (TMOS, Spectrum 97%, Alfa Aesar 98%), Tetraethoxysilane (TEOS, Alfa Aesar 99+%) Tetra-n-propoxysilane (TPOS, Alfa Aesar 97%), Tetra-n-butoxysilane (TBOS, Alfa Aesar 97%), Nochromix and sulfuric acid (98%) were purchased from Fischer Scientific, amidine and carboxyl/sulfate polystyrene latex spheres were purchased from Invitrogen Corporation and one side polished (n type, <100>) single-crystal silicon wafers were purchased from Montco Silicon Technologies Ltd. All chemicals were used as received.

4.2.2 Solution Preparation – Protocols

Vesicular solution of (2% wt. total surfactant CTAB/SPFO, at 1:4 wt. ratio) was prepared as described in Chapter 2.2.2. The pH of the vesicular solution was adjusted within the range of 3.0-3.5, with HCl drop wise, and the solution was filtered (Nylon filter, 450 nm pore size, Whatman). Then the silica precursor (TMOS) was added to the vesicular solution (10 mL) and was stirred for 5-10 min in order to obtain a single phase. TMOS concentration was chosen in the range of 50-100 mM. After the initial 5-10 min of the reaction, the stirring was stopped. The solutions

were monitored by dynamic light scattering (DLS) and were kept at room temperature without stirring.

4.2.3 Methods

Atomic Force Microscopy

Contact mode Atomic Force Microscopy (AFM) operates by scanning a tip attached to the end of a cantilever across the sample surface while monitoring the change in cantilever deflection with a split photodiode detector. A feedback loop maintains a constant deflection between the cantilever and the sample by vertically moving the scanner at each (x, y) data point to maintain a "setpoint" deflection (Figure 4.1). By maintaining a constant cantilever deflection, the force between the tip and the sample remains constant. The force is calculated from Hooke's Law:

$$F = -k\,x$$

where:

F = Force

k = spring constant

x = cantilever deflection.

Force constants usually range from 0.01 to 1.0 N/m, resulting in forces ranging from nN to μN in an ambient atmosphere. The distance the scanner moves vertically at

each (x, y) data point is stored by the computer to form the topographic image of the sample surface. Operation can take place in both ambient and liquid environments. A drop of the hollow silica spheres solution was placed on a polished silicon wafer and was air dried. The polished silicon wafers (with a roughness of ~1 Å as measured by AFM) were cleaned by sonicating in a mixture of Nochromix and 98% sulfuric acid for about 30 min, followed by successive water rinsing. The cleaned substrates were stored under water at room temperature and dried in a stream of dry nitrogen just before use.

Transmission Electron Microscopy

Transmission electron microscopy (TEM) is a technique whereby a beam of electrons is transmitted through an ultra thin specimen and interacts with the specimen as it passes through. An image is formed from the interaction of the electrons transmitted through the specimen and is either magnified and focused onto an imaging device (such as a fluorescent screen) on a layer of photographic film, or detected by a sensor such as a CCD camera. Transmission electron microscopy (TEM) images were obtained by using the Zeiss EM 902, operating at 80kV with a line resolution of 0.34 nm and a point resolution of 0.5 nm. We also employed a negative staining procedure with uranyl acetate solution (4% wt.). 6 μL drops of hollow silica spheres solution were placed on copper coated grids. A strip of filter paper was used to blot the excess fluid from the grid and the grid was air-dried.

Scanning Transmission Electron Microscopy

Scanning Transmission Electron Microscopy (STEM) was performed using a Zeiss Supra 55VP (A thermal field emission type SEM with a maximum resolution of 1 nm). A scanning transmission electron microscope (STEM) is a type of transmission electron microscope (TEM). The electrons pass through a sufficiently thin specimen. However, STEM is distinguished from conventional transmission electron microscopes (TEM) by focusing the electron beam into a narrow spot, which is scanned over the sample in a raster. The rastering of the beam across the sample makes these microscopes suitable for analysis techniques such as mapping by energy dispersive X-ray (EDXS) spectroscopy. Samples were prepared as in transmission electron microscopy, however, the samples were not negatively stained.

4.3 Results and Discussion

Hollow silica spheres (silica shells) were synthesized by acidic hydrolysis and cross-linking of an inorganic alkoxide precursor (tetramethoxysilane, TMOS)[130,131] onto the surface of unilamellar catanionic vesicles consisting of Cetyltrimethylammonium Bromide (CTAB) and Sodium Perfluorooctanoate (SPFO). In the acidic conditions that the shells are formed, the negatively charged silicate species are attracted to the positively charged CTAB component of the vesicles. The templates (2% wt. total surfactant CTAB/SPFO, at 1:4 wt. ratio) were equilibrated for a minimum of 14 days.

Transmission electron microscopy images, in Figure 4.1, revealed the hollow structure of the vesicle templated spheres, Their size ranged from 30 to 120 nm. The TMOS concentration was chosen at 0.1 M. As shown in Figure 4.2 and Figure 4.3 it can be found that the particles have a hollow spherical morphology and a uniform silica shell thickness of 9.37 nm. Vesicle templated hollow spheres were further characterized with atomic force microscopy (Figure 4.4), which showed silica particles with sharp-edged morphologies.

Using dynamic light scattering, we monitored the hydrodynamic average diameter (based on intensity) of the vesicle templated hollow silica spheres over time (Figure 4.5). The first point of data, for t=0, corresponds to the hydrodynamic average diameter of the template (2% wt. total surfactant CTAB/SPFO, at 1:4 wt. ratio) before the initiation of the reaction of TMOS (0.1 mM) which was 84 nm. The

hydrolysis and condensation of TMOS took place in acidic conditions (pH=3.00). Dynamic light scattering measurements of silica hollow spheres started 20 min after the initiation of the reaction. We observed an increase of 12 nm of the diameter of the hollow silica spheres and their size (96 nm) remained constant for the first 6 hours of the reaction. A small shrinkage was observed from 6-12 hours due to condensation reactions of adsorbed TMOS onto the surface of the vesicles. Their size was constant for the remaining time of the reaction, up to 17 hours. We did not observe any significant second (smaller size) population of particles, which confirmed that gelation time in acidic conditions is maximized, but did not preclude the presence of fractal-shaped polymerized oligomers of TMOS and TMOS/surfactant. Also, more importantly, the absence of any larger size particles in the duration of the reaction (17 hours) ruled out any possible agglomeration phenomena between the hollow silica spheres. The colloidal solution of hollow silica spheres remained stable for 17 hours at a pH=3 close to the isoelectric point of silica (pH≈2) when the silica surfaces expected to have a minimum charge.

Complete hydrolysis and condensation of TMOS would produce stoichiometrically four times the amount (molar) of methanol (eq. 2, Chapter 3). Methanol can significantly perturb the phase behavior of the vesicular template during synthesis. Integrity of the template is essential in transcriptive synthesis. Solutions of catanionic vesicles (2% wt. total surfactant CTAB/SPFO, at 1:4 wt. ratio) were prepared in water with added methanol as a co-solvent at concentrations of 0.5, 1, 5, 10 and 15% vol.. Figure 4.6 shows CTAB/SPFO vesicles with size distributions

obtained with dynamic light scattering (Intensity vs. Diameter) for the above five concentrations. The size of the CTAB/SPFO vesicles increases slightly for the solutions with concentrations of 0.5, 1, 5% vol. methanol. Their size monodispersity remains practically the same (Figure 4.7), which indicates that the phase of the CTAB/SPFO mixture remains vesicular. The size distributions of the solutions with concentrations of 10% and 15% vol. of methanol show a dramatic increase in size with a secondary intensity peak at 2500 nm (same for both size distributions). Polydispersity index for the solutions of 10% and 15% vol. of methanol increases 20% and 50% respectively. These results suggest a phase transition of the CTAB/SPFO mixture that contains vesicular and lamellar phases. When the catanionic vesicular solution was used for templated synthesis of hollow silica spheres, the TMOS concentration was chosen at 0.1 M, which if it would be fully hydrolyzed and condensed would release methanol up to 0.4 M concentration or 1.6% vol., a level that cannot alternate the phase of the vesicular solution as it was shown experimentally above.

The vesicle templated synthesis of hollow silica spheres, as a reverse-casting, transcriptive synthesis, uses the vesicles surface for silica adsorption and structuring. Solutions of catanionic vesicles (2% wt. total surfactant CTAB/SPFO, at 1:4 wt. ratio) have a main spherical vesicular population in co-existence with cylindrical and disc shaped bilayers (Chapter 2, §2.3). Scanning electron micrograph of vesicle templated hollow spheres (Figure 4.8) shows intact hollow silica spheres and hollow silica spheres with a thin-ruptured silica shell. Transmission electron

migrograph (Figure 4.9) captured the petrified disc-shaped vesicular template and scanning electron micrograph (Figure 4.10) shows the half of a cylindrical shaped silica shell templated from cylindrical CTAB/SPFO bilayers. The above electron microscopy observations of encapsulated spherical disc-shaped and cylindrical CTAB/SPFO bilayers confirm the high rigidity of the bilayer and that the vesicular template did not undergo any phase transition during the template synthesis. Energy dispersive X-ray spectroscopy (EDXS) (shown in Figure 4.11) performed on a hollow spherical silica particle, indicates that the particle consist of silica, but also exhibits a fluorine peak confirming the existence of the trapped fluorocarbon surfactant (SPFO) due to the template's presence in the hollow interior.

Solutions of catanionic vesicles of 2% wt. total surfactant CTAB/SPFO concentration and 1:4 wt. ratio, have a molar ratio of CTAB/SPFO 23/77%. Non-ideal mixing of CTAB and SPFO in the vesicles bilayers (Chapter 2, §2.1) leads to a different molar ratio of the two surfactants in the two layers of the bilayer. The bulkier CTAB head group and the tendency of CTAB to form high curvature rod-like micelles indicates the existence of a higher CTAB/SPFO molar ratio in the outer layer of the bilayer than 23/77% (Figure 4.12). The affinity of the positively charged trimethyl-ammonium group of CTAB for the hydrolyzed TMOS monomers was investigated by using a solid template such as polystyrene latex, with a similar size (diameter of 90 nm) as the vesicular templates, and a positive charge due to their functionalization with amidine groups. Amidine functionalized polystyrene spherical particles are shown in scanning electron and transition electron micrographs in Figure 4.13. The

area per amidine group was 3.1 nm^2 and there were 8,200 charge groups per particle. Therefore, the charged surface coverage was 25% for a spherical polystyrene particle with a diameter of 90 nm, which is almost identical to the CTAB group surface coverage for CTAB/SPFO vesicles. The polystyrene templated hollow silica particles were obtained using the same concentrations and reaction conditions as the vesicle templated ones and they exhibit a higher surface roughness as shown in Figure 4.14. A comparison of their size distributions (obtained with scanning electron micrographs) before and after the templated synthesis (Figure 4.15) reveals a thin silica coating with a thickness of 3.5 nm. A broken detached shell in Figure 4.16 shows the smoother polystyrene surface compared to the silica coating and a silica thickness of 7 nm. Figure 4.17 shows the adsorption pattern of the hydrolyzed species of TMOS onto the polystyrene amidine functionalized surface, as the particle seemed to be partially coated with silica before further adsorption and condensation of silica would fully cover the templates' surface. The smallest island of adsorbed silica on the surface of the particle had an area of 3.66 nm^2, which is in a remarkable agreement with the specifications of the amidine polystyrene particles as the area per amidine group was 3.1 nm^2. The polystyrene core was removed by treatment with tetrahydrofuran (THF), and Figure 4.18 shows the hollow structure of amidine functionalized polystyrene templated hollow silica spheres. Negative functionalized (carboxyl-sulfate) polystyrene spherical particles of the same size (90 nm) were used to investigate the effect of the negative charged carboxyl-sulfate groups in the templated silica synthesis. Using identical reaction conditions, silica coated particles were not observed. Figure 4.19 shows a carboxyl-sulfate polystyrene particle with no

roughness, as in the case of the amidine functionalized particles that indicates no presence of silica. Energy dispersive X-ray spectroscopy (EDXS) (shown in Figure 4.20) performed on three carboxyl-sulfate polystyrene particle generated spectra with no existence of silica.

As the adsorbed silicate species increase their surface coverage locally on the vesicle surface, condensation of the silicate species occurs. This reaction is in direct competition with the condensation of the silicates that takes place in the bulk solution forming long silicate chains that leads to gelation, which compromises our ability to recover separated clean discreet particles. Even though the gelation time of TMOS in pure water under acidic conditions (pH=3) is very large, there is a factor in our system that significantly minimizes the gelation time: as this vesicular phase is a component of the thermodynamic phase diagram of the mixture, these vesicles are in coexistence with free monomeric surfactant molecules of CTAB and SPFO. CTAB free monomeric molecules act as nucleation sites for hydrolyzed TMOS monomers and oligomers and promote nucleation and polymerization in the bulk. More specifically, for pH=3 (Figure 4.21), size distributions of the template (CTAB/SPFO vesicles) obtained by dynamic light scattering, and the templated hollow silica spheres show a uniform increase in their diameter with a silica shell thickness of 8-12 nm and not a significant difference in polydispersity. Figure 4.22 shows a similar behavior for the same reaction system in pH=4. But in Figure 4.23, and for pH=5.05, we observed a large increase of the size of the particles and polydispersity which indicates non-uniform silica adsorption and particle agglomeration. Size

distributions for higher pH such as pH=5.75 (Figure 4.24) show three different peaks at 100, 500, 2000 nm that suggest gel-formation. Transmission electron micrographs for the pH=5.75 sample, (Figure 4.25), confirmed a gel-formation that with time, trapped and caged the hollow silica particles that formed initially in the reaction.

Vesicle templated silica syntheses were attempted by using different alkoxysilanes such as tetraethoxysilane (TEOS), tetra-n-propoxysilane (TPOS) and tetra-n-butoxysilane (TBOS). In the case of TEOS we observed very few hollow silica templated particles (Figure 4.26) and the majority of the characterized sample consisted of triangular shaped silica solid particles. The same phenomena were observed for the TPOS sample (Figure 4.27). In the case of TBOS, the solution exceeded 24 hours in order to achieve a single phase and precipitation occurred. The longer hydrolysis rate for TPOS, TBOS, and the produced alcohols due to their hydrolysis and condensation reactions directly affect the vesicular phase of the catanionic vesicles of CTAB/SPFO and the integrity of the template. TEOS seems to have the same influence during the templated synthesis with an exemption of the existence of a few hollow structures.

4.4 Conclusion

Catanionic vesicle templated hollow silica spheres were synthesized, using tetramethoxysilane as the silica precursor in acidic conditions. The templated synthesis produced hollow silica spheres in co-existence with a smaller population of cylindrical and disc-shaped shaped hollow particles, which confirms a transcriptive synthesis as the templating mechanism. Energy dispersive X-ray spectroscopy (EDXS) technique was used to characterize the silica particles and confirmed the presence of fluorine due to the trapped fluorocarbon surfactant (SPFO) in the interior of the hollow silica spheres. The hollow silica particles solution was colloidally stable for at least 18 hours after the initiation of the reaction, maintaining a single particle size distribution and a relatively constant hydrodynamic average diameter. Methanol produced from the hydrolysis and condensation reactions of TMOS did not have any influence to the integrity and rigidity of the vesicular template. The transcriptive synthesis was successful in a pH range of 3-5, with increasing size polydispersity as pH increased, but for higher pH values samples exhibited gel-formation and hollow particles were trapped into the silica gel. The template's surface functionality – charge influenced the adsorption and condensation of the hydrolyzed silica precursor's species. A positively charged, (amidine functionalized polystyrene), template directed the adsorption and condensation of hydrolyzed TMOS species onto the template's surface and formed hollow silica spheres, whereas a negatively charged, (carboxyl-sulfate functionalized polystyrene), template did not exhibit any specificity for hydrolyzed silica species in the reaction solution and did

not produce any hollow silica particles. Catanionic vesicle template synthesis of silica hollow spheres with TEOS, TPOS and TBOS was unsuccessful, resulting in non-spherical solid silica particles.

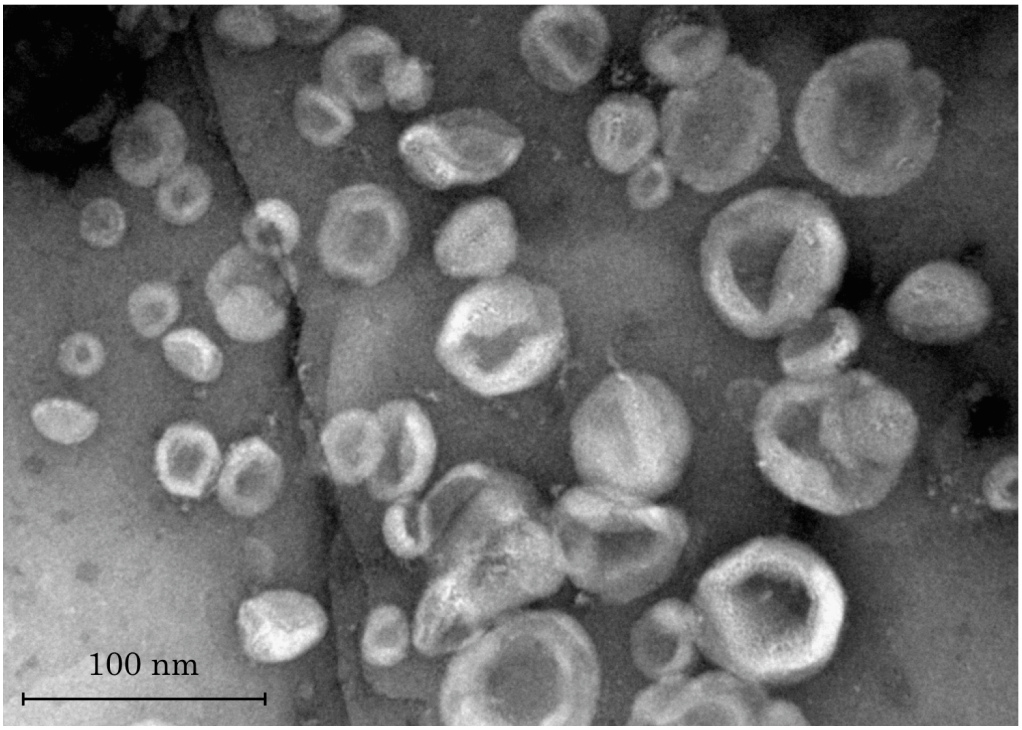

Figure 4.1 Transmission electron micrograph of vesicle templated hollow silica spheres.

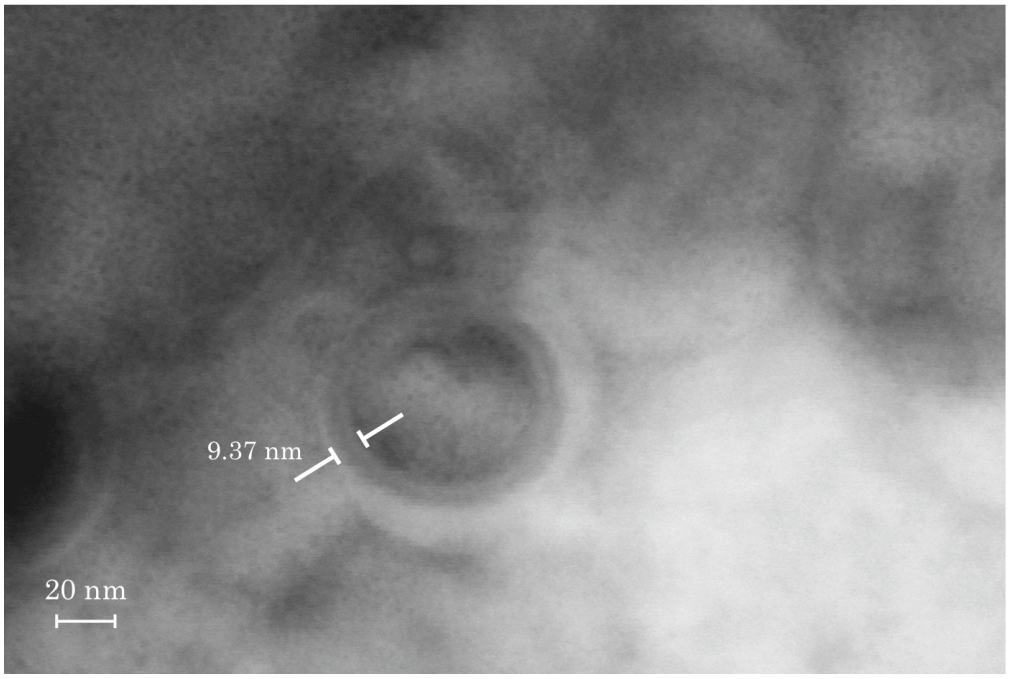

Figure 4.2 Scanning transmission electron micrograph of a vesicle templated hollow silica sphere with a silica shell thickness of 9.37 nm.

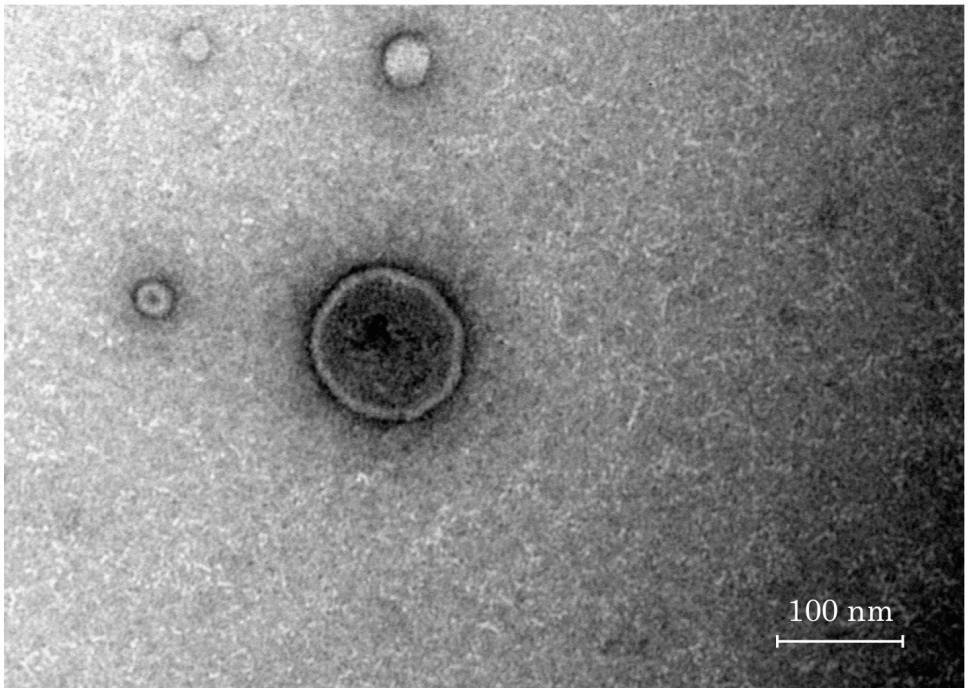

Figure 4.3 Transmission electron micrograph of a vesicle templated hollow silica sphere with a diameter of 110 nm. The sample was negatively stained with uranyl acetate solution (4% wt.).

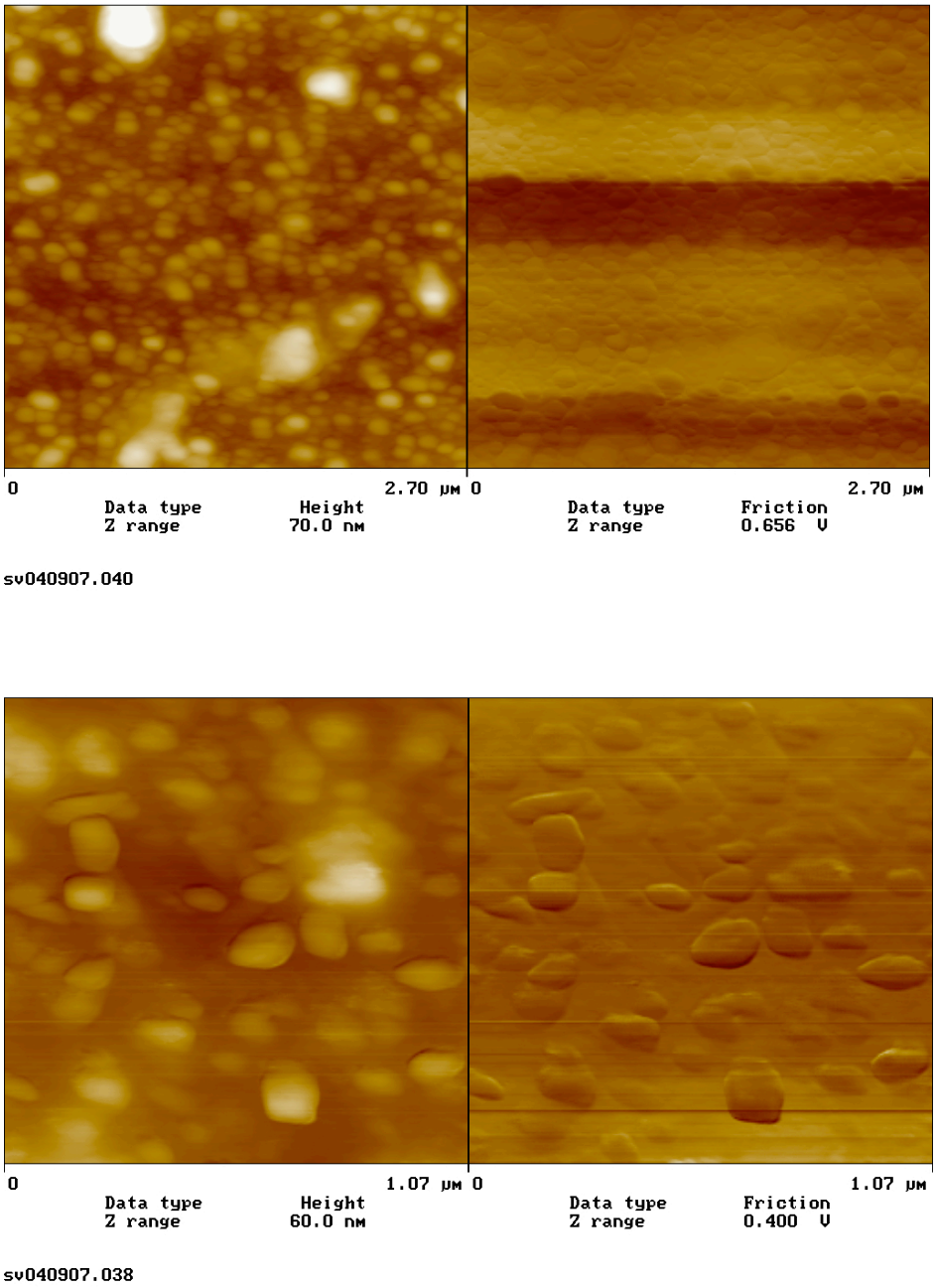

Figure 4.4 Atomic force micrographs of vesicle templated silica spheres.

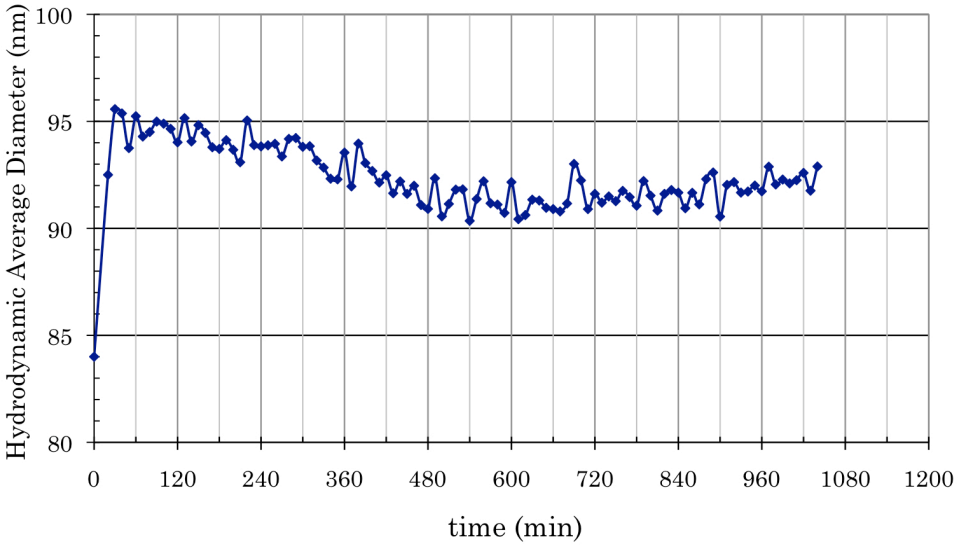

Figure 4.5 Hydrodynamic average diameter of vesicle templated silica hollow particles, obtained by dynamic light scattering, vs. time. The first point of data, for t = 0, corresponds to the hydrodynamic average diameter of the template (2% wt. total surfactant CTAB/SPFO, at 1:4 wt. ratio) before the initiation of the reaction of TMOS.

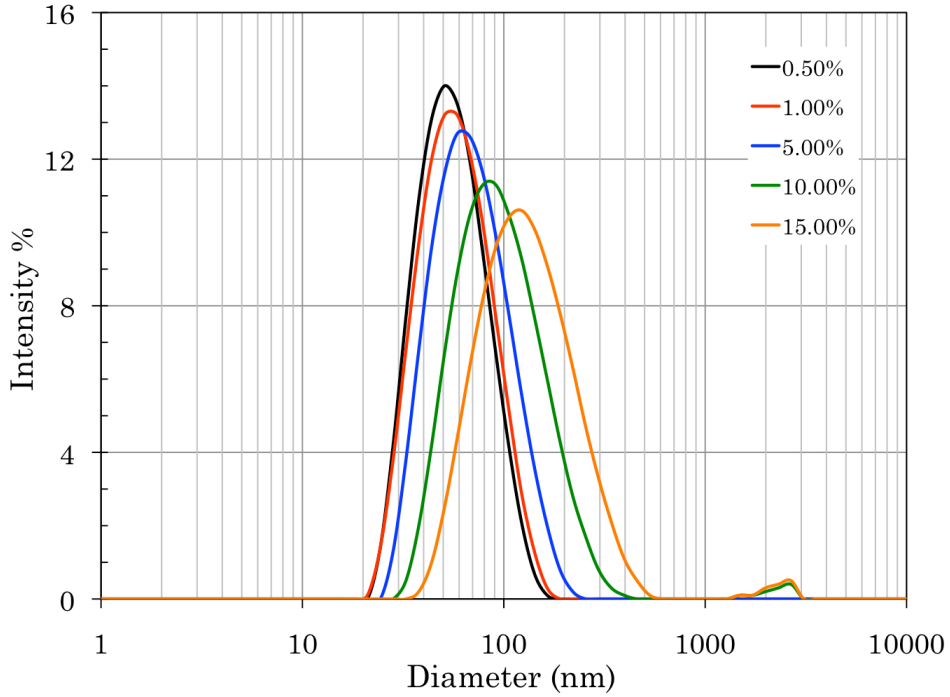

Figure 4.6 Dynamic light scattering data (Intensity vs. Diameter) of catanionic vesicles (2% wt. total surfactant CTAB/SPFO, at 1:4 wt. ratio) in H_2O with 0.5, 1, 5, 10, 15% vol. methanol.

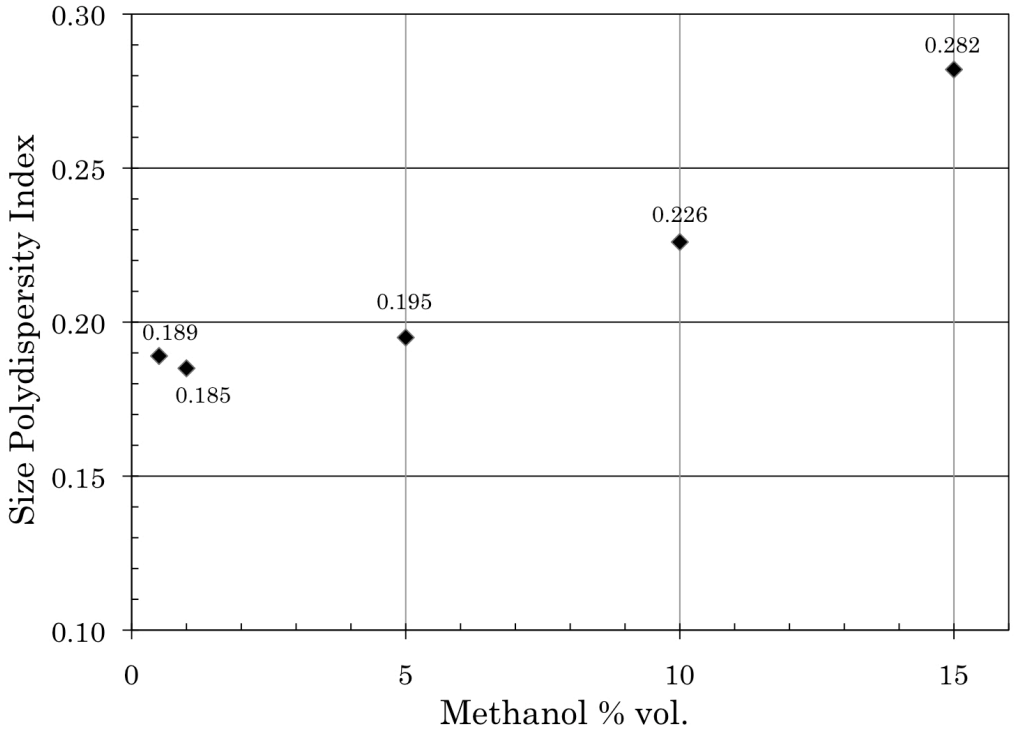

Figure 4.7 Size polydispersity index vs. methanol % vol., obtained with dynamic light scattering, of catanionic vesicles (2% wt. total surfactant CTAB/SPFO, at 1:4 wt. ratio) in H_2O with 0.5, 1, 5, 10, 15% vol. methanol.

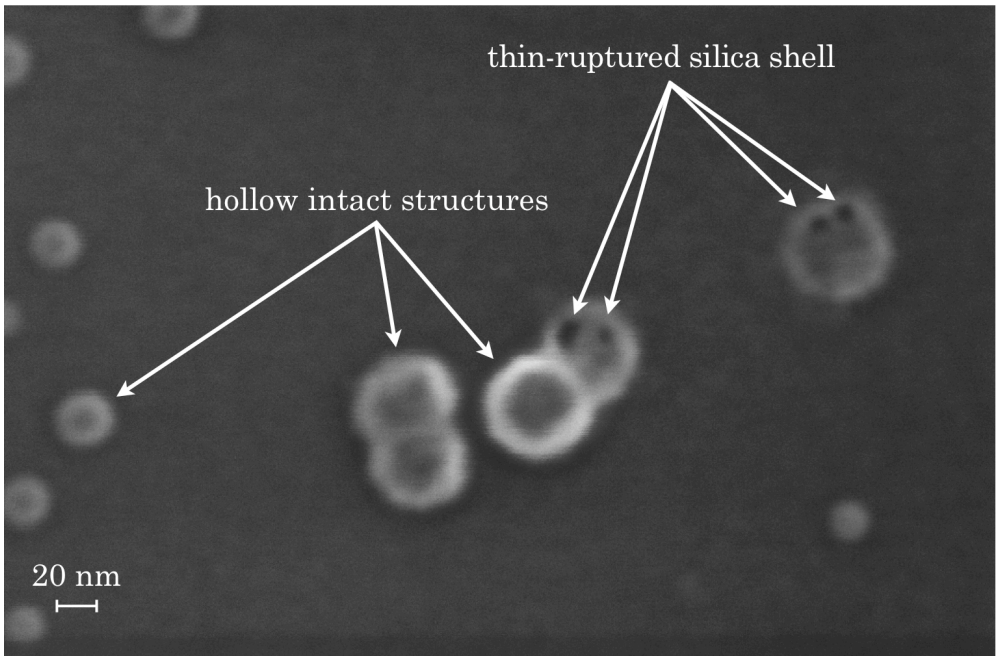

Figure 4.8 Scanning electron micrograph of hollow silica spheres. White arrows indicate hollow intact structures and ruptured (dark holes), due to their extreme thin shells.

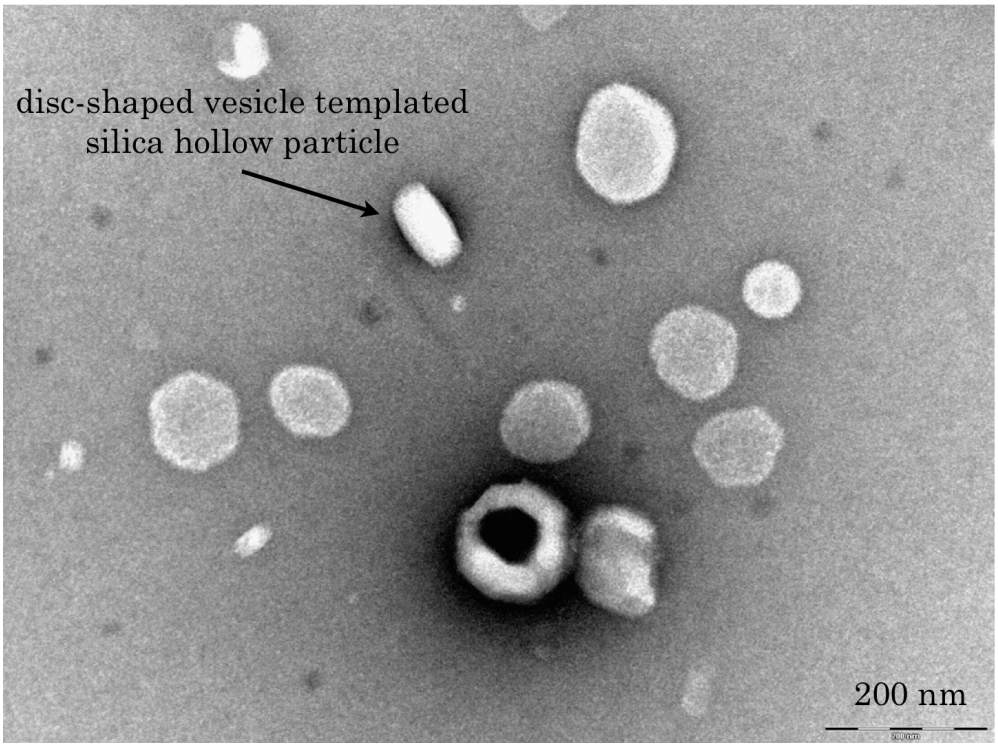

Figure 4.9 Transmission electron micrograph of a disk-shaped vesicle templated hollow silica particle. The sample was negatively stained with uranyl acetate solution (4% wt.).

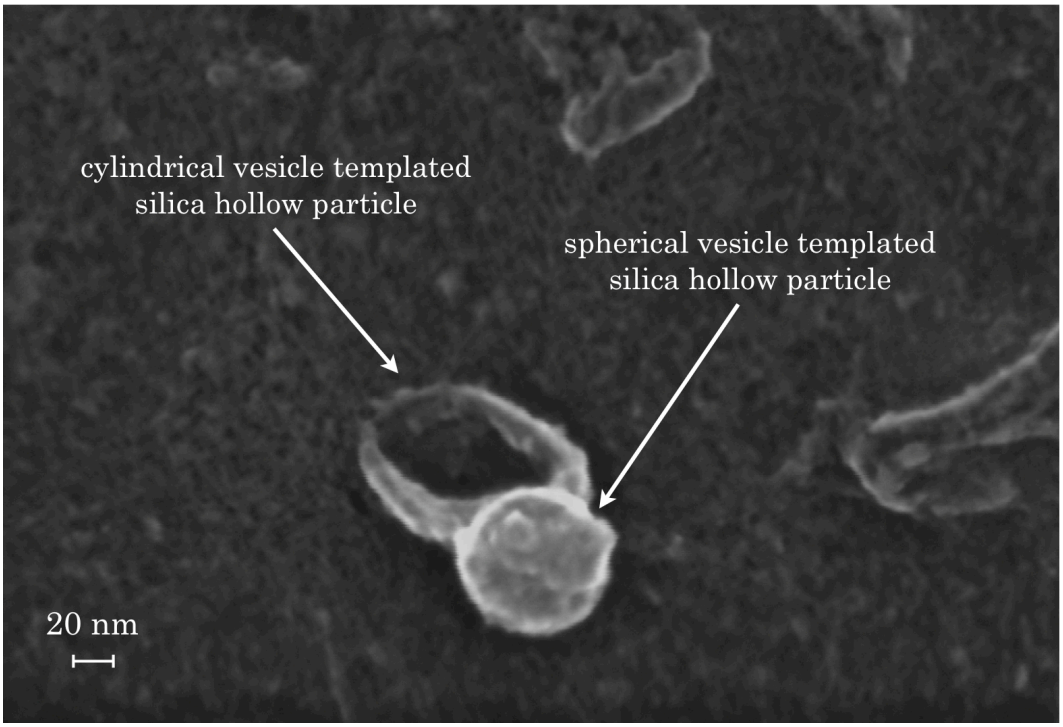

Figure 4.10 Scanning electron micrograph of a cylindrical vesicle templated hollow half silica particle, and a spherical vesicle templated hollow intact silica particle.

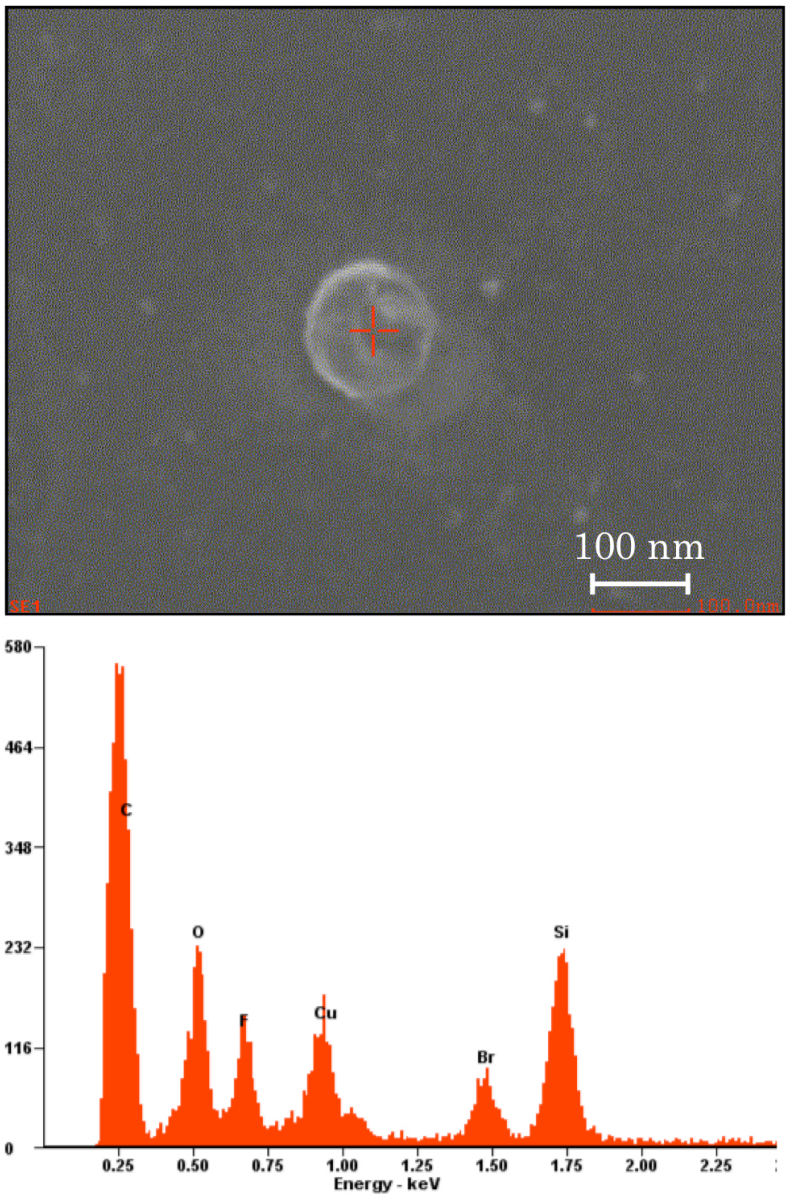

Figure 4.11 Scanning electron micrograph and energy dispersive X-ray spectroscopy of a hollow silica sphere.

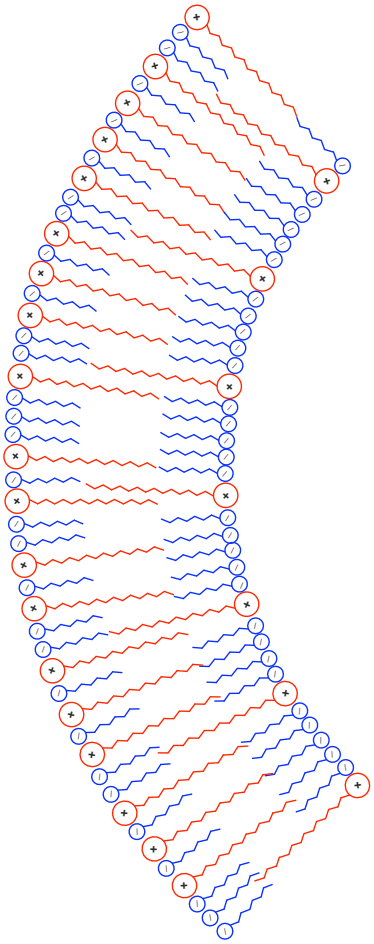

Figure 4.12 Higher CTAB/SPFO molar ratio on the outer layer of the bilayer due to the non-ideal mixing.

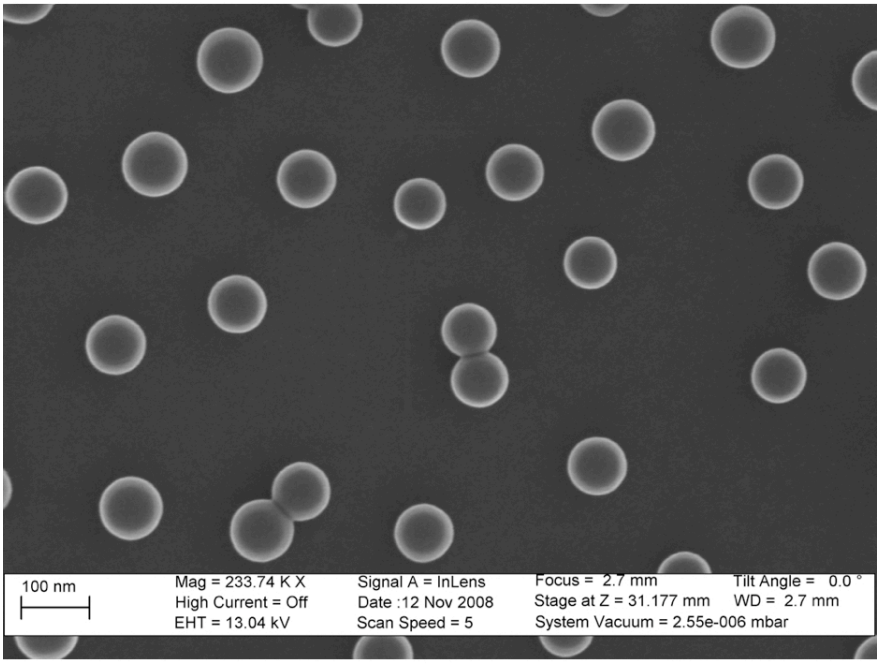

(a)

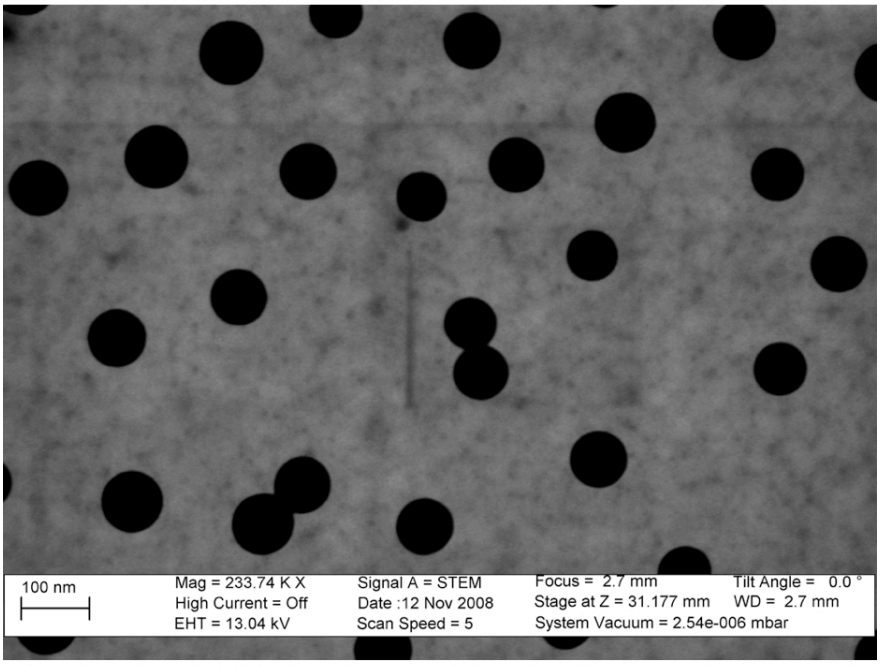

(b)

Figure 4.13 Amidine functionalized polystyrene beads, (a) scanning electron micrograph, (b) transmission electron micrograph.

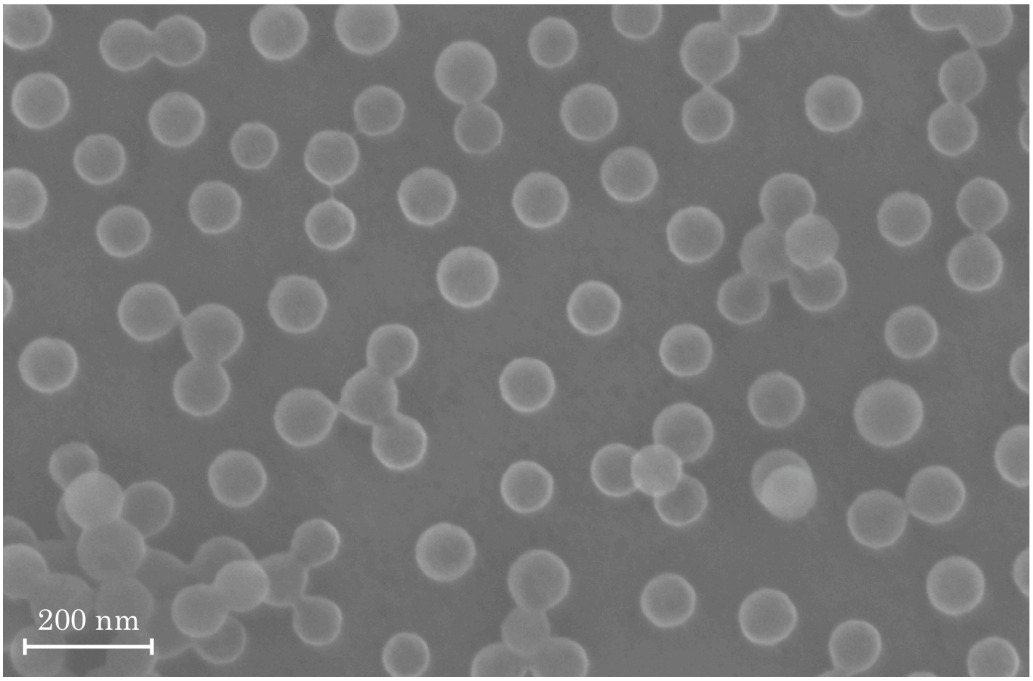

Figure 4.14 Scanning electron micrograph of silica spheres with a core of amidine functionalized polystyrene beads.

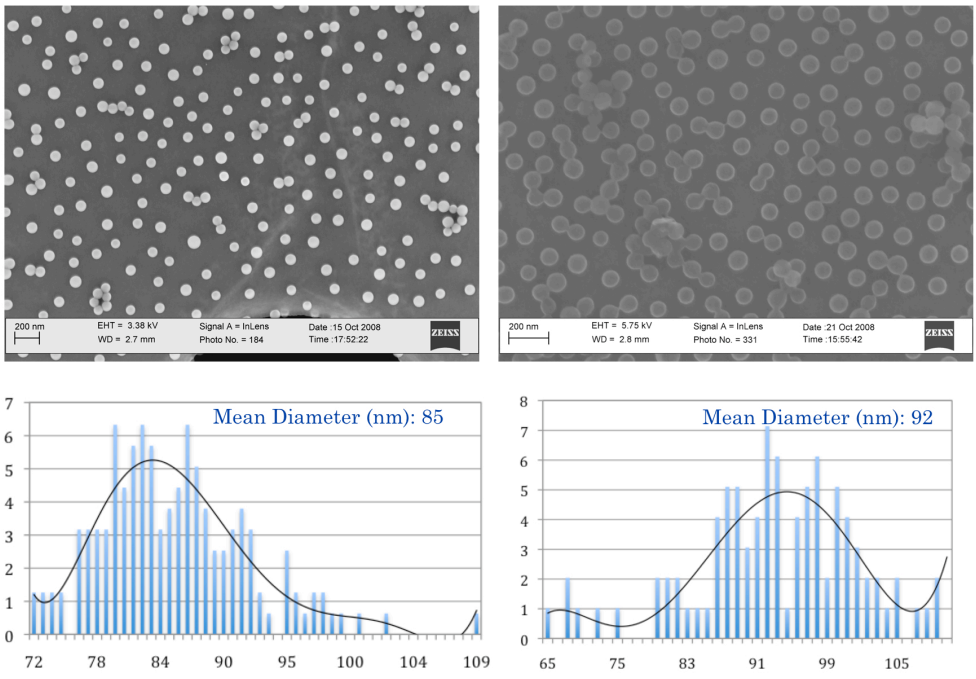

Figure 4.15 Scanning electron micrographs of polystyrene spheres and silica coated polystyrene spheres. Size distributions comparison, obtained from the two micrographs, indicates a silica shell thickness of 3.5 nm.

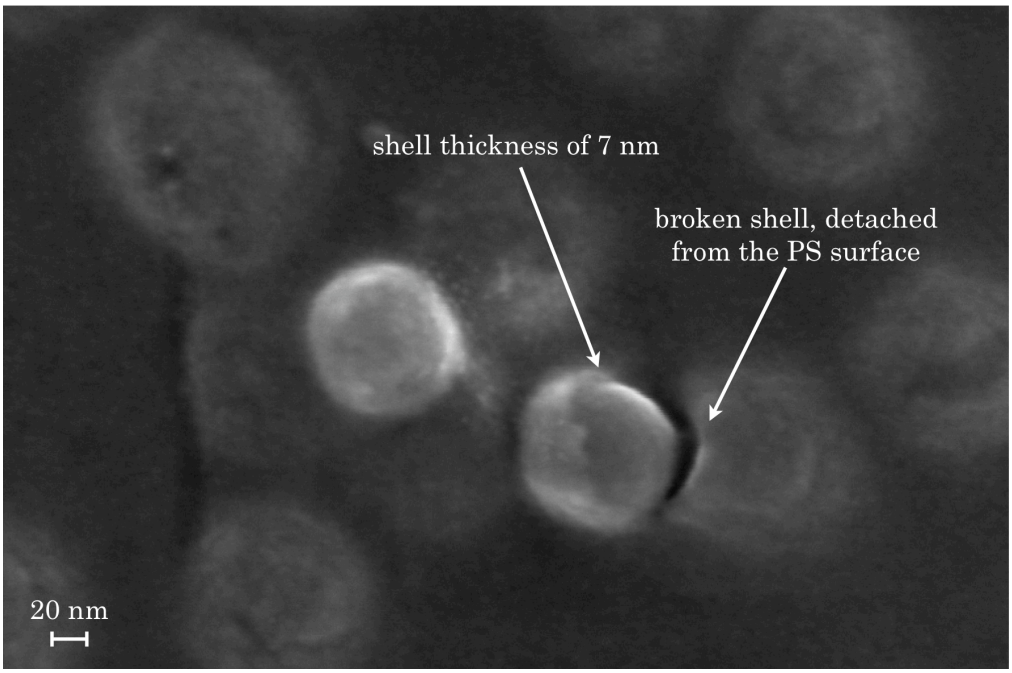

Figure 4.16 Scanning electron micrograph of silica spheres with a core of amidine functionalized polystyrene beads. Arrows indicate the shell thickness and broken/detached silica shell from the core polystyrene bead.

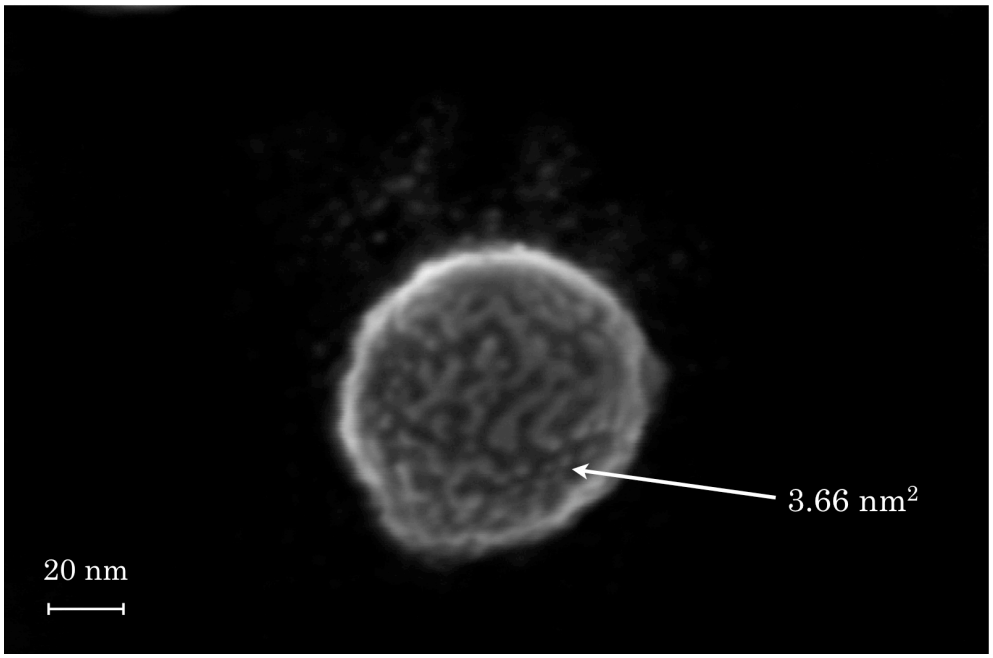

Figure 4.17 Scanning electron micrograph showing the pattern of silica adsorption on the surface of the amidine polystyrene bead. The arrow indicates a small island of adsorbed silica of area of 3.66 nm^2.

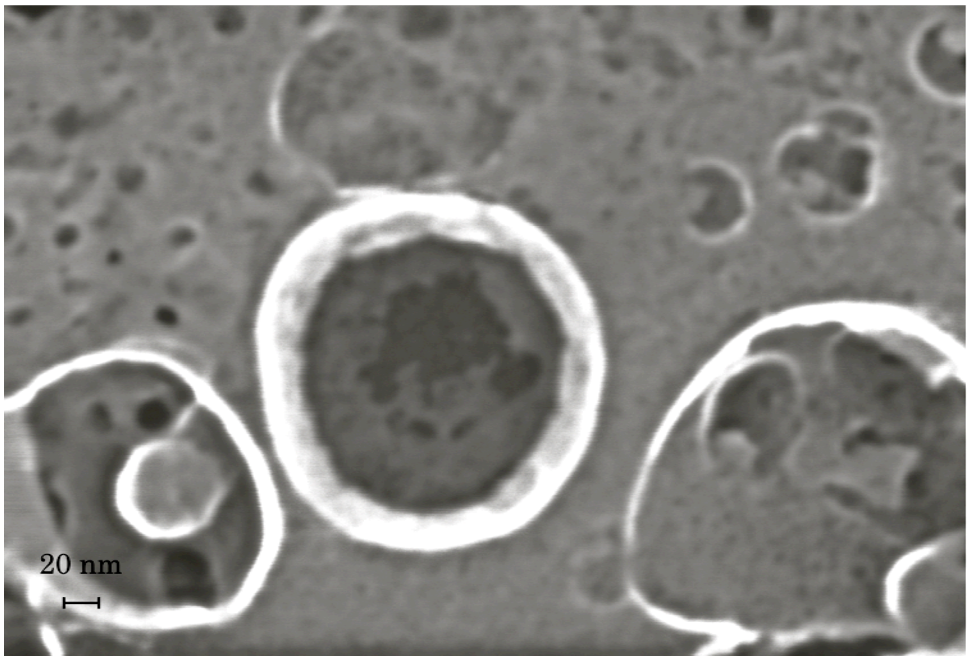

Figure 4.18 Scanning electron micrograph of amidine polystyrene latex templated silica shells after removing the polystyrene core with treatment with tetrahydrofuran (THF).

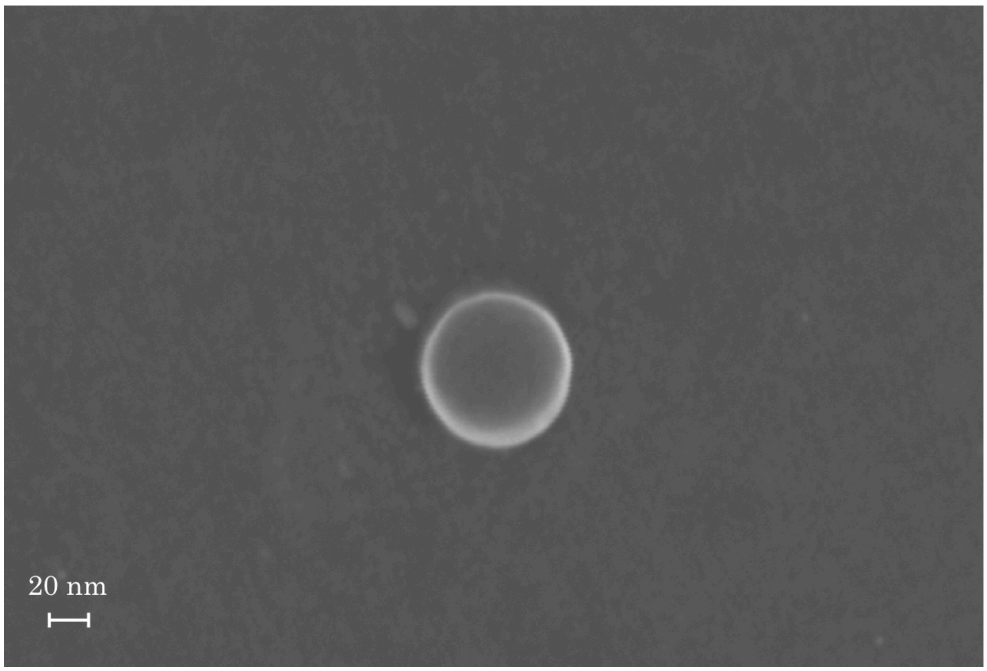

Figure 4.19 Scanning electron micrograph of carboxyl-sulfate functionalized polystyrene bead after the templated synthesis.

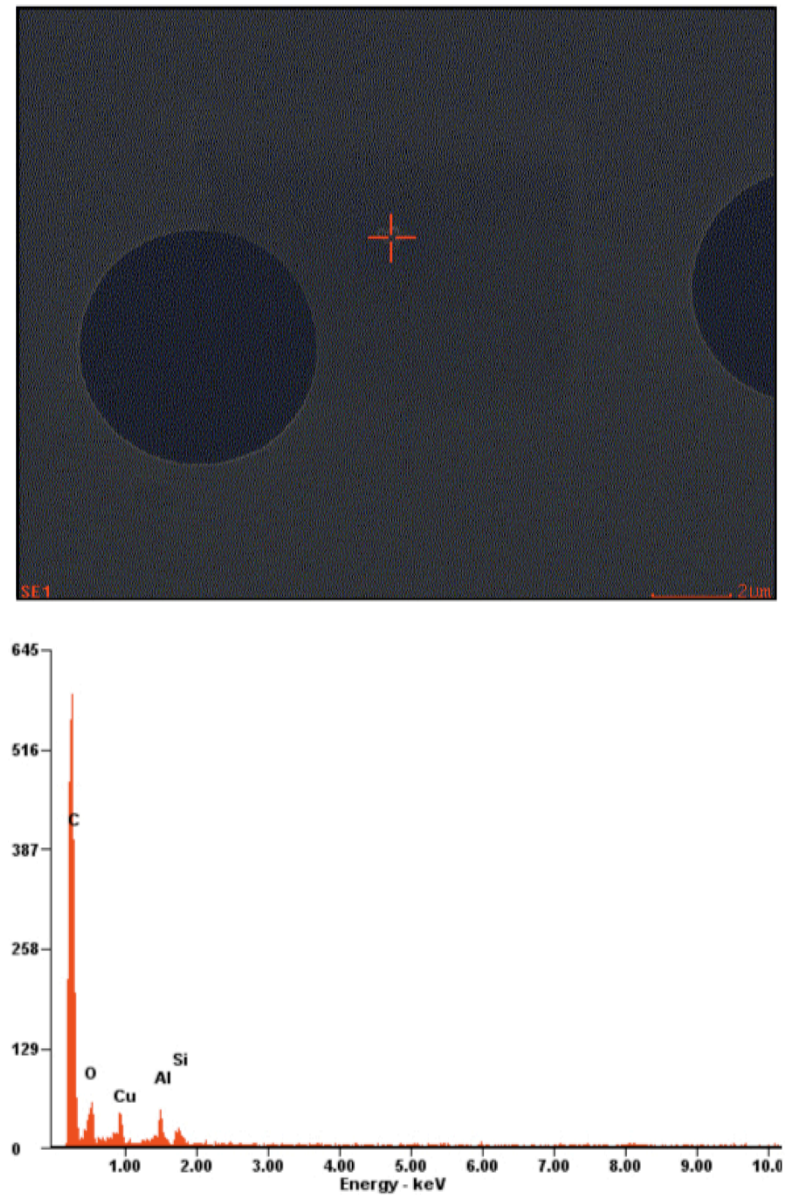

Figure 4.20 Scanning electron micrograph and energy dispersive X-ray spectroscopy of three uncoated carboxyl-sulfate polystyrene beads, showing just traces of silicon oxide.

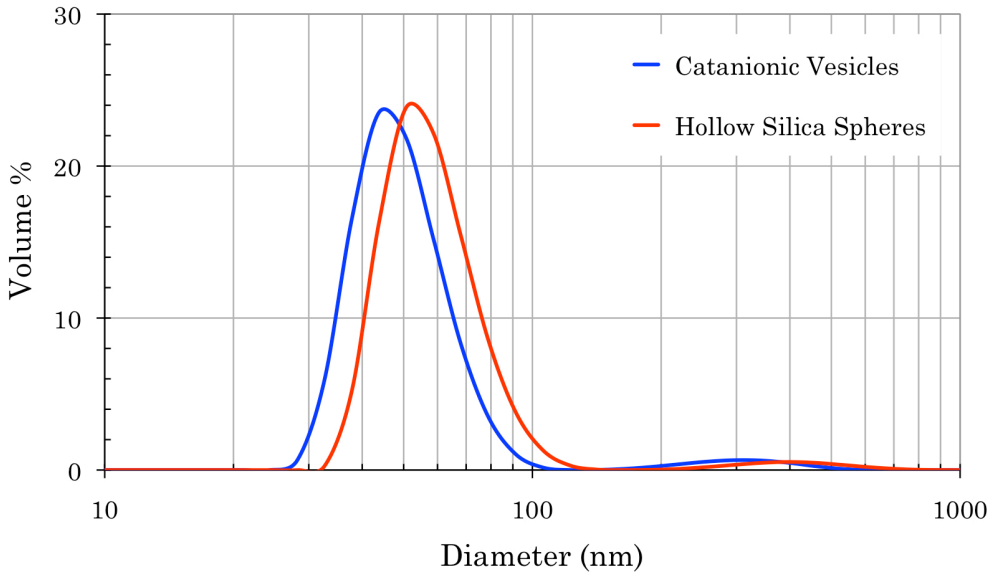

Figure 4.21 Size distributions, obtained by dynamic light scattering, of catanionic vesicles and hollow silica spheres at pH=3.

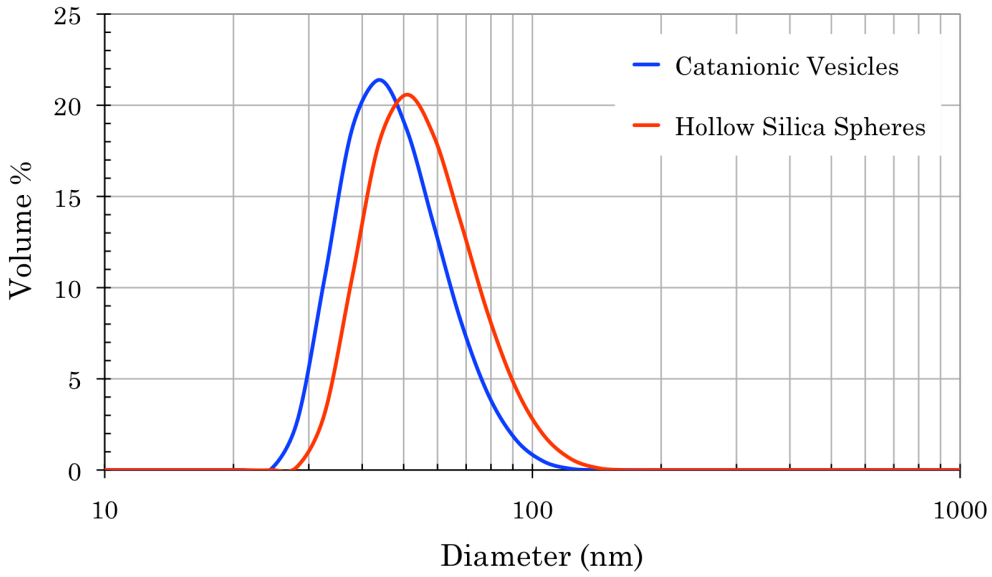

Figure 4.22 Size distributions, obtained by dynamic light scattering, of catanionic vesicles and hollow silica spheres at pH=4.

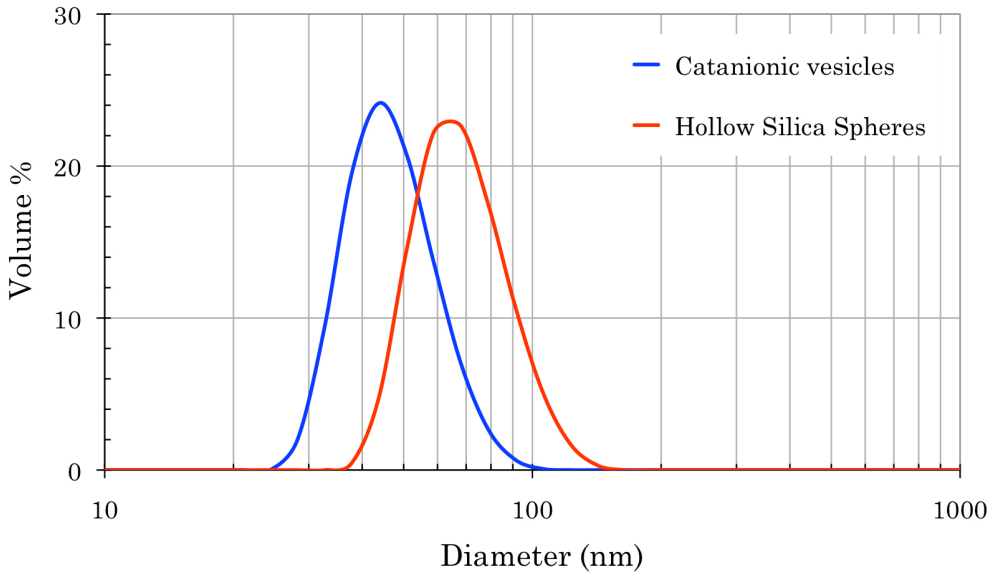

Figure 4.23 Size distributions, obtained by dynamic light scattering, of catanionic vesicles and hollow silica spheres at pH=5.05.

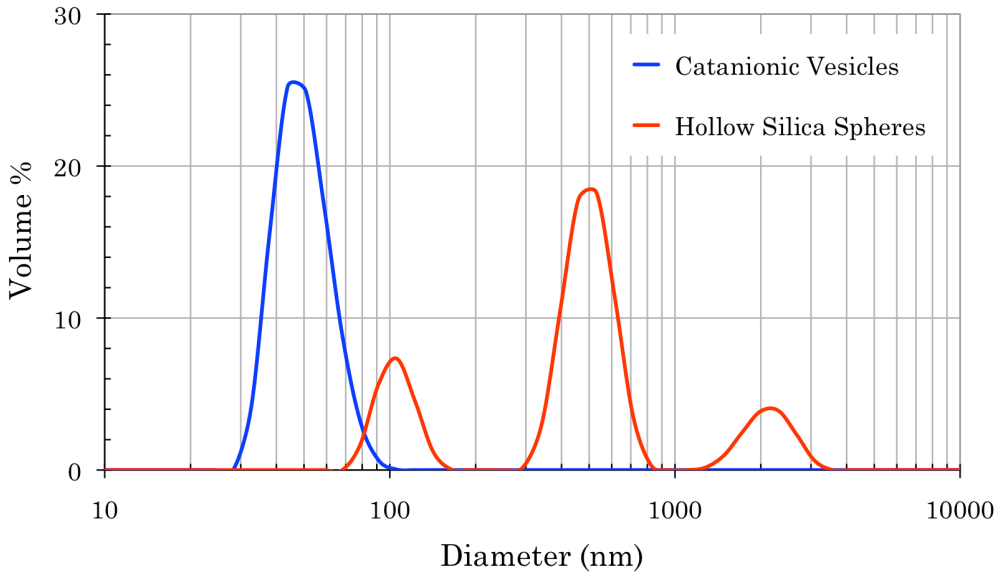

Figure 4.24 Size distributions, obtained by dynamic light scattering, of catanionic vesicles and hollow silica spheres at pH=5.75.

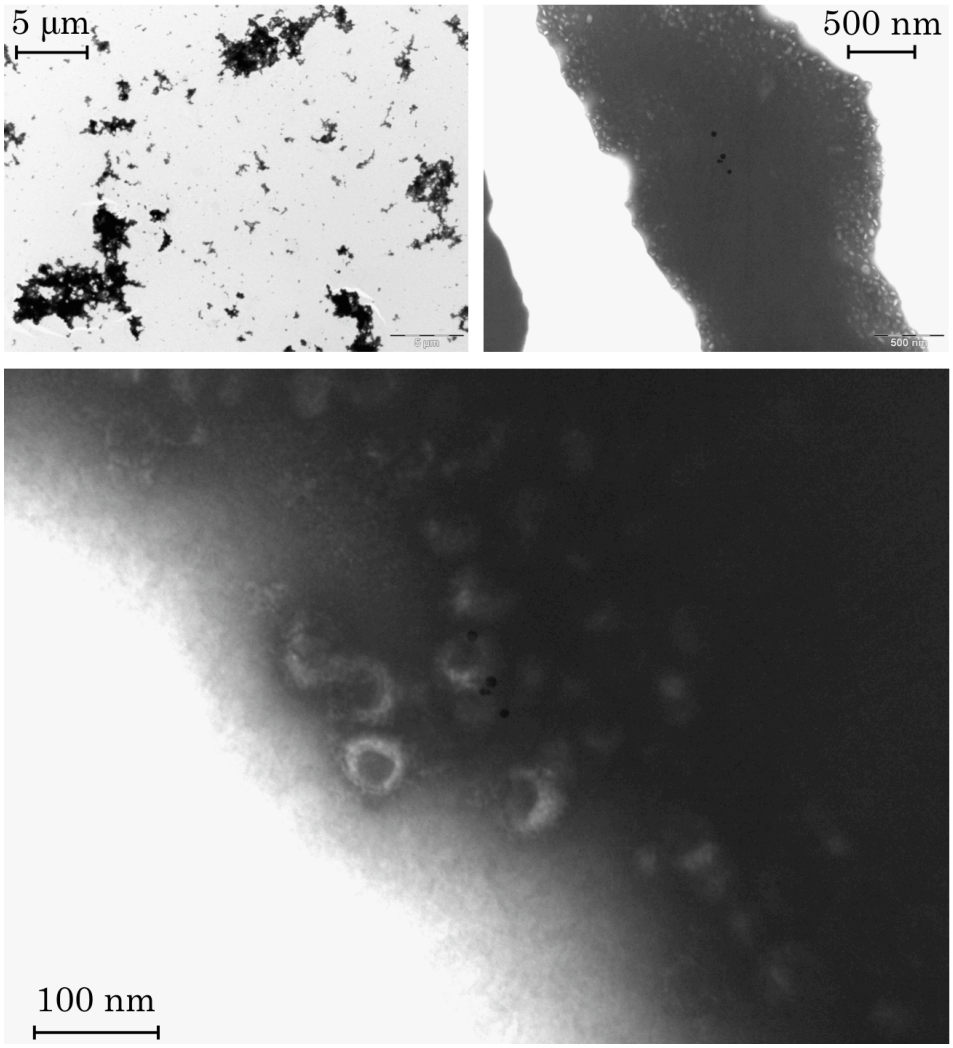

Figure 4.25 Transmission electron micrographs of templated hollow silica spheres at pH=5.75.

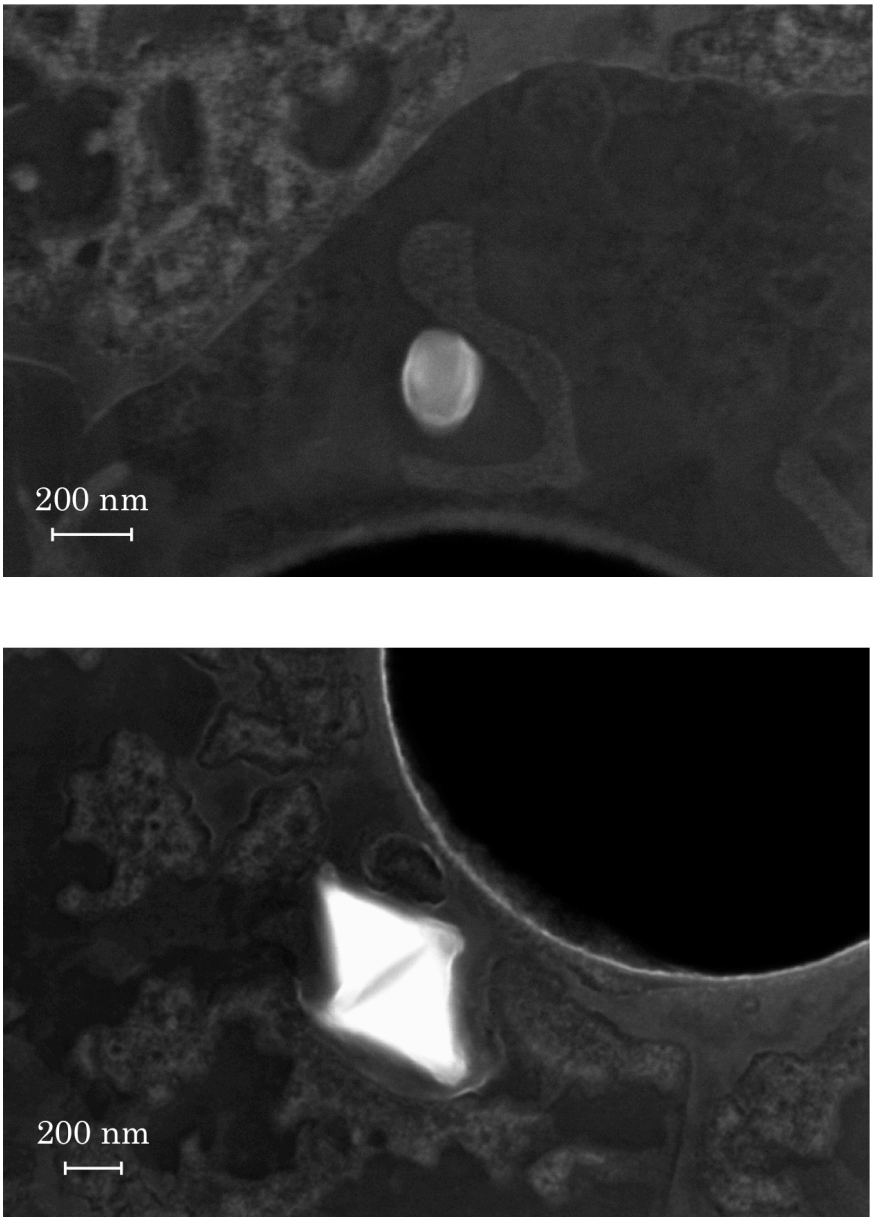

Figure 4.26 Scanning electron micrographs of vesicle templated silica synthesis sample with tetraethoxysilane (TEOS).

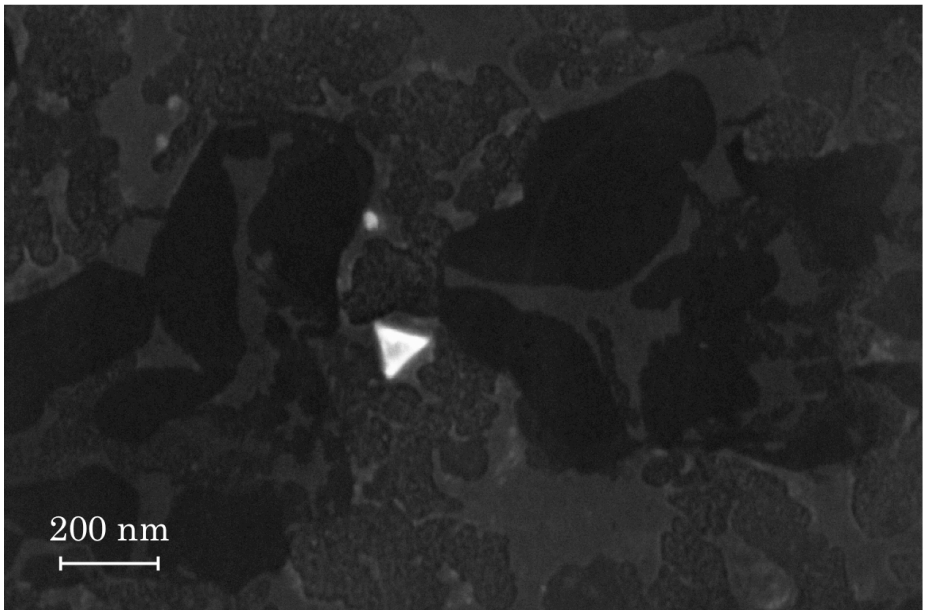

Figure 4.27 Scanning electron micrographs of vesicle templated silica synthesis sample with tetra-n-propoxysilane (TPOS).

CHAPTER 5

OPTIMIZATION - ADSORPTION AND SEPARATION

5.1 Introduction

In this chapter, we report a method to synthesize hollow silica spheres using a two-step synthesis. The first step involved the acidic hydrolysis and cross-linking of an inorganic alkoxide precursor (tetramethoxysilane, TMOS) onto the surface of unilamellar catanionic vesicles of Cetyltrimethylammonium Bromide (CTAB) and Sodium Perfluorooctanoate (SPFO) as described in Chapter 4. The second step consisted of the condensation of the hydrolyzed TMOS species in basic conditions, forming solid silica spheres.

Typically, the sol-gel process is described by an initial hydrolysis reaction that leads to the formation of reactive silanol species. These species then react with each other, releasing water (water condensation) or alcohol (alcohol condensation) to form silica. In acidic conditions, hydrolysis is preceded by fast protonation of the alkoxy groups, followed by the nucleophilic attack of water on the silicon atoms and the release of alcohol.[123,125,126] Overall, in acidic conditions, hydrolysis reactions are fast and condensation reactions are the rate-limiting steps.

In acidic conditions that the shells are formed, the negatively charged silicate species are attracted to the positively charged CTAB component of the vesicles. As the adsorbed silicate species increase their surface coverage locally on the vesicle surface, condensation of the silicate species occurs. This reaction is in direct competition with the condensation of the silicates that takes place in the bulk

solution forming long silicate chains that leads to gelation, which compromises our ability to recover separated clean discreet particles. In order to minimize the gelation phenomena, we want to stop the polymerization of the silicates in the bulk and instead drive the species to forming particles. We achieve this goal by introducing a second step that is similar to the Stöber synthesis.[109, 132] As a result, upon changing the pH of the solution from acidic to basic, we accelerate the condensation reactions that were originally rate determining, and as such, direct the silicate species present in the solution to form particles, much in the sense of the Stöber process.

5.2 Experimental Section

5.2.1 Materials

Sodium Perfluorooctanoate (SPFO, Alfa Aesar 97%), Cetyltrimethylammonium Bromide (CTAB, Alfa Aesar 98%), Tetramethoxysilane (TMOS, Spectrum 97%, Alfa Aesar 98%), ammonium hydroxide solution (28-30% NH_3, Fisher Scientific), 2-propanol (ACS reagent grade, Fisher Scientific), and 1-butanol (ACS reagent grade, Fisher Scientific) were used as received.

5.2.2 Solution Preparation – Protocols

The pH of the solutions was adjusted in the range of 3.0-3.5 by adding hydrochloric acid (HCl) in order to facilitate the hydrolysis of the tetramethoxysilane (TMOS) and maximize the gelation time.[93] The solutions were filtered and stirred at room temperature for 21 days to reach an equilibrium size. We then introduced the silica precursor TMOS (final concentration of 50 mM) into the 10 mL of vesicular solution. Silica hollow spheres were obtained after one hour of the initiation of the reaction.

Then we proceeded to the second step. Typically, 1 mL of the first step (hollow silica spheres) was added to 16.38 mL of 2-propanol and was immediately mixed with 1.18 mL of ammonia (28-30 %wt. in water) and 1.38 mL of water, while mechanically stirring throughout the process. The resulting solids were rinsed three times with

water and air dried before imaging the samples using scanning electron microscopy. Also, in the case of 1-butanol, all concentrations remained the same.

5.3 Results and Discussion

In our two-step synthesis, the first step (acidic hydrolysis of tetramethoxysilane in aqueous solution) provides a safe route to template the catanionic vesicles,[39] since the vesicles do not survive in alcoholic solvents. Therefore we obtain hollow silica spheres with a thin silica shell and a large number of hydrolyzed TMOS species in a short period of time. Acidic pH in the range of 2-4 maximizes the gelation time[93,106,107] and near the isoelectric point of silica (pH≈2) condensation rate for silica is quite low due to lack of strong nucleophiles ($Si\text{-}O^-$) or ($Si\text{-}O^+HR$). However, acidic hydrolysis of an alkoxysilane and the presence of free monomeric surfactant molecules of CTAB and SPFO, will eventually involve polycondensation and cyclization reactions[133-135] in the bulk, that promote gelation. Control of temperature, pH, and concentrations is not sufficient enough to eliminate gel behavior and enhance adsorption and cross-linking of the hydrolyzed species onto the vesicles' surface.

The second step consisted of templated hollow silica spheres, non-adsorbed prehydrolyzed monomer species, and oligomers of TMOS provided from the first step. Hydrolysis is not the rate-limiting step and a second population of solid silica particles was formed by the aggregation of oligomers and aggregation-addition of soluble species to the particle surface.[121] The concentration of ammonia, water, and the type of alcohol (second step) dictates the particle size at which colloidal stability occurs[111] and when aggregation stops. It is difficult to separate hydrolysis from condensation in this complex multi-reaction system. In most cases condensation

reactions will start rapidly during and after hydrolysis. Hydrolysis and condensation of an alkoxysilane in alcoholic solutions cause an incomplete hydrolysis and lead to a remarkable amount of non-hydrolyzed ≡Si-O-R groups[105,122] and transesterification products ≡Si-O-R′ (where R′ corresponds to the 2-propanol alkyl group), that incorporate into the silica network.[136]

The vesicle templated silica hollow spheres survived the second step (Figure 5.1) and thin silica shells revealed the hollow structure of the particles. Their size population was monodisperse with sizes in the range of 80-120 nm. Hollow particles obtained with the two step synthesis have smoother surfaces (see figure 5.1) than the corresponding ones from the first step (Chapter 4). It was observed, from SEM images, that they still do not exhibit a perfect spherical geometry but sharp-edged morphologies as those obtained from the first step were not perceptible. Figure 5.2 shows two distinct populations of hollow and solid silica particles, which are the result of changing the conditions of the reaction in the second step. Conditions close to Stöber synthesis as our proposed synthesis, produce highly monodisperse, dense silica particles. The slow hydrolysis of alkoxysilane monomers, in basic conditions, is overall (in both, reaction or diffusion limiting) the rate-limiting step,[93,126] and provides the hydrolyzed monomers that nucleate and grow with a monomer addition-aggregation mechanism; and growth stops once they obtain colloidal stability.[115,121] Independently on the mechanism of silica particle growth (discussed in Chapter 3), the size monodispersity of the silica particles is a product of the self-sharpening mechanism with time.[116] During the initial time of the Stöber synthesis (after the

initial nucleation and polycondensation) the silica particle size appears polydisperse and with time becomes highly monodisperse.

Dense solid Stöber silica particles were obtained using our proposed two-step synthesis, but in the absence of a vesicular template (Figure 3). Concentrations and reaction times for the entire synthesis were identical to the vesicle templated two-step synthesis. More specifically, in the first step, TMOS hydrolyzes in acidic (pH=3) aqueous solution for 30 min (acidic hydrolysis of TMOS can be completed within 10-15 min) and an appropriate volume of the aqueous TMOS solution was immersed into a 2-propanol/NH_3/H_2O solution and was left for 3 hours. As it was observed, (Figure 5.3), the particles had a perfect spherical geometry and their size population was highly polydisperse with sizes in the range of 20-130 nm. The size polydispersity of the sample was expected to be high, due to the limited time of the second step. If the second step was not stopped by 3 hours, size monodispersity would eventually be achieved as discussed above. One important comparative observation between Figure 5.1 and Figure 5.3 was that in vesicle templated two-step synthesis, and in identical concentrations/synthesis/reaction time conditions, we obtained a highly monodisperse templated hollow silica spheres population (Figure 5.1), with sizes similar to the ones obtained after the first step (see Chapter 4). Their morphology did not have a uniform spherical geometry, like the solid ones obtained without the vesicular template (Figure 5.3). This is consistent with the results we obtained for vesicle templated hollow silica spheres after the first step (Chapter 4) and is attributed to the mechanical stresses caused by the condensation of the growing

silica network on the vesicles surface, and by the sample preparation-drying on the electron microscopy grids. The second, dense solid silica spheres, population we obtained with the two step synthesis (Figure 5.2) rules out the monomer addition growth model,[115] for our system. It would be very *convenient* to actually coat the existing vesicle templated hollow silica spheres with the non-adsorbed monomers-oligomers of TMOS in the bulk, but this is not the case for this particular system. Since the vesicular solution of mixtures of CTAB/SPFO is in an equilibrium with free monomeric surfactant molecules of CTAB and SPFO, makes our reaction system highly complex compared to the classic, surfactant free, Stöber synthesis. CTAB free monomeric molecules should act as nucleation sites for hydrolyzed TMOS monomers and oligomers and also promote nucleation and polymerization in the bulk during both acidic (1^{st}) and basic (2^{nd}) steps. Upon introduction of the vesicle templated hollow silica spheres and the hydrolyzed monomers and oligomers from the first (acidic) step into the second (basic) step, the solution has already developed nucleation complex sites of monomers/oligomers/ CTAB that accelerate aggregation and undergo polymerization until they collapse and condense, forming dense particles that further aggregate in order to achieve colloidal stability. The system develops selectivity for solid silica particle growth, along with smoothing of the vesicle templated hollow silica particles surface without any significant growth (compared to the solid silica particles growth). The growth of the solid silica particles is directly dependent on the remained TMOS hydrolyzed species in the bulk, and they are not expected to have the same density of the silica structure of surfactant free Stöber particles, due to incorporation of more CTAB, and less SPFO in the silica

network, non-hydrolyzed ≡Si-O-CH_3 groups, and up to 10 different transesterification products of ≡Si-O-$CH(CH_3)_2$ (see Table 5.1).

Size distributions obtained with dynamic light scattering experiments of the templates (catanionic vesicles), hollow silica spheres (1st step), and hollow/solid silica spheres (2nd step) are shown in Figure 5.4. Intensity vs. diameter data for the 2nd step (see Figure 5.4.a) show size distributions of the two populations for the 2nd step of hollow silica spheres (lower intensity and diameter) and solid silica spheres (higher intensity and diameter). Their corresponding dynamic light scattering size distribution data for number of particles vs. diameter (see Figure 5.4.b) reveals a higher number of hollow silica spheres and a lower number of large solid silica spheres.

Energy dispersive X-ray spectroscopy (EDXS) elemental analysis [shown in Figure 5.5 (top schematic)], performed on the small diameter population of the particles, indicates that the particles consisted of silica, but also exhibit a fluorine peak confirming the existence of the trapped fluorocarbon surfactant (SPFO) due to the template's presence in the hollow interior. Figure 5.5 (lower schematic) shows the EDXS spectra for the large diameter population of particles, indicating that they are solely solid silica beads. These beads do not exhibit the template's fluorine signature peak, confirming that they were formed in the second step of the synthesis.

The type of the alcoholic solvent used plays a significant role in particle formation.

Van Blaaderen and Kentgens,[136] reported that the rate of hydrolysis and condensation for TEOS follows the sequence 1-butanol>methanol>1-propanol> ethanol>2-propanol. The authors suggested that hydrogen bonding and steric hindrance of the alcoholic solvent are the factors that influence the reaction rates. Sadasivan et al.,[137] showed that particle size increases proportionally to the alcoholic solvent molecular weight, 1-butanol>2-propanol>1-propanol>ethanol>methanol. They suggested that steric hindrance may be the predominant factor for lower alcohols, and weaker hydrogen bonding may be the predominant one for the higher alcohols. They concluded that the final particle size seems to depend on solvent polarity. High polarity alcohols, such as methanol, will produce small particle size, whereas the low polarity of 2-propanol favorites the aggregation of larger particle sizes in order to obtain colloidal stability. However, the alcoholic solvent in our synthesis (2^{nd} step) most influences the condensation reactions, since TMOS has been hydrolyzed in the 1^{st} step.

The alcoholic solvent of 2-propanol produces solid silica spherical particles up to 6 - 7 times the diameter of the vesicles templated hollow silica spheres (Figure 5.1, Figure 5.2). The two distinct different size populations of silica spheres can be easily separated by centrifugation due to their significant difference in weight.

Instead of 2-propanol, methanol or ethanol would produce smaller solid silica particles in the same size range of vesicle templated hollow silica spheres and would make separation more difficult. A higher molecular weight alcohol (1-butanol) was

used as an alcoholic solvent under identical reaction conditions. Vesicle templated silica spheres survived the process as is shown in the scanning electron micrographs in Figure 5.6. Solid silica particles were observed (Figure 5.7) in the range of 700-800 nm in coexistence with microspheres (5-10 μm) consisting of vesicle hollow spheres. The system was unstable and promoted vesicle templated hollow spheres agglomeration, which created uniform spherical geometries with a sponge-like morphology.

5.4 Conclusion

In conclusion, we described a two step method in order to fabricate vesicle templated hollow silica spheres using an acid-catalyzed sol-gel synthesis for templating catanionic vesicles and minimizing the homogeneous nucleation in the bulk by rapid condensation of the remaining hydrolyzed TMOS species by introducing a second step and changing the solvent and pH. Acidic pH, during the first step, facilitates the hydrolysis of TMOS and maximizes the gelation time. However, gel formation cannot be avoided by just tuning the pH, and without the second step, hollow silica particles would eventually get trapped/caged into the gel. In the second step, the already hydrolyzed species of TMOS, which have not been adsorbed onto the vesicles surface will be the inventory in the presence of ammonia and 2-propanol, as a solvent, to quickly condense, aggregate and form the solid silica beads. A low polarity alcohol (2-propanol) was used to obtain large solid silica beads. The two populations (hollow silica spheres with diameters in the range of 80-100 nm, and silica beads with diameters in the range of 500-600 nm) can be easily separated by centrifugation due to their significant difference in density. However, when using 1-butanol as a solvent, instead of 2-propanol, the same system was unstable, promoting vesicle templated hollow spheres agglomeration and creating uniform micron size spherical geometries with a sponge-like morphology.

The second step optimizes the synthesis of vesicle templated hollow nanoparticles, not only by increasing the yield of the process (as high molecular weight polymerized

species of TMOS produce solid particles, rather than a gel, which would eventually encage the hollow spheres) but also provides an easy mechanical separation route for producing fine monodisperse hollow and solid powders. The most important factor for scaling-up the process is that in both (batch-process) steps, were not introduced any additional degrees of freedom (such as filtration, dilution, ethanol / acid washing, or centrifugation and washing cycles for surfactant removal), which would elevate the complexity of the system. Even though the above techniques are very common in material synthesis for obtaining and characterizing powders, are difficult to formulate (which limits reproducibility), time consuming, and limit the process to rather small batch volumes of reaction solutions.

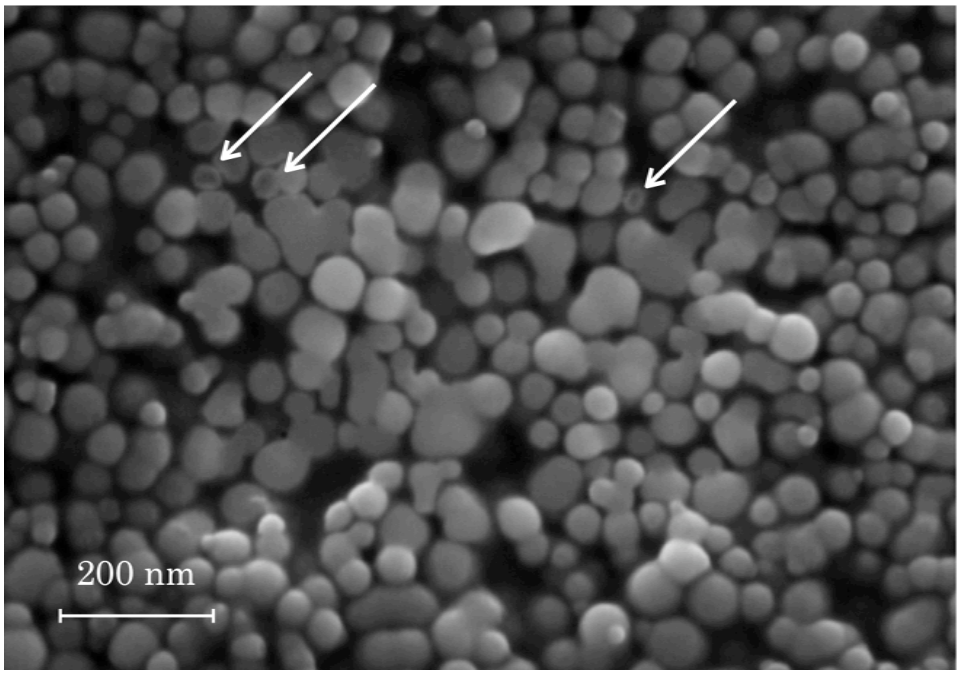

Figure 5.1 Scanning electron micrograph of templated hollow silica spheres after the 2nd step. The white arrows show spheres with extremely thin shell that indicates their hollow structure.

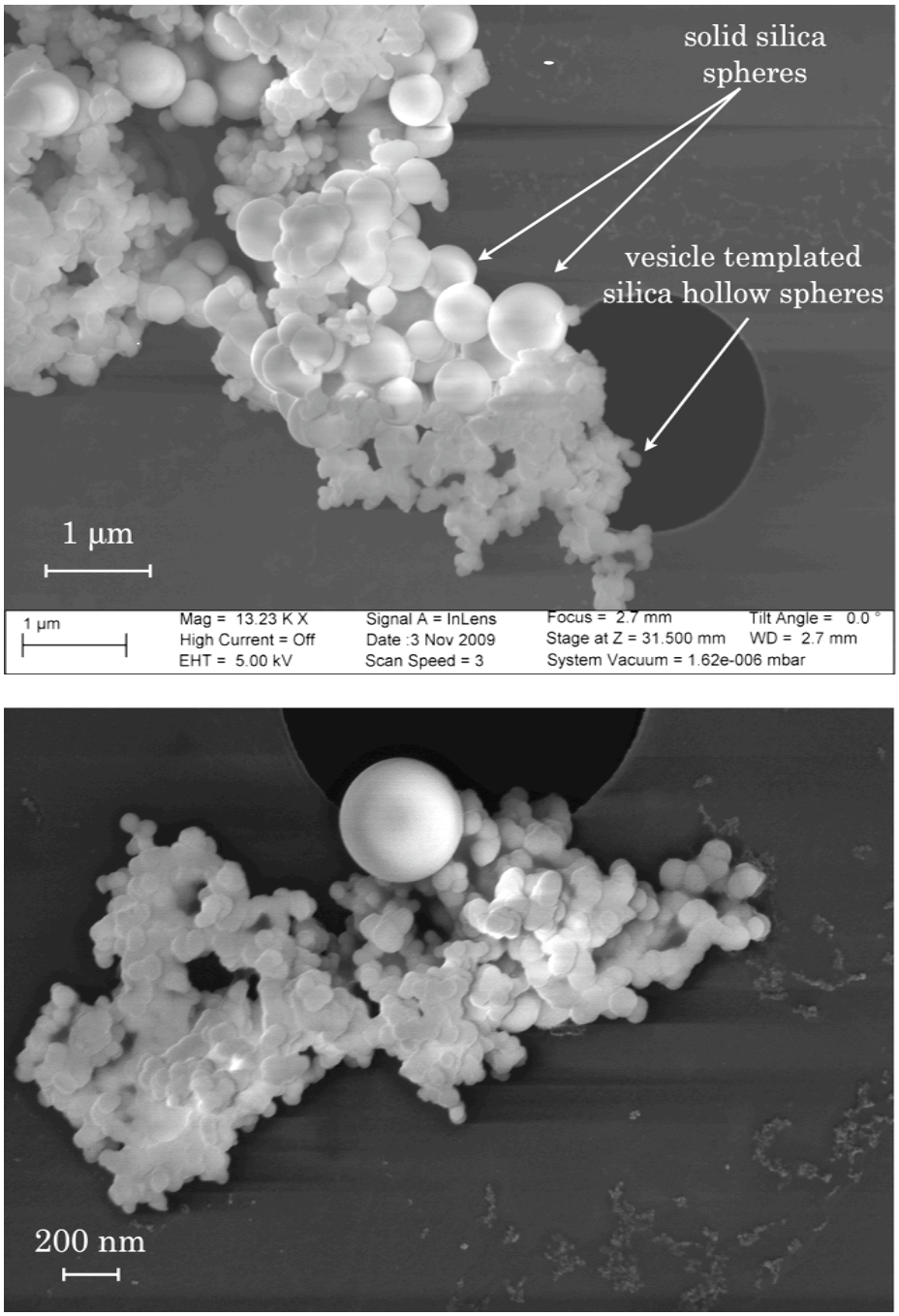

Figure 5.2 Scanning electron micrographs of hollow silica spheres in the range of 30-120 nm and solid silica spheres in the range of 400-700 nm.

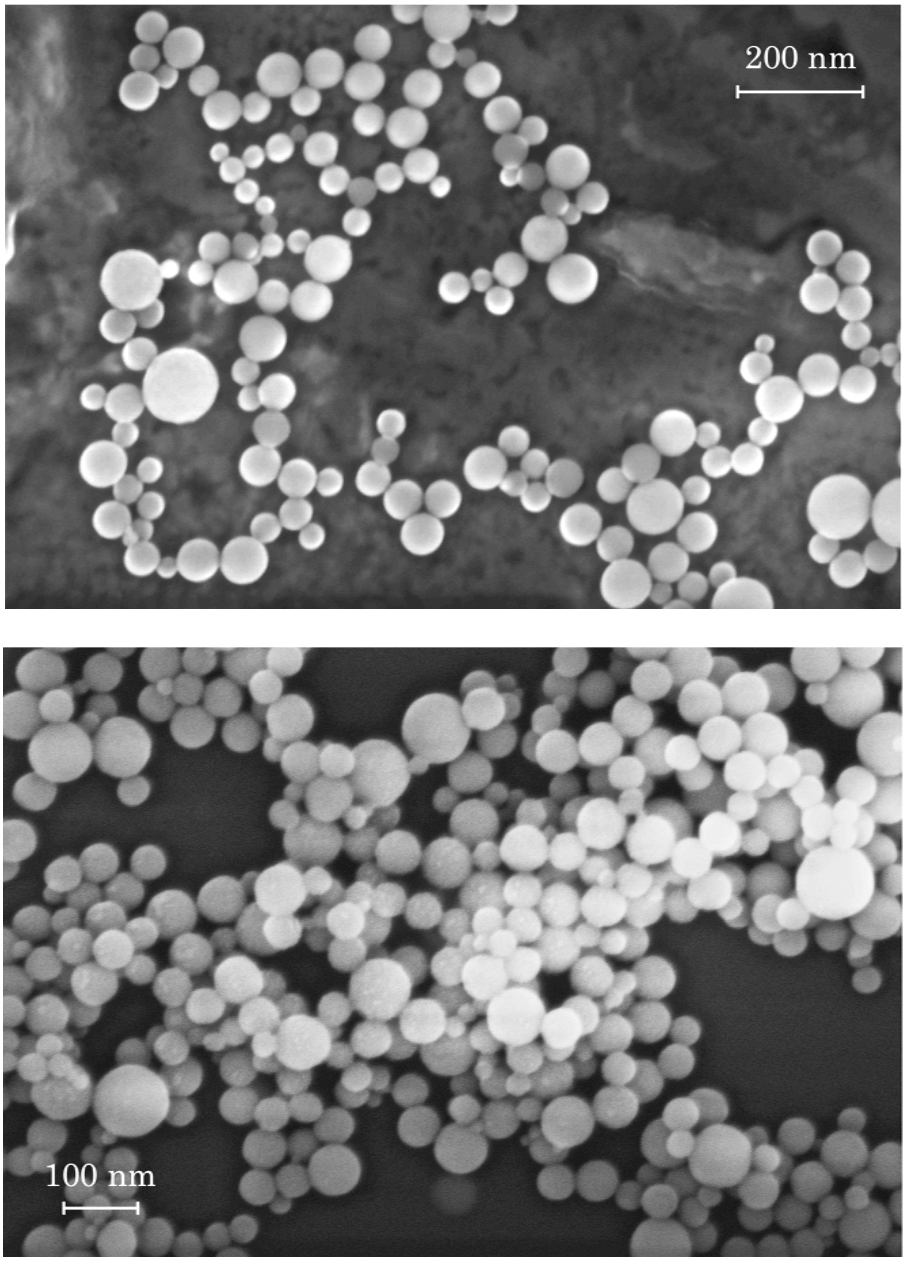

Figure 5.3 Scanning electron micrographs of a polydisperse population of solid silica spheres synthesized in two steps. The first step consist of pre-hydrolyzed TMOS in acidic conditions without the presence of any template, and the second step is identical to the proposed synthesis.

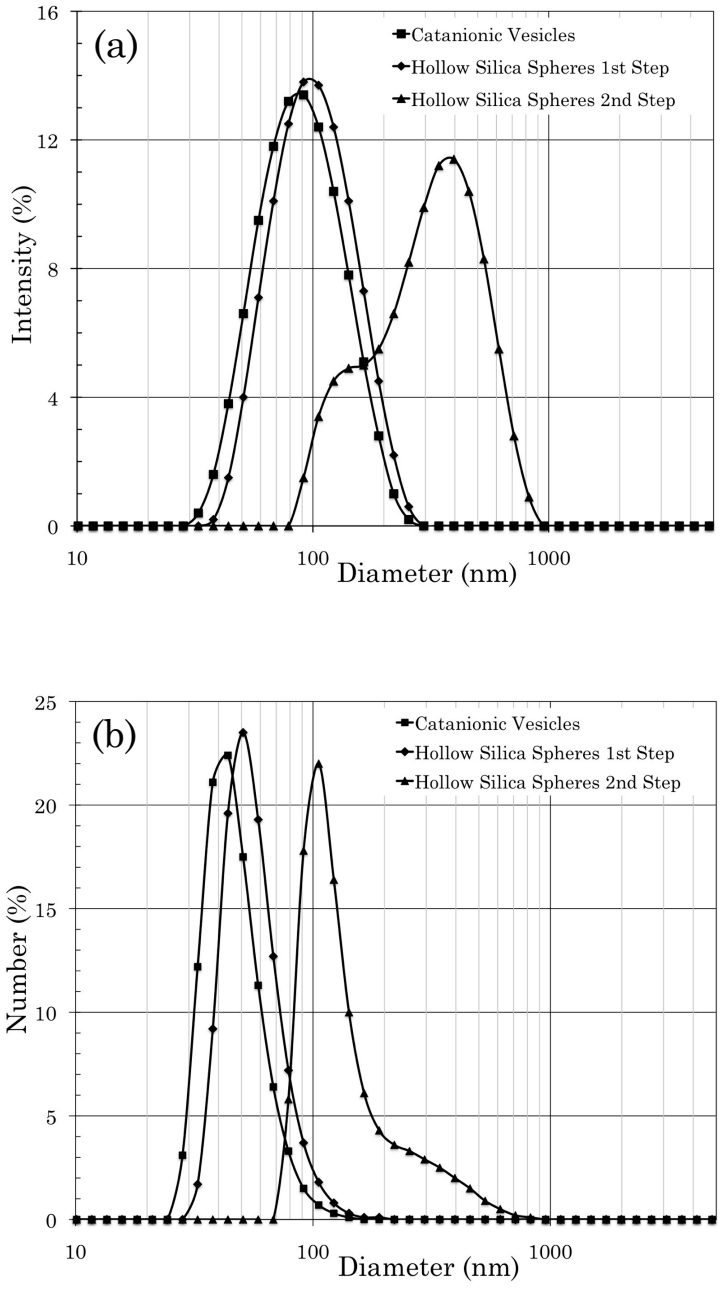

Figure 5.4 Dynamic light scattering data of (■) catanionic CTAB/SPFO vesicles, (◆) hollow silica spheres (1st step), and (▲) hollow and solid silica spheres (2nd step); (a) intensity vs. diameter, (b) number vs. diameter.

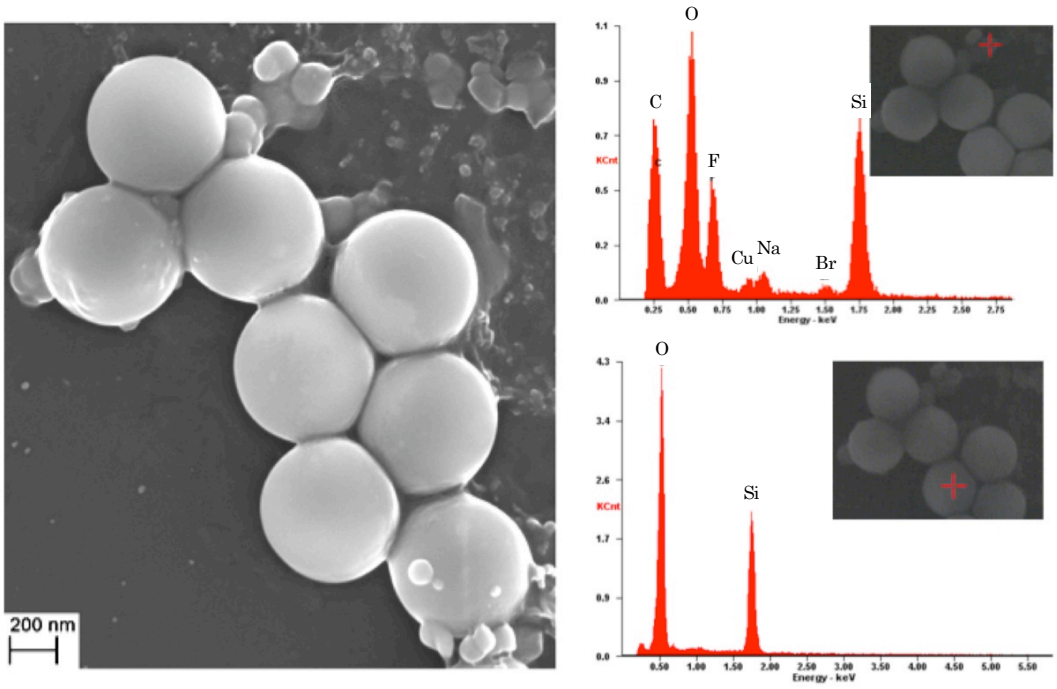

Figure 5.5 Scanning electron micrograph and energy dispersive X-ray spectroscopy of hollow templated spheres (top schematic) and solid silica spheres (bottom schematic).

Table 5.1 List of monomer species of TMOS, after hydrolysis, in 2-propanol /NH_3/H_2O solution.

Silanol Monomer Species of TMOS in 2-Propanol/NH_3/H_2O Solution
$Si(OCH_3)_4$
$Si(OCH_3)_3(OH)$
$Si(OCH_3)_2(OH)_2$
$Si(OCH_3)(OH)_3$
$Si(OH)_4$
$Si[OCH(CH_3)_2](OCH_3)$
$Si[OCH(CH_3)_2](OCH_3)_2(OH)$
$Si[OCH(CH_3)_2](OCH_3)(OH)_2$
$Si[OCH(CH_3)_2](OH)_3$
$Si[OCH(CH_3)_2]_2(OCH_3)_2$
$Si[OCH(CH_3)_2]_2(OCH_3)(OH)$
$Si[OCH(CH_3)_2]_2(OH)_2$
$Si[OCH(CH_3)_2]_3(OCH_3)$
$Si[OCH(CH_3)_2]_3(OH)$
$Si[OCH(CH_3)_2]_4$

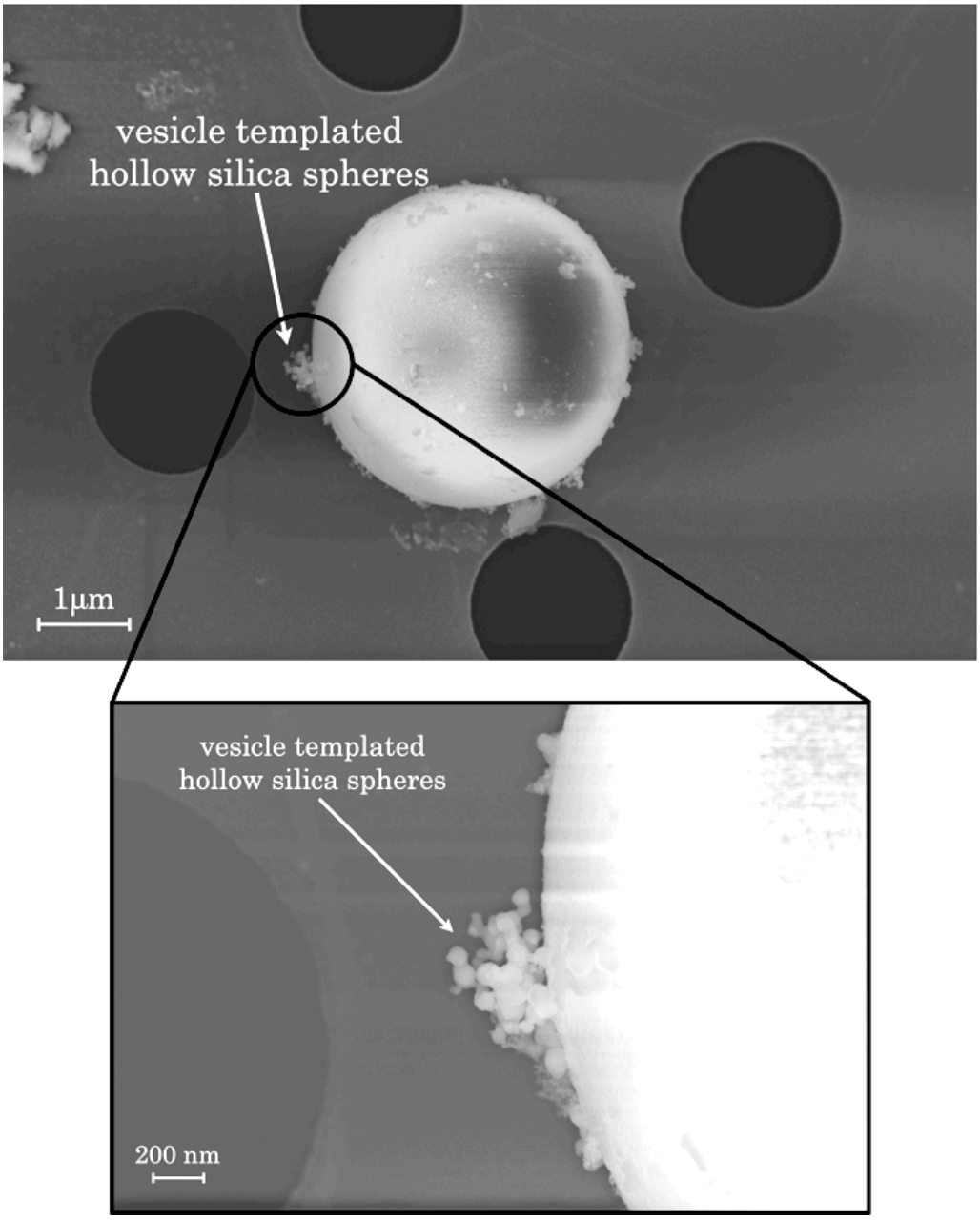

Figure 5.6 Scanning electron micrograph of a large solid silica sphere and its magnification. Alcoholic solvent for the second step was 1-butanol. White arrow indicates vesicle templated silica hollow spheres.

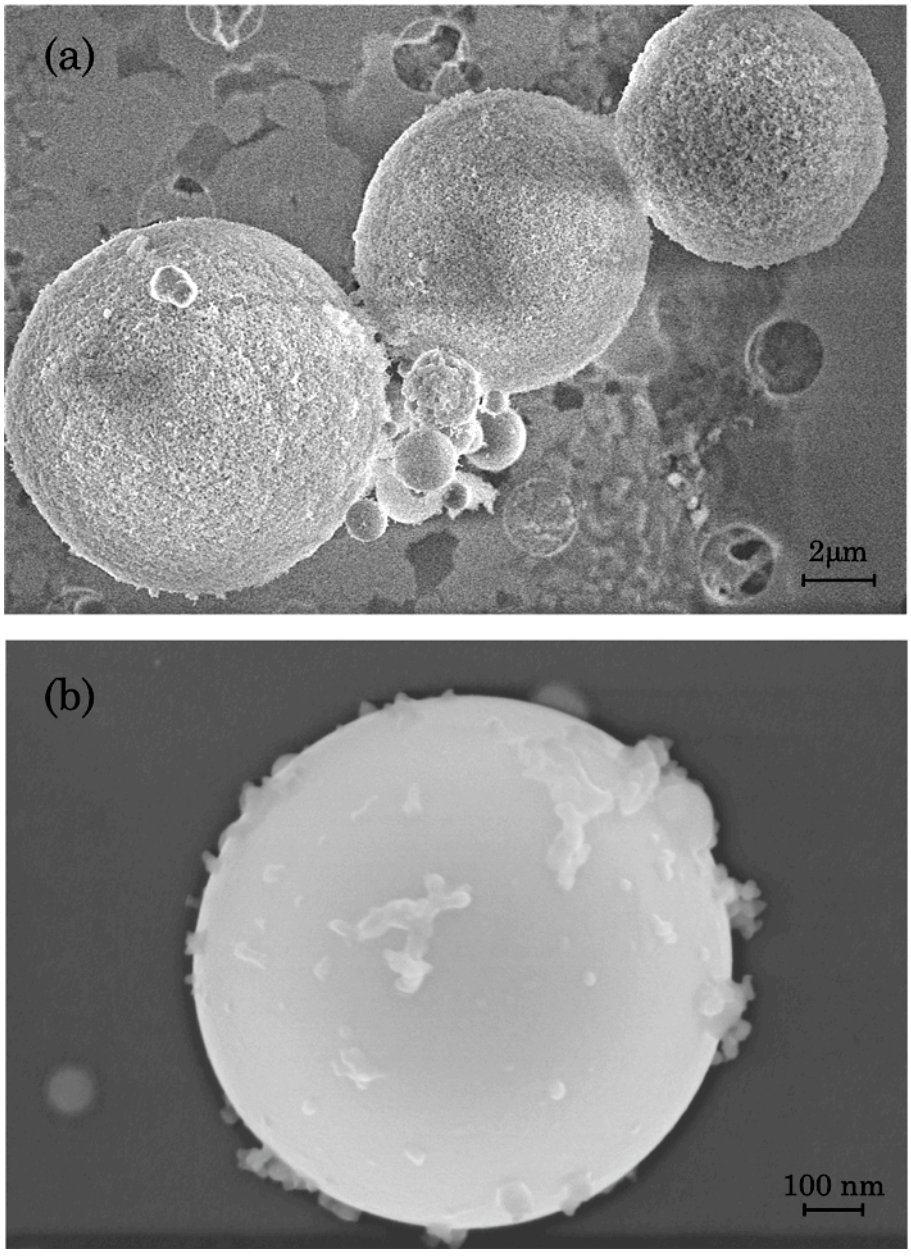

Figure 5.7 Scanning electron micrographs of (a) large silica micro-spheres with sponge-like morphology consisted of agglomerated templated hollow silica spheres; and (b) solid dense silica nano-sphere. Both images were obtained from the same sample and the alcoholic solvent, for the second step, was 1-butanol.

CHAPTER 6

FUTURE WORK

Further optimization of the process of the synthesis of hollow silica spheres could be to introduce and disperse the reaction solution (hollow silica spheres after the 2nd step) into a viscous organic media (e.g., water-starch solution) and afterwards calcine it with a slow heat rate (1-2°C min^{-1}). The organic matrix would ensure minimum contact of the hollow silica spheres with each other during the critical temperature of evaporation of their surface water. Silica networks would condense (at least on the surface) before the combustion of the organic matrix, and would minimize agglomeration phenomena, producing highly monodisperse fine powders.

In the case of 1-butanol (Chapter 5, 2nd step), it will be of a great interest to attempt to functionalize the surface of the sponge-like spherical particles (made of agglomerates of hollow silica spheres) and then coat the surface with a different inorganic material, obtaining composite sponge-like particles. These composite powders can be used in catalysis, as they should exhibit a high specific surface area and an extremely low density due to their sponge microstructure and hollow nanostructure.

Lipids with hydrophilic polymers grafted at the polar head group, such as polyethylene-glycol can stabilize vesicles by enhancing steric interaction (inhibiting vesicle fusion),[138] and lead to unilamellar vesicles at low concentrations.[139,140] However, enthapically stabilized vesicles, such as CTAB/SPFO, are expected to be more sensitive than entropically stabilized ones because the grafted lipid polymer would directly affect elastic constants[141] and curvature of the bilayer, and thus the

stability mechanism.[67] Potential use of sodium perfluoroexanoate instead of sodium perfluorooctanoate (SPFO) with CTAB would form entropically stabilized vesicles[62] that can overcome stability mechanism restrictions but will form polydisperse vesicular systems. We successfully synthesized vesicles of CTAB/SPFO/polyethylene-glycol dimyristoylphosphatidylcholine (PEG2000-DMPE) of [(2% wt. total surfactant CTAB/SPFO at 1:4 wt. ratio) and 1:100 molar (PEG2000-DMPE):CTAB/SPFO]. We introduced the silica precursor (TMOS) in acidic conditions to coat the vesicle-PEG template. Size distributions of CTAB/SPFO/PEG-DMPE vesicles observed in cryo-TEM images (Figure 6.1) were highly polydisperse compared to the CTAB/SPFO ones and the findings were confirmed with dynamic light scattering experiments. We observed vesicle fusion in some of our samples as shown in Figure 6.1. Silica templating with TMOS was successful, obtaining hollow silica spherical morphologies with irregularities appearing on the outer surface of the particle as shown in atomic force micrographs (Figure 6.3). Transmission electron microscopy confirmed the presence of particles with morphologies (Figure 6.3) that resemble Jung et al.,[142] description of parachute-like morphologies, when he observed phase separation phenomena during polymerization and silica templating (TMOS), using vesicle/polymer architectures as templates.

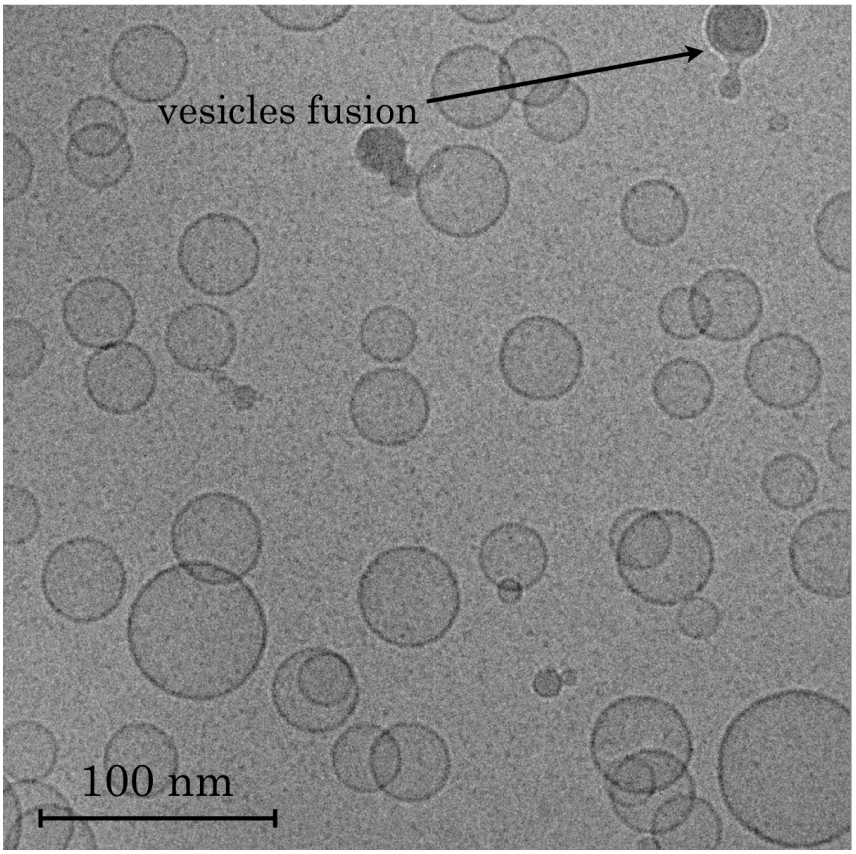

Figure 6.1 Cryo-TEM micrograph of vesicle/PEG-lipid [2% wt. total surfactant CTAB/SPFO at 1:4 wt. ratio, 1:100 molar (PEG-DMPE):CTAB/SPFO].

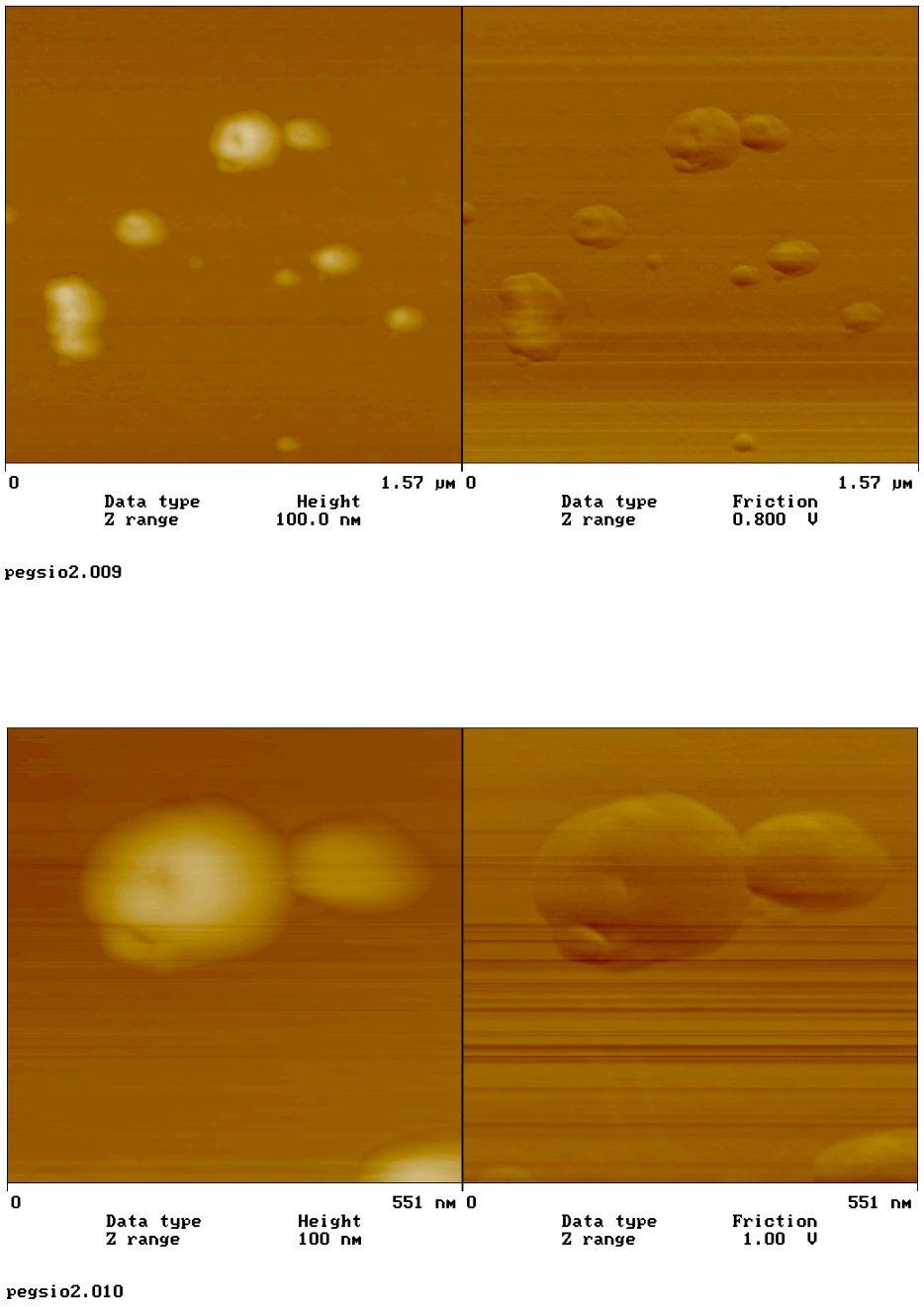

Figure 6.2 Atomic force micrograph of vesicle/PEG-lipid templated hollow silica spheres [2% wt. total surfactant CTAB/SPFO at 1:4 wt. ratio, 1:100 molar (PEG-DMPE):(CTAB/SPFO), and 2%wt of TMOS].

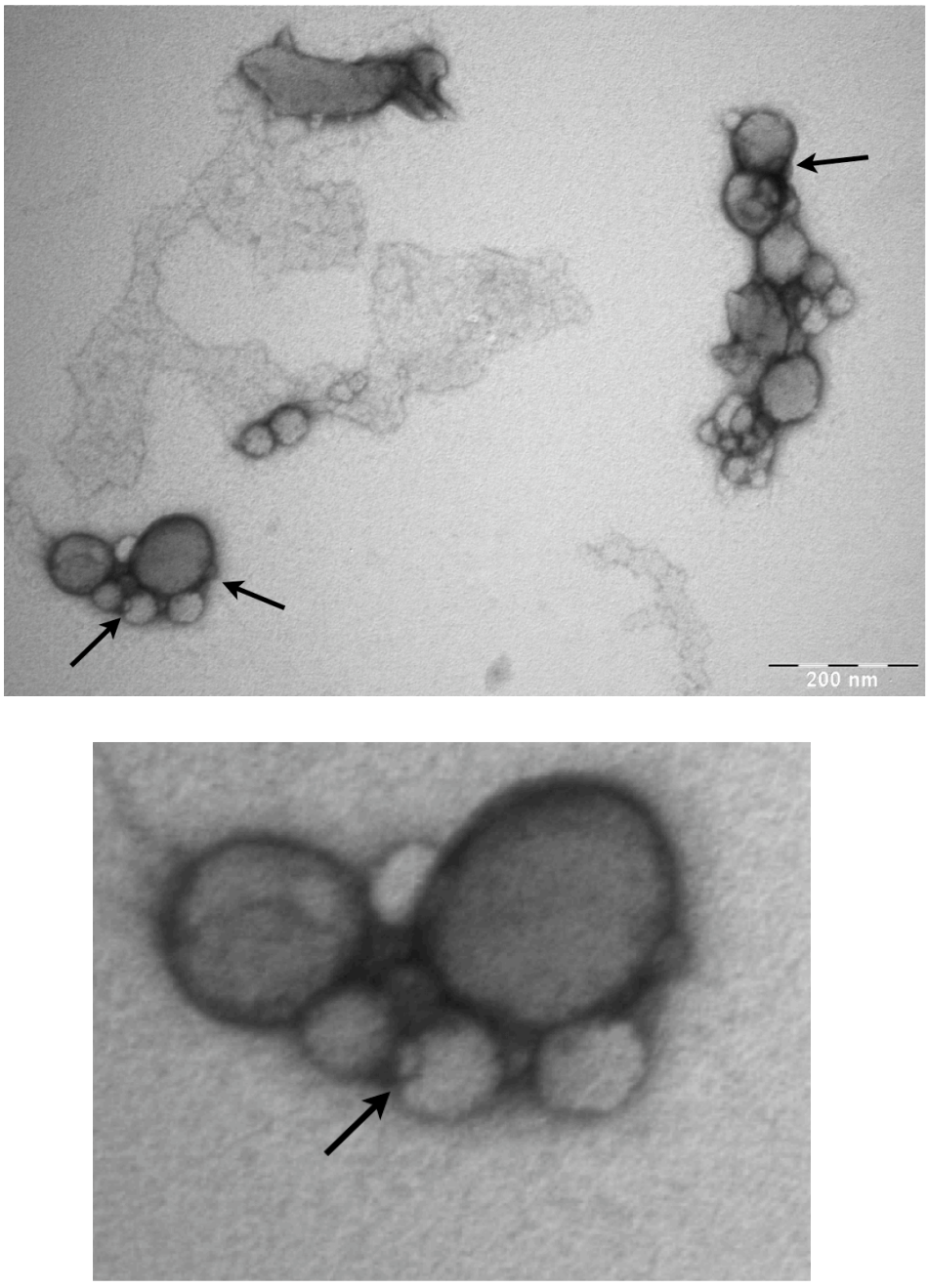

Figure 6.3 Transmission electron micrograph of vesicle/PEG-lipid templated hollow silica particles. Black arrows indicate the irregularities on the particles surface. The sample was negatively stained with uranyl acetate solution (4 %wt.).

BIBLIOGRAPHY

1. Graham, T., Liquid diffusion applied to analysis. *Phil. Trans. Roy. Soc. London* **1861,** *151*, 183-224.

2. Von Weymarn, P. P., *Kolloid-Z.* **1908,** (2), 199, 230, 275, 301 326.

3. Ostwald, W., *Kolloid-Z.* **1907,** (1), 291,331.

4. Ostwald, W., Die Welt der Vernachlässigten Dimensionen (The world of neglected dimensions). *Theodor Steinkopff, Dresden, Germany;* **1914**.

5. Weiser, H. B., Colloid Chemistry. *John Wiley & Sons, Inc., New York* **1939**.

6. Caruso, R. A.; Antonietti, M., Sol-gel nanocoating: An approach to the preparation of structured materials. *Chemistry of Materials* **2001,** *13* (10), 3272-3282.

7. Corma, A., From microporous to mesoporous molecular sieve materials and their use in catalysis. *Chem. Rev.* **1997,** *97* (6), 2373-2419.

8. Beck, J. S.; Vartuli, J. C.; Kennedy, G. J.; Kresge, C. T.; Roth, W. J.; Schramm, S. E., Molecular or supramolecular templating - Defining the role of surfactant chemistry in the formation of microporous and mesoporous molecular - sieves. *Chemistry of Materials* **1994,** *6* (10), 1816-1821.

9. Raman, N. K.; Anderson, M. T.; Brinker, C. J., Template-based approaches to the preparation of amorphous, nanoporous silicas. *Chemistry of Materials* **1996,** *8* (8), 1682-1701.

10. Davis, M. E., Materials science - organizing for better synthesis. *Nature* **1993,** *364* (6436), 391-393.

11. Lu, Y. F.; Fan, H. Y.; Stump, A.; Ward, T. L.; Rieker, T.; Brinker, C. J., Aerosol-assisted self-assembly of mesostructured spherical nanoparticles. *Nature* **1999,** *398* (6724), 223-226.

12. Huang, J. X.; Xie, Y.; Li, B.; Liu, Y.; Qian, Y. T.; Zhang, S. Y., In-situ source-template-interface reaction route to semiconductor CdS submicrometer hollow spheres. *Advanced Materials* **2000,** *12* (11), 808-811.

13. Fowler, C. E.; Khushalani, D.; Mann, S., Facile synthesis of hollow silica microspheres. *J. Mater. Chem.* **2001,** *11* (8), 1968-1971.

14. Velikov, K. P.; van Blaaderen, A., Synthesis and characterization of monodisperse core-shell colloidal spheres of zinc sulfide and silica. *Langmuir* **2001,** *17* (16), 4779-4786.

15. LizMarzan, L. M.; Giersig, M.; Mulvaney, P., Synthesis of nanosized gold-silica core-shell particles. *Langmuir* **1996,** *12* (18), 4329-4335.

16. Demirors, A. F.; van Blaaderen, A.; Imhof, A., Synthesis of eccentric titania-silica core-shell and composite particles. *Chemistry of Materials* **2009,** *21* (6), 979-984.

17. Cornelissen, J. J. L. M.; Connor, E. F.; Kim, H. C.; Lee, V. Y.; Magibitang, T.; Rice, P. M.; Volksen, W.; Sundberg, L. K.; Miller, R. D., Versatile synthesis of nanometer sized hollow silica spheres. *Chem. Commun.* **2003,** (8), 1010-1011.

18. Bourlinos, A. B.; Karakassides, M. A.; Petridis, D., Synthesis and characterization of hollow clay microspheres through a resin template approach. *Chem. Commun.* **2001,** (16), 1518-1519.

19. Rhodes, K. H.; Davis, S. A.; Caruso, F.; Zhang, B. J.; Mann, S., Hierarchical assembly of zeolite nanoparticles into ordered macroporous monoliths using core-shell building blocks. *Chemistry of Materials* **2000,** *12* (10), 2832-+.

20. Caruso, F.; Caruso, R. A.; Mohwald, H., Nanoengineering of inorganic and hybrid hollow spheres by colloidal templating. *Science* **1998,** *282* (5391), 1111-1114.

21. Yang, J.; Lind, J. U.; Trogler, W. C., Synthesis of hollow silica and titania nanospheres. *Chemistry of Materials* **2008,** *20* (9), 2875-2877.

22. Imhof, A., Preparation and characterization of titania-coated polystyrene spheres and hollow titania shells. *Langmuir* **2001,** *17* (12), 3579-3585.

23. Hadiko, G.; Han, Y. S.; Fuji, M.; Takahashi, M., Synthesis of hollow calcium carbonate particles by the bubble templating method. *Mater. Lett.* **2005,** *59* (19-20), 2519-2522.

24. Hubert, D. H. W.; Jung, M.; German, A. L., Vesicle templating. *Advanced Materials* **2000,** *12* (17), 1291-+.

25. Hubert, D. H. W.; Jung, M.; Frederik, P. M.; Bomans, P. H. H.; Meuldijk, J.; German, A. L., Vesicle-directed growth of silica. *Advanced Materials* **2000,** *12* (17), 1286-1290.

26. Tanev, P. T.; Pinnavaia, T. J., Biomimetic templating of porous lamellar silicas by vesicular surfactant assemblies. *Science* **1996,** *271* (5253), 1267-1269.

27. Hotz, J.; Meier, W., Vesicle-templated polymer hollow spheres. *Langmuir* **1998,** *14* (5), 1031-1036.

28. Kim, S. S.; Zhang, W. Z.; Pinnavaia, T. J., Ultrastable mesostructured silica vesicles. *Science* **1998,** *282* (5392), 1302-1305.

29. Nelson, K.; Deng, Y. L., The shape dependence of core-shell and hollow titania nanoparticles on coating thickness during layer-by-layer and sol-gel synthesis. *Nanotechnology* **2006,** *17* (13), 3219-3225.

30. Davis, S. A.; Burkett, S. L.; Mendelson, N. H.; Mann, S., Bacterial templating of ordered macrostructures in silica and silica-surfactant mesophases. *Nature* **1997,** *385* (6615), 420-423.

31. Imhof, A.; Pine, D. J., Ordered macroporous materials by emulsion templating. *Nature* **1997,** *389* (6654), 948-951.

32. Schacht, S.; Huo, Q.; VoigtMartin, I. G.; Stucky, G. D.; Schuth, F., Oil-water interface templating of mesoporous macroscale structures. *Science* **1996,** *273* (5276), 768-771.

33. Liu, J.; Yang, Q. H.; Zhang, L.; Yang, H. Q.; Gao, J. S.; Li, C., Organic-inorganic hybrid hollow nanospheres with microwindows on the shell. *Chemistry of Materials* **2008,** *20* (13), 4268-4275.

34. Liu, J.; Fan, F.; Feng, Z.; Zhang, L.; Bai, S.; Yang, Q.; Li, C., From hollow nanosphere to hollow microsphere: Mild buffer provides easy access to tunable silica structure. *J. Phys. Chem. C* **2008,** *112* (42), 16445-16451.

35. Heuer, A. H.; Fink, D. J.; Laraia, V. J.; Arias, J. L.; Calvert, P. D.; Kendall, K.; Messing, G. L.; Blackwell, J.; Rieke, P. C.; Thompson, D. H.; Wheeler, A. P.; Veis, A.; Caplan, A. I., Innovative materials processing strategies - A biomimetic approach. *Science* **1992,** *255* (5048), 1098-1105.

36. Tanev, P. T.; Pinnavaia, T. J., Biomimetic assembly of porous lamellar silica molecular sieves with a vesicular particle architecture. *Supramol. Sci.* **1998,** *5* (3-4), 399-404.

37. Qiao, S. Z.; Lin, C. X.; Jin, Y. G.; Li, Z.; Yan, Z. M.; Hao, Z. P.; Huang, Y. N.; Lu, G. Q., Surface-functionalized periodic mesoporous organosilica hollow spheres. *J. Phys. Chem. C* **2009,** *113* (20), 8673-8682.

38. Tan, B.; Lehmler, H. J.; Vyas, S. M.; Knutson, B. L.; Rankin, S. E., Fluorinated-surfactant-templated synthesis of hollow silica particles with a single layer of mesopores in their shells. *Advanced Materials* **2005,** *17* (19), 2368-2371.

39. Hentze, H. P.; Raghavan, S. R.; McKelvey, C. A.; Kaler, E. W., Silica hollow spheres by templating of catanionic vesicles. *Langmuir* **2003,** *19* (4), 1069-1074.

40. Ojogun, V. A.; Lehmler, H.-J.; Knutson, B. L., Cationic-anionic vesicle templating from fluorocarbon/fluorocarbon and hydrocarbon/fluorocarbon surfactants. *J Colloid Interface Sci* **2009,** *338* (1), 82-91.

41. Graf, C.; Vossen, D. L. J.; Imhof, A.; van Blaaderen, A., A general method to coat colloidal particles with silica. *Langmuir* **2003,** *19* (17), 6693-6700.

42. Rosen, M. J., Surfactants and Interfacial Phenomena, 2nd ed. *Wiley, New York;* **1989**.

43. Bangham, A. D.; Standish, M. M.; Watkins, J. C., Diffusion of univalent ions across lamellae of swollen phospholipids. *J. Mol. Biol.* **1965,** *13* (1), 238-252.

44. Israelachvili, J. N.; Mitchell, D. J.; Ninham, B. W., Theory of self-assembly of hydrocarbon amphiphiles into micelles and bilayers. *Journal of the Chemical Society-Faraday Transactions Ii* **1976,** *72*, 1525-1568.

45. Israelachvili, J. N.; Mitchell, D. J.; Ninham, B. W., Theory of self-assembly of lipid bilayers and vesicles. *Biochimica Et Biophysica Acta* **1977,** *470* (2), 185-201.

46. Mitchell, D. J.; Ninham, B. W., Micelles, vesicles and micro-emulsions. *Journal of the Chemical Society-Faraday Transactions Ii* **1981,** *77*, 601-629.

47. Tartar, H. V.; Lelong, A. L. M., Micellar molecular weights of some paraffin chain salts by light scattering. *J. Phys. Chem.* **1956,** *59* (12), 1185-1190.

48. Tanford, C., Micelle shape and size. *J. Phys. Chem.* **1972,** *76* (21), 3020-3024.

49. Tanford, C., The Hydrophobic Effect: Formation of Micelles and Biological Membranes. *John Wiley & Sons, New York;* **1973**.

50. Israelachvili, J. N., Intermolecular and surface forces, 2nd ed. *London, Academic Press;* **1992**.

51. Jokela, P.; Jonsson, B.; Wennerstrom, H., Phase-equilibria in systems containing both an anionic and a cationic amphiphile - a thermodynamic model calculation. *Progress in Colloid and Polymer Science* **1985,** *70*, 17-22.

52. Hargreaves, W. R.; Deamer, D. W., Liposomes from ionic, single chain amphiphiles. *Biochemistry* **1978,** *17* (18), 3759-3768.

53. Kaler, E. W.; Murthy, A. K.; Rodriguez, B. E.; Zasadzinski, J. A. N., Spontaneous vesicle formation in aqueous mixtures of single-tailed surfactants. *Science* **1989,** *245* (4924), 1371-1374.

54. Herrington, K. L.; Kaler, E. W.; Miller, D. D.; Zasadzinski, J. A.; Chiruvolu, S., Phase-behavior of aqueous mixtures of dodecyltrimethylammonium bromide (DTAB) and sodium dodecyl-sulfate (SDS). *J. Phys. Chem.* **1993,** *97* (51), 13792-13802.

55. Fukuda, H.; Kawata, K.; Okuda, H.; Regen, S. L., Bilayer-forming ion-pair amphiphiles from single-chain surfactants. *J. Am. Chem. Soc.* **1990,** *112* (4), 1635-1637.

56. Kamenka, N.; Chorro, M.; Talmon, Y.; Zana, R., Study of mixed aggregates in aqueous-solutions of sodium dodecyl-sulfate and dodecyltrimethylammonium bromide. *Colloids and Surfaces* **1992,** *67*, 213-222.

57. Sjobom, M. B.; Edlund, H., Dependence of alkyl chain asymmetry on the phase equilibria of three catanionic surfactant mixtures containing dodecyltrimethylammonium chloride, sodium alkylcarboxylate, water. *Langmuir* **2002,** *18* (22), 8309-8317.

58. Lasic, D. D., Recent developments in medical applications of liposomes: sterically stabilized liposomes in cancer therapy and gene delivery in vivo. *J. Control. Release* **1997,** *48* (2-3), 203-222.

59. Lasic, D. D., Liposomes: From Physics to Applications. *Elsevier, Amsterdam;* **1993**.

60. Fendler, J. H., Membrane Mimetic Chemistry. *Wiley: New York, Ch. 6* **1983**.

61. Brasher, L. L.; Herrington, K. L.; Kaler, E. W., Electrostatic effects on the phase-behavior of aqueous cetyltrimethylammonium bromide and sodium octyl sulfate mixtures with added sodium-bromide. *Langmuir* **1995,** *11* (11), 4267-4277.

62. Iampietro, D. J.; Kaler, E. W., Phase behavior and microstructure of aqueous mixtures of cetyltrimethylammonium bromide and sodium perfluorohexanoate. *Langmuir* **1999,** *15* (25), 8590-8601.

63. Lasic, D. D., On the thermodynamic stability of liposomes. *Journal of Colloid and Interface Science* **1990,** *140* (1), 302-304.

64. Porte, G.; Ligoure, C., Mixed amphiphilic bilayers - bending elasticity and formation of vesicles. *J. Chem. Phys.* **1995,** *102* (10), 4290-4298.

65. Chiruvolu, S.; Israelachvili, J. N.; Naranjo, E.; Xu, Z.; Zasadzinski, J. A.; Kaler, E. W.; Herrington, K. L., Measurement of forces between spontaneous vesicle-forming bilayers. *Langmuir* **1995,** *11* (11), 4256-4266.

66. Helfrich, W., Elastic properties of lipid bilayers - theory and possible experiments *Z.Naturforsch.(C)* **1973,** *C 28* (11-1), 693-703.

67. Safran, S. A.; Pincus, P.; Andelman, D., Theory of spontaneous vesicle formation in surfactant mixtures. *Science* **1990,** *248* (4953), 354-356.

68. Safran, S. A.; Pincus, P. A.; Andelman, D.; Mackintosh, F. C., Stability and phase-behavior of mixed surfactant vesicles. *Physical Review A* **1991,** *43* (2), 1071-1078.

69. Safran, S. A., Statistical thermodynamics of soft surfaces. *Surf. Sci.* **2002,** *500* (1-3), 127-146.

70. Helfrich, W., Steric interaction of fluid membranes in multilayer systems. *Z. Naturfors. Sect. A-J. Phys. Sci.* **1978,** *33* (3), 305-315.

71. Lipowsky, R.; Sackmann, E., Structure and Dynamics of Membranes. *North Holland, Amsterdam;* **1995**.

72. Herve, P.; Roux, D.; Bellocq, A. M.; Nallet, F.; Gulikkrzywicki, T., Dilute and concentrated phases of vesicles at thermal - equilibrium. *J. Phys. II* **1993,** *3* (8), 1255-1270.

73. Safran, S. A., Statistical Thermodynamics of Surfaces, Interfaces, and Membranes. *Addision-Wesley, Reading, MA;* **1994**.

74. Jung, H. T.; Coldren, B.; Zasadzinski, J. A.; Iampietro, D. J.; Kaler, E. W., The origins of stability of spontaneous vesicles. *Proc. Natl. Acad. Sci. U. S. A.* **2001,** *98* (4), 1353-1357.

75. Jung, H. T.; Lee, S. Y.; Kaler, E. W.; Coldren, B.; Zasadzinski, J. A., Gaussian curvature and the equilibrium among bilayer cylinders, spheres, and discs. *Proc. Natl. Acad. Sci. U. S. A.* **2002,** *99* (24), 15318-15322.

76. Dubois, M.; Deme, B.; Gulik-Krzywicki, T.; Dedieu, J. C.; Vautrin, C.; Desert, S.; Perez, E.; Zemb, T., Self-assembly of regular hollow icosahedra in salt-free catanionic solutions. *Nature* **2001,** *411* (6838), 672-675.

77. Kaler, E. W.; Herrington, K. L.; Iampietro, D. J.; Coldren, B. A.; Jung, H. T.; Zasadzinski, J. A., Phase behavior and microstructure in aqueous mixtures of cationic and anionic surfactants. In *Mixed Surfactant Systems*, Marcel Dekker: New York, 2005; Vol. 124, pp 289-337.

78. Wang, K.; Karlsson, G.; Almgren, M.; Asakawa, T., Aggregation behavior of cationic fluorosurfactants in water and salt solutions. A cryoTEM survey. *J. Phys. Chem. B* **1999,** *103* (43), 9237-9246.

79. Blanco, E.; Gonzalez-Perez, A.; Ruso, J. M.; Pedrido, R.; Prieto, G.; Sarmiento, F., A comparative study of the physicochemical properties of perfluorinated and hydrogenated amphiphiles. *Journal of Colloid and Interface Science* **2005,** *288* (1), 247-260.

80. Kissa, E., Fluorinated Surfactants Synthesis, Properties, Applications. *Marcel Dekker, New York;* **1994**.

81. Rahl, F. J.; Reimschu.Ac; Evanco, M. A.; Frederic.Rj, Studies of morphology of emulsion-grade polytetrafluoroethylene. *Journal of Polymer Science Part a-2-Polymer Physics* **1972,** *10* (7), 1337-&.

82. Riess, J. G.; Krafft, M. P., Fluorinated phosphocholine-based amphiphiles as components of fluorocarbon emulsions and fluorinated vesicles. *Chemistry and Physics of Lipids* **1995,** *75* (1), 1-14.

83. Bates, T. W.; Stockmay.Wh, Conformational properties of isolated polytetrafluoroethylene chains. *J. Chem. Phys.* **1966,** *45* (6), 2321-&.

84. Hoffmann, H.; Wurtz, J., Unusual phenomena in perfluorosurfactants. *J. Mol. Liq.* **1997,** *72* (1-3), 191-230.

85. Ristori, S.; Appell, J.; Porte, G., Spontaneous formation of monodisperse vesicles in dilute aqueous solutions of PFPE and betaine. *Langmuir* **1996,** *12* (3), 686-690.

86. Alam, T. M.; McIntyre, S. K., Self-assembly and magnetic alignment in cetyltrimethylammonium bromide/sodium perfluorooctanoate surfactant mixtures investigated using H-2 nuclear magnetic resonance spectroscopy. *Langmuir* **2008,** *24* (24), 13890-13896.

87. Dubois, M.; Lizunov, V.; Meister, A.; Gulik-Krzywicki, T.; Verbavatz, J. M.; Perez, E.; Zimmerberg, J.; Zemb, T., Shape control through molecular segregation in giant surfactant aggregates. *Proc. Natl. Acad. Sci. U. S. A.* **2004,** *101* (42), 15082-15087.

88. Schmolzer, S.; Grabner, D.; Gradzielski, M.; Narayanan, T., Millisecond-range time-resolved small-angle x-ray scattering studies of micellar transformations. *Phys. Rev. Lett.* **2002,** *88* (25), 4.

89. Weiss, T. M.; Narayanan, T.; Wolf, C.; Gradzielski, M.; Panine, P.; Finet, S.; Helsby, W. I., Dynamics of the self-assembly of unilamellar vesicles. *Phys. Rev. Lett.* **2005,** *94* (3), 4.

90. Bartlett, P.; Ottewill, R. H., A neutron-scattering study of the structure of a bimodal colloidal crystal. *J. Chem. Phys.* **1992,** *96* (4), 3306-3318.

91. Andrianov, K. A., Organic Silicon Compounds (state Scientific Publishing House for Chemical Literature, Moscow, 1955). *translation 59-11239,U.S. Dept. of Commerce, Washington, D.C.*

92. Ebelmen, M., *Ann. Chim. Phys.* **1845,** *15*, 319.

93. Brinker, C. J. S., G. W., Sol-Gel Science: the physics and chemistry of sol-gel-processing. *Academic Press: Boston;* **1990**, p xiv, 908.

94. Mendeleyev, D. I., *Khim. Zhur. sok. i Eng.* **1860,** *4*, 65.

95. Ebelmen, M., *Ann. Chim. Phys.* **1846,** (57), 319.

96. Friedel, C.; Crafts, J., *Ann.* **1865,** *136*, 203.

97. Friedel, C.; Ladenburg, A., *Ann.* **1867,** *143*, 118.

98. Friedel, C.; Ladenburg, A., **1868,** *145*, 179.

99. Konrad, E.; Bachle, O.; Signer, R., Polymer Kiesel acid esters. *Justus Liebigs Ann. Chem.* **1929,** *474*, 276-295.

100. Bechtold, M. F.; Vest, R. D.; Plambeck, L., Silicic acid from tetraethyl silicate hydrolysis. Polymerization and properties. *J. Am. Chem. Soc.* **1968,** *90* (17), 4590-4598.

101. Sakka, S.; Kamiya, K., The sol-gel transition in the hydrolysis of metal alkoxides in relation to the formation of glass-fibers and films. *Journal of Non-Crystalline Solids* **1982,** *48* (1), 31-46.

102. Yoldas, B. E., Introduction and effect of structural variations in organic polymers and glass networks. *Journal of Non-Crystalline Solids* **1982,** *51* (1), 105-121.

103. Weyl, W. A., *Miner. Ind. Exp. Stn. Bull* **1951,** *57*, 56.

104. Iler, R. K., The Chemistry of Silica. *Wiley, New York;* **1979**.

105. Schmidt, H.; Scholze, H.; Kaiser, A., Principles of hydrolysis and condensation reaction of alkoxysilanes *Journal of Non-Crystalline Solids* **1984,** *63* (1-2), 1-11.

106. Meixner, D. L.; Dyer, P. N., Influence of sol-gel synthesis parameters on the microstructure of particulate silica xerogels. *J. Sol-Gel Sci. Technol.* **1999,** *14* (3), 223-232.

107. Margaca, F. M. A.; Salvado, I. M. M.; Teixeira, J., Small angle neutron scattering study of silica gels: influence of pH. *Journal of Non-Crystalline Solids* **1999,** *258* (1-3), 70-77.

108. Kolbe, G., Das komplexchemische Verhalten der Kieselsaure. *Dissertation, Jena;* **1956**.

109. Stober, W.; Fink, A.; Bohn, E., Controlled growth of monodisperse silica spheres in micron size range. *Journal of Colloid and Interface Science* **1968,** *26* (1), 62-69.

110. Vanhelden, A. K.; Jansen, J. W.; Vrij, A., Preparation and characterization of spherical monodisperse silica dispersions in non-aqueous solvents. *Journal of Colloid and Interface Science* **1981,** *81* (2), 354-368.

111. Bogush, G. H.; Tracy, M. A.; Zukoski, C. F., Preparation of monodisperse silica particles - control of size and mass fraction. *Journal of Non-Crystalline Solids* **1988,** *104* (1), 95-106.

112. Green, D. L.; Lin, J. S.; Lam, Y. F.; Hu, M. Z. C.; Schaefer, D. W.; Harris, M. T., Size, volume fraction, and nucleation of Stober silica nanoparticles. *Journal of Colloid and Interface Science* **2003,** *266* (2), 346-358.

113. Lamer, V. K.; Dinegar, R. H., Theory, production and mechanism of formation of monodispersed hydrosols. *J. Am. Chem. Soc.* **1950,** *72* (11), 4847-4854.

114. Matsoukas, T.; Gulari, E., Dynamics of growth of silica particles from ammonia-catalyzed hydrolysis of tetra-ethyl-orthosilicate. *Journal of Colloid and Interface Science* **1988,** *124* (1), 252-261.

115. Matsoukas, T.; Gulari, E., Monomer-addition growth with a slow initiation step-a growt-model for silica particles from alkoxides. *Journal of Colloid and Interface Science* **1989,** *132* (1), 13-21.

116. Matsoukas, T.; Gulari, E., Self-sharpening distributions revisited polydispersity in growth by monomer addition. *Journal of Colloid and Interface Science* **1991,** *145* (2), 557-562.

117. Bogush, G. H.; Zukoski, C. F., Studies of the kinetics of the precipitation of uniform silica particles through the hydrolysis and condensation of silicon alkoxides. *Journal of Colloid and Interface Science* **1991,** *142* (1), 1-18.

118. Bogush, G. H.; Zukoski, C. F., Uniform silica particle-precipitation - An aggregative growth-model. *Journal of Colloid and Interface Science* **1991,** *142* (1), 19-34.

119. Kim, S.; Zukoski, C. F., A model of growth by heterocoagulation in seeded colloidal dispersions. *Journal of Colloid and Interface Science* **1990,** *139* (1), 198-212.

120. Bailey, J. K.; Mecartney, M. L., Formation of colloidal silica particles from alkoxides. *Colloids and Surfaces* **1992,** *63* (1-2), 151-161.

121. Vanblaaderen, A.; Vangeest, J.; Vrij, A., Monodisperse colloidal silica spheres from tetraalkoxysilanes - particle formation and growth - mechanism. *Journal of Colloid and Interface Science* **1992,** *154* (2), 481-501.

122. Aelion, R.; Loebel, A.; Eirich, F., Hydrolysis of ethyl silicate. *J. Am. Chem. Soc.* **1950,** *72* (12), 5705-5712.

123. Assink, R. A.; Kay, B. D., Sol-gel kinetics. 1. Functional-group kinetics. *Journal of Non-Crystalline Solids* **1988,** *99* (2-3), 359-370.

124. Brinker, C. J., Hydrolysis and condensation of silicates - effects on structure. *Journal of Non-Crystalline Solids* **1988,** *100* (1-3), 31-50.

125. Sanchez, J.; McCormick, A., Kinetic and thermodynamic study of the hydrolysis of silicon alkoxides in acidic alcohol - solutions. *J. Phys. Chem.* **1992,** *96* (22), 8973-8979.

126. Sefcik, J.; McCormick, A. V., Kinetic and thermodynamic issues in the early stages of sol-gel processes using silicon alkoxides. *Catal. Today* **1997,** *35* (3), 205-223.

127. Green, D. L.; Jayasundara, S.; Lam, Y. F.; Harris, M. T., Chemical reaction kinetics leading to the first Stober silica nanoparticles - NMR and SAXS investigation. *Journal of Non-Crystalline Solids* **2003,** *315* (1-2), 166-179.

128. Harris, M. T.; Brunson, R. R.; Byers, C. H., The base-catalyzed-hydrolysis and condensation-reactions of dilute and concentrated TEOS solutions. *Journal of Non-Crystalline Solids* **1990,** *121* (1-3), 397-403.

129. Mann, S.; Burkett, S. L.; Davis, S. A.; Fowler, C. E.; Mendelson, N. H.; Sims, S. D.; Walsh, D.; Whilton, N. T., Sol-gel synthesis of organized matter. *Chemistry of Materials* **1997,** *9* (11), 2300-2310.

130. Matsuyama, I.; Satoh, S.; Katsumoto, M.; Susa, K., Raman and GC-MS study of the initial-stage of the hydrolysis of tetramethoxysilane in acid and base-catalyzed sol-gel processes. *Journal of Non-Crystalline Solids* **1991,** *135* (1), 22-28.

131. Zhang, Z. Y.; Sakka, S., Hydrolysis and polymerization of dimethyldiethoxysilane, methyltrimethoxysilane and tetramethoxysilane in

presence of aluminum acetylacetonate. A complex catalyst for the formation of siloxanes. *J. Sol-Gel Sci. Technol.* **1999,** *16* (3), 209-220.

132. Bele, M.; Siiman, O.; Matijevic, E., Preparation and flow cytometry of uniform silica-fluorescent dye microspheres. *Cytometry* **2002**, 128-128.

133. Rankin, S. E.; Macosko, C. W.; McCormick, A. V., Importance of cyclization during the condensation of hydrolyzed alkoxysilanes. *Chemistry of Materials* **1998,** *10* (8), 2037-+.

134. Wilcock, D. F., Liquid methylpolysiloxane systems. *J. Am. Chem. Soc.* **1947,** *69* (3), 477-486.

135. Sanchez, J.; McCormick, A. V., Intramolecular vs intermolecular condensation rates in the acidic polymerization of octaethoxytrisiloxane. *Journal of Non-Crystalline Solids* **1994,** *167* (3), 289-294.

136. Vanblaaderen, A.; Kentgens, A. P. M., Particle morphology and chemical microstructure of colloidal silica spheres made from alkoxysilanes. *Journal of Non-Crystalline Solids* **1992,** *149* (3), 161-178.

137. Sadasivan, S.; Dubey, A. K.; Li, Y. Z.; Rasmussen, D. H., Alcoholic solvent effect on silica synthesis - NMR and DLS investigation. *J. Sol-Gel Sci. Technol.* **1998,** *12* (1), 5-14.

138. Holland, J. W.; Hui, C.; Cullis, P. R.; Madden, T. D., Poly(ethylene glycol)-lipid conjugates regulate the calcium-induced fusion of liposomes composed of phosphatidylethanolamine and phosphatidylserine. *Biochemistry* **1996,** *35* (8), 2618-2624.

139. Rovira-Bru, M.; Thompson, D. H.; Szleifer, I., Size and structure of spontaneously forming liposomes in lipid/PEG-lipid mixtures. *Biophys. J.* **2002,** *83* (5), 2419-2439.

140. Kang, S. Y.; Seong, B. S.; Han, Y. S.; Jung, H. T., Self-organization of amphiphilic polymer in vesicle bilayers composed of surfactant mixtures. *Biomacromolecules* **2003,** *4* (2), 360-365.

141. Marsh, D., Elastic constants of polymer-grafted lipid membranes. *Biophys. J.* **2001,** *81* (4), 2154-2162.

142. Jung, M.; Hubert, D. H. W.; Bomans, P. H. H.; Frederik, P. M.; Meuldijk, J.; van Herk, A. M.; Fischer, H.; German, A. L., New vesicle-polymer hybrids: The parachute architecture. *Langmuir* **1997,** *13* (26), 6877-6880.